RSC Advances

REVIEW

View Article Online
View Journal | View Issue

Cite this: *RSC Adv.*, 2014, **4**, 28537

Adsorption of metal ions by clays and inorganic solids

Susmita Sen Gupta[a] and Krishna G. Bhattacharyya*[b]

Received 22nd April 2014
Accepted 11th June 2014

DOI: 10.1039/c4ra03673e

www.rsc.org/advances

This review deals with adsorption of metal ions, particularly those considered as hazardous, on clays and some inorganic solids and covers the publication years 2000–2013 describing and quantifying the use of isotherms to obtain the adsorption capacities of the solids. The inorganic solids in the review include clays and clay minerals, their modified forms (obtained by treatment with acids and alkalis, organic functionalization, *etc.*), zeolites, silica gel, soil, river sediment, activated alumina, inorganic polymers, red mud, inorganic oxides, fly ash, *etc.* The use of two parameter and three parameter linear isotherms are only discussed with a view to obtain quantitative description of adsorptive accumulation and separation of metal ions from aqueous solution on the solids. The extensively used isotherms are those of Freundlich, Langmuir, Dubinin–Radushkevich and Redlich–Peterson. How these isotherms are being used to obtain the adsorption capacities along with their interpretations form the bulk of the review. The review is divided into sections, each describing the use of a particular isotherm. The metal cations receiving immense importance in adsorption studies are As(III)/As(V), Cd(II), Cr(III)/Cr(VI), Cu(II), Co(II), Pb(II), Ni(II), Hg(II), and Zn(II), and the review covers both the cationic and the anionic metal ions. A few other cations such as Mn(II), Fe(III), Se(V), which have not received much attention, are also covered.

1. Introduction

Inorganic solids like oxides, clay minerals, zeolites, *etc.*, play a leading role in maintaining environmental purity by adsorbing and separating undesirable components from the liquid phase. Equilibrium relationships between the quantity adsorbed in the solid phase and that remaining unadsorbed in the solution at a fixed temperature help in evaluating the adsorption capacities of the solids.[1] The equilibrium relationship illustrates how a constituent in the liquid phase interacts with the solid adsorbent and how the adsorption mechanism can be optimised for practical applications.[2,3] The isotherms are often used to predict modeling procedures for analysis and design of a particular system and for theoretical evaluation and interpretation of thermodynamic parameters.[4]

The equilibrium isotherm yields a range of quantitative information about the performance of a solid[5] such as the absorbability, amount adsorbed per unit mass, maximum

[a]*Department of Chemistry, B N College, Dhubri 783324, Assam, India*
[b]*Department of Chemistry, Gauhati University, Guwahati 781014, Assam, India. E-mail: kgbhattacharyya@gmail.com; Tel: +91 9864031987*

Susmita Sen Gupta is an Assistant Professor of Chemistry at B N College under Gauhati University (India). She did her Ph.D. in Chemistry from Gauhati University in 2008 on clay–metal interactions: a study with respect to kaolinite and montmorillonite with and without pillaring (supervisor K. G. Bhattacharyya). Her research interests include adsorption on clay minerals and modified clay minerals, photocatalytic removal of pollutants from water and material characterization.

Krishna Gopal Bhattacharyya is a professor of physical chemistry at Gauhati University (India). He received his Ph.D. degree from Imperial College, University of London in 1984 (Supervisor David Hayward). His research interests include adsorption on solids from solutions, heterogeneous catalysis with zeolites, clays and oxides, and environmental chemistry of water, air and soil.

amount that can be removed from solution, the sensitivity of the adsorbent to changes in adsorbate concentration, *etc.* The isotherm suffers from the limitation that it is strictly applicable to equilibrium conditions without any time restriction, and hence if true equilibrium is difficult to ascertain, the applicability of the isotherm will remain uncertain. Further, long-term chemical and biological effects are not accounted for by the isotherm.

A solid is a good adsorbent if it has high internal volume accessible to the adsorbate molecules or ions. Surface area,

Table 1 Composition of some inorganic adsorbents

Absorbent	Composition	Ion exchange capacity (mmol per 100 g)	Ref.
Kaolin	SiO_2 (46.70%), Al_2O_3 (37.33%), TiO_2 (<0.01%), Fe_2O_3 (0.75%), Na_2O (<0.10%), K_2O (0.93%), CaO (<0.10%), MgO (<0.10%), MnO (0.04%)	11.3	27
Ballclay	SiO_2 (62.96%), Al_2O_3 (22.61%), TiO_2 (0.51%), Fe_2O_3 (1.49%), Na_2O (<0.10%), K_2O (2.01%), CaO (0.51%), MgO (0.51%), MnO (0.02%)	14.9	
Turkish kaolinite	SiO_2 (59.46%), Al_2O_3 (14.92%), K_2O (2.45%), MgO (1.98%), Fe_2O_3 (5.18%), CaO (4.75%), SO_3 (0.10%), Na_2O (0.98%), TiO_2 (0.73%), Kuvars (quartz) (16.64%), calcite (8.14%), anorthite (11.53%), illite (42.58%), chlorite (21.11%)	—	31
Montmorillonite K-10	SiO_2 (65.34%), Al_2O_3 (12.89%), Fe_2O_3 (2.38%), MgO (0.95%), TiO_2 (0.52%), CaO (0.24%), Na_2O (0.53%), K_2O (1.54%), P_2O_5 (7.85%)	45.1	33
Natural Brazilian bentonite	SiO_2 (57.85%), Al_2O_3 (16.74%), Fe_2O_3 (8.78%), MgO (2.73%), TiO_2 (1.24%), CaO (1.08%), Na_2O (0.73%), K_2O (0.43%), P_2O_5 (0.27%)	74.8	
Turkish bentonite	SiO_2 (71.90%), Al_2O_3 (13.85%), Fe_2O_3 (0.68%), TiO_2 (0.09%), CaO (2.42%), MgO (1.27%), Na_2O (0.39%), K_2O (1.62%)	45.5 (pH 5.0) 51.9 (pH 6.4) 62.4 (pH 8.0)	34
Sepiolite	SiO_2 (58.7%), MgO (25.0%), Al_2O_3 (0.5%), CaO (0.5%), FeO + Fe_2O_3 (0.05%), TiO_2 (0.05%), Na_2O (0.05%)	—	151
Vermiculite	SiO_2 (39.0%), MgO (20.0%), Al_2O_3 (12.0%), Fe_2O_3 (8.0%), K_2O (4.0%), CaO (3.0%)	100.0	90
Laterite	Fe-oxide (47.26%), SiO_2 (28.67%), aloxide (21.13%), MnO_2 (0.78%), Na_2O (0.69%)	—	208
Muscovite	SiO_2 (61.32%), Al_2O_3 (23.90%), K_2O (7.12%), CaO (2.48%), MgO (2.07%), Fe_2O_3 (1.31%), TiO_2 (0.26%), Na_2O (0.15%)	0.3	43
Perlite	SiO_2, Al, K, Na	—	161
Attapulgite	C (2.63%), H (1.12%), N (9.65%)	—	132
Tourmaline	SiO_2 (41.56%), Al_2O_3 (26.3%), Fe_2O_3 (12.19%), TiO_2 (0.26%), B_2O_3 (9.33%), FeO (5.4%), CaO (0.52%), MgO (0.55%), K_2O (0.14%), Na_2O (1.2%), P_2O_5 (0.22%), Fe_2O_3 (1.59%), LiO_2 (1.87%), MnO (0.04%), F (1.06%)	384.0	122
Dolomite	$MgCO_3$ (44.0%), $CaCO_3$ (53.0%), (SiO_2 and Fe as impurities)	—	205
Beidellite	SiO_2 (58.08%), Al_2O_3 (29.92%), MgO (5.48%), Fe_2O_3 (2.96%), Na_2O (1.85%), CaO (0.63%), K_2O (0.2%)	—	181
Natural clinoptilolite	SiO_2 (69.12%), Al_2O_3 (12.05%), CaO (2.23%), K_2O (3.61%), Na_2O (0.32%), Fe_2O (0.98%), MgO (1.30%)	190.0–220.0	85
Zeolite	SiO_2 (46.5%), MgO (2.3%), Al_2O_3 (15%), Fe_2O_3 (3%), K_2O (6%), CaO (10%), Na_2O_2 (0.6%), TiO_2 (0.3%)	170.0	90
Natural zeolitic volcanic tuff	SiO_2 (69.57%), Al_2O_3 (10.59%), CaO (2.23%), K_2O (5.37%), Na_2O (1.50%), Fe_2O_3 (1.33%), MgO (0.77%), TiO_2 (0.22%)	—	82
Low-grade phosphate	P_2O_5 (26.35%), CaO (48.13%), SiO_2 (10.04%), CO_2 (8.64%), Cl^- (360 ppm), organic carbon (0.17%), moisture (1.32%)	—	209
Pumice	SiO_2 (72.0%), MgO (0.1%), Al_2O_3 (11.9%), Fe_2O_3 (2.1%), K_2O (5.1%), CaO (0.6%), TiO_2 (0.1%)	30.0	90
Polymetallic sea nodule	MnO_2 (31.8%), Fe_2O_3 (21.2%), SiO_2 (14.2%) with traces of Cu, Ni, Co, Ca, K, Na and Mg	—	222
Vanadium mine tailing	C (28.47%), O (36.2%), Mg (0.88 %), Al (5.99%), Si (21.1%), K (2.48%), V (1.45%), Fe (1.09%)	—	223
Activated alumina	SiO_2 (0.03 %), Fe_2O_3 (0.03 %), Al_2O_3 (93.1 %), Na_2O (0.1 %)	—	111
Loess soil	SiO_2 (63.68%), Al_2O_3 (12.77%), CaO (9.56%), MgO (3.14%), K_2O (3.01%), Fe_2O_3 (2.74%), Na_2O (2.35%), FeO (0.89%), TiO_2 (0.78%), MnO (0.09%)	11.2	123
Fly ash (sugar industry)	SiO_2 (60.5%), Al_2O_3 (15.4%), CaO (2.90%), Fe_2O_3 (4.90%), MgO (0.81%)	—	231
Fly ash (thermal power plant)	SiO_2 (52.0%), Al_2O_3 (27.0%), Fe_2O_3 (6.0%), MgO (0.70%), CaO (0.11%), TiO_2 (1.01%)	—	235
Pit coal fly ash	SiO_2 (47.39%), Al_2O_3 (23.49%), Fe_2O_3 (8.55%), CaO (4.67%), Na_2O (1.36%)	—	233
Clarified sludge	SiO_2 (12.6%), Fe_2O_3 (48.0%), CaO (23.4%), MgO (2.5%), MnO (0.2%), Na_2O (0.7%), K_2O (0.5%)	—	239
	Fe_2O_3 (48.0%), CaO (23.4%), MgO (2.5%), MnO (0.2%), SiO_2 (12.6%), Na_2O (0.7%), K_2O (0.5%)	—	240
Red mud	SiO_2 (9.64%), Al_2O_3 (17.28%), Fe_2O_3 (38.80%), TiO_2 (18.80%), Na_2O (6.86%)	—	237
Electric furnace slag	SiO_2 (27.54%), Fe_2O_3 (0.49%), FeO (7.11%), CaO (26.74%), MgO (22.84%), Mn_2O_3 (9.71%), Al_2O_3 (4.52%), P_2O_5 (0.019%), S (0.015%), K_2O (0.60%), Na_2O (0.23%)	—	137

particularly the internal pore surface and pore size distribution determine the extent of adsorption. How quickly the adsorbing molecules reach the adsorption sites is another important criterion for consideration.[6] The physical size and form of the solid particles, the chemistry of the adsorbent, namely, degree of ionization at the surface, the types of functional groups present and the degree to which these properties change in contact with an aqueous solution are important considerations in determining the adsorption capacity of a solid.

During the last few years, a good number of reviews have appeared on water treatment through adsorption. A few of these reviews include (i) arsenic remediation by different types of adsorbents,[7] (ii) advanced adsorption methods that specialize in the composition, structure, function and characteristics of the solids for water treatment,[8] (iii) use of low cost inorganic and biomass-based adsorbents for wastewater treatment,[9] (iv) utilization of agro-industrial and municipal wastes for detoxification of water,[10] (v) natural and modified zeolites as adsorbents for water and wastewater treatment,[11] (vi) natural and modified kaolinite and montmorillonite as adsorbents for metal ions removal,[12–14] (vii) development and potential applications of adsorption isotherms,[3] *etc.*

The present work reviews adsorption of metal cations and anions on inorganic solids since 2000 and the use of isotherms to characterize the solids in terms of the adsorption capacities. The inorganic adsorbents included in this review are clays and clay minerals, zeolites, silica gel, soil, river sediment, activated alumina, inorganic polymer, red mud, inorganic oxides (*viz.*, hydrous zirconium oxide, titanium oxide, stannic oxide, ferric oxide), fly ash, *etc.* These substances are used as they are found in nature and also modified chemically through various treatments. Table 1 summarises a list of such inorganic adsorbents with their compositions.

2. Quantitative treatment of the adsorption equilibrium

Adsorption is described as one of the fascinating phenomena related with the behaviour of fluids in a force field exerted by the solid surface.[15] While chemical equilibrium in a homogeneous system is driven by a reduction of the free energies of the bulk system, the same for a heterogeneous surface reaction comes from a reduction in the surface energy.

In formulating an adsorption isotherm, three basic approaches are followed, namely, (i) consideration of adsorption as a state of dynamic equilibrium involving both adsorption and desorption,[16] (ii) thermodynamic treatment of adsorption that provides a framework to obtain a number of isotherm models[17,18] and (iii) potential energy profiles of the adsorbate as it comes close to the adsorbent.[19] In many cases, more than one approach is utilised in obtaining an isotherm that makes it possible to interpret the adsorption phenomenon.[20]

This review considers the use of linear isotherms to obtain adsorption capacities of clays and other inorganic solids with respect to adsorptive accumulation and separation of metal ions from aqueous solution. Freundlich and Langmuir isotherms continue to be most extensively and inbariably used by all adsorption scientists, while Dubinin–Radushkevich, Redlich–Peterson, Temkin and Toth isotherms have also been explored in a number of works. The estimation of the adsorption capacities of clays and other inorganic solids based on these isotherms form the bulk of this review. There are, however, wide disparities in the nomenclature and the units used for expressing the adsorption capacities and other coefficients (including no use of units in some cases) and the review is therefore confined to those cases where these entities are well defined and are unambiguous. Molecular simulation studies, particularly with respect to adsorption isotherms and adsorbate–adsorbent interactions, have also been referred to in this review.

2.1. Freundlich isotherm and its applications

The Freundlich isotherm,[21] one of the most widely used adsorption equilibrium model, started on an empirical ground, but was shown latter to be thermodynamically rigorous for adsorption on heterogeneous surfaces.[22] Any non-uniform distribution of adsorption heat and affinities over a heterogeneous surface leading to multilayer adsorption can be described with this isotherm.[23] Freundlich model proposed that the stronger binding sites on a solid surface were occupied first until adsorption energy decreased to a value when no further adsorbate–adsorbent interactions were possible.[3,24,25]

The Freundlich isotherm and its linearized form,

$$q_e = K_F C_e^n \quad (1)$$

$$\log q_e = \log K_F + n \log C_e \quad (2)$$

give the relationship between C_e and q_e, the equilibrium liquid phase and solid phase concentrations of the adsorbate, K_F and n being Freundlich coefficients, representing adsorption capacity and adsorption intensity respectively. The value of n is qualitatively related to the distribution of site-binding energies and thus reflects the type of sorption sites. When $n = 1$, all surface sites are considered similar.[26] For a heterogeneous surface, n is <1, which is considered as the sufficient condition for adsorption to be favourable. A selection of literature on use of this isotherm is presented below. Freundlich capacities for adsorption of metal ions on some inorganic adsorbents are summarized in Table 2.

2.1.1. Clays. Freundlich adsorption capacities of Thai kaolin and ballclay for Cd(II), Cr(III), Cu(II), Ni(II), Pb(II) and Zn(II) were shown as:[27]

(i) Kaolin: 6.22×10^{-4}, 1.13×10^{-3}, 4.20×10^{-4}, 5.11×10^{-5}, 7.73×10^{-5} and 1.07×10^{-3} mmol g^{-1}.

(ii) Ballclay: 3.11×10^{-3}, 2.31×10^{-2}, 7.16×10^{-3}, 5.62×10^{-3}, 4.01×10^{-3} and 5.32×10^{-3} mmol g^{-1} respectively for Cd(II), Cr(III), Cu(II), Ni(II), Pb(II) and Zn(II). The ballclay having 2 : 1 layer structure has higher charges in both tetrahedral and octahedral sheets resulting from isomorphous substitution, whereas kaolin (1 : 1) has little such substitution. This explains the higher adsorption capacity of ball clay. The highest adsorption affinity of Cr(III) on both the clays was attributed to

Table 2 Freundlich capacities for adsorption of metal ions on some inorganic adsorbents

Metal cation/adsorbent	Experimental variables		Freundlich capacity (K_F)		Ref.
As(III)					
$MnFe_2O_4$	293 K	pH 7.0	29.6	$mg^{1-1/n}\ L^{1/n}\ g^{-1}$	104
$CoFe_2O_4$			36.9		
Fe_3O_4			15.2		
Natural muscovite	293 K	As(III) 0–100 mg L^{-1}, pH 6.0	0.029	$mg^{1-1/n}\ L^{1/n}\ g^{-1}$	43
As(V)					
Natural muscovite	293 K	As(V) 0–100 mg L^{-1}, pH 6.0	0.200	$mg^{1-1/n}\ L^{1/n}\ g^{-1}$	43
Laterite	305 K	As(V) 0.5–2.0 mg L^{-1}, pH 5.5	0.498	mg L^{-1}	208
		As(V) 2.0–20.0 mg L^{-1}, pH 5.5	0.147		
		As(V) 0.2–20.0 mg L^{-1}, pH 7.0	0.234		
		As(V) 3.0–20.0 mg L^{-1}, pH 7.0	0.124		
		As(V) 0.2–20.0 mg L^{-1}, pH 5.5	0.306		
	293 K	As(V) 0.5–2.0 mg L^{-1}, pH 7.0	0.124		
		As(V) 2.0–20.0 mg L^{-1}, pH 7.0	0.105		
	315 K	As(V) 0.5–2.0 mg L^{-1}, pH 5.5	0.665		
		As(V) 2.0–20.0 mg L^{-1}, pH 5.5	0.245		
		As(V) 0.5–2.5 mg L^{-1}, pH 7.0	0.174		
		As(V) 2.5–20.0 mg L^{-1}, pH 7.0	0.144		
		As(V) 3.5–20.0 mg L^{-1}, pH 5.5	0.381		
$MnFe_2O_4$	293 K	pH 3.0	59.7	$mg^{1-1/n}\ L^{1/n}\ g^{-1}$	104
$CoFe_2O_4$			49.4		
Fe_3O_4			19.2		
Fe modified beydellite	298 K	As(III) 250–5000 μg L^{-1}	26.46	μg g^{-1}	181
	308 K		36.79		
	318 K		45.63		
Fe–Ce modified zeolite	298 K		10.40		
	308 K		11.51		
	318 K		15.05		
Fe modified sepiolite	298 K		7.98		
	308 K		10.34		
	318 K		11.21		
Iron oxide-coated perlite	303 K	pH 6.5–7.0	0.76	L mg^{-1}	161
Al-loaded-zeolite	297 K	As(V) 1.3 mμ	0.122	mmol g^{-1}	86
			0.088		
Chitosan–clay–magnetite composite	296 ± 2 K	pH 5.0	0.282	L g^{-1}	178
Activated red mud	288 K	As(V) 5.74–182.57 μM, pH 7.0 ± 0.1	5.93	L μmol^{-1}	138
	293 K	As(V) 7.70–136.50 μM, pH 7.0 ± 0.1	6.71		
	296 ± 1 K	As(V) 2.0–151.87 μM, pH 7.0 ± 0.1	17.98		
	323 K	As(V) 6.91–152.18 μM, pH 7.0 ± 0.1	16.85		
	296 ± 1 K	As(V) 7.03–220.85 μM, pH 4.5 ± 0.1	63.29		
Cd(II)					
Kaolin	303 K		6.22×10^{-4}	mmol g^{-1}	27
Ball clay			3.11×10^{-3}		
Bentonite	303 K	Cd(II) 50–300 mg L^{-1}	46.56	mg g^{-1}	36
Montmorillonite K 10	298 K		0.42	mg g^{-1}	33
Brazilian bentonite			1.74		
Acid-activated kaolinite	303 K	pH 5.5	0.80	mg g^{-1}	46
Acid-activated montmorillonite			12.90		
Montmorillonite	293 K		3775.5	$\mu M^{1-n}\ kg^{-1}\ L^{n}$	26
Hydroxy-Al interlayered montmorillonite			507.0		
Fe-pillared bentonite		Cd(II) 0.178–5.34 mmol L^{-1}	0.451	L g^{-1}	63
Fe/Cr-pillared bentonite			0.347		
Cr-pillared bentonite			0.264	$mg^{1-1/n}\ L^{1/n}\ g^{-1}$	47
Kaolinite	303 K	pH 5.5	0.38		
ZrO-kaolinite			0.33		
TBA-kaolinite			0.32		
Montmorillonite			6.76		
ZrO-montmorillonite			1.20		
TBA-montmorillonite			2.21		
Bentonite	303 K	pH 6.02	0.82	mg g^{-1}	58
	323 K		2.40		

Table 2 (*Contd.*)

Metal cation/adsorbent	Experimental variables		Freundlich capacity (K_F)		Ref.
Bentonite + goethite	303 K		0.70		
	323 K		1.08		
Bentonite + humic acid	303 K		1.89		
	323 K		2.82		
Bentonite + geothite + humic acid	303 K		1.61		
	323 K		2.65		
Goethite	300 ± 1 K	Cd(II) 5–25 mg L^{-1}	2.140	L g^{-1}	113
Boehmite (γ-AlOOH)	298 K	Cd(II) 50 mg L^{-1}, pH 6.0	0.111	$mg^{1-1/n}$ $L^{1/n}$ g^{-1}	114
Goethite (γ-FeOOH)			0.074		
Vermiculite	298 K	Cd(II) 0–500 μM	0.65	L g^{-1}	90
Zeolite			0.55		
Pumice			0.69		
Natural muscovite	293 K	Cd(II) 0–100 mg L^{-1}, pH 6.0	0.007	$mg^{1-1/n}$ $L^{1/n}$ g^{-1}	43
Zeolite-based geopolymer			6.603	L g^{-1}	89
NiO	303 K	Cd(II) 100–600 mg L^{-1}	6.616	mg g^{-1}	201
Hydrous MnO_2	298 K	pH 3.5–4.0	1.367	$mmol^{1-n}$ L^{n} g^{-1}	96
Iron oxide-immobilized sand	298 ± 1 K		0.179	mg g^{-1}	128
Thiol-functionalized silica	298 K	Cd(II) 20–250 mg L^{-1}	25.65 ± 1.43	L g^{-1}	117
Loess soils	278 K	Cd(II) 25–150 mg L^{-1}	8.80	mg g^{-1}	123
	288 K		4.02		
	298 K		4.05		
	308 K		4.26		
	318 K		4.87		
Titanate nanotube	298 ± 1 K	Cd(II) 0.1–3.0 mmol L^{-1}	0.92	mmol g^{-1}	80
Silico-antimonate ion exchanger	298 ± 1 K		0.79	mmol g^{-1}	133
Activated alumina	303 K	pH 5.0	4.34	$mg^{1-1/n}$ $L^{1/n}$ g^{-1}	111
Clarified sludge	303 ± 0.5 K	pH 5.0	4.37	$mg^{1-1/n}$ $L^{1/n}$ g^{-1}	240
Dithiocarbamate chelating resin	298 K	Cd(II) 1–25 mmol L^{-1}	0.831	mmol L^{-1}	136
Co(II)					
Bentonite	293 K	pH 3.0	0.460	mg g^{-1}	34
		pH 5.0	1.093		
		pH 7.0	2.290		
		pH 9.0	3.834		
Kaolinite	303 K	pH 5.8	1.1	$mg^{1-1/n}$ $L^{1/n}$ g^{-1}	50
Acid-activated kaolinite			1.5		
Montmorillonite			4.6		
Acid-activated montmorillonite			6.0		
ZrO-kaolinite	303 K	Co(II) 10–250 mg L^{-1}, pH 5.7	0.8	$mg^{1-1/n}$ $L^{1/n}$ g^{-1}	49
ZrO-montmorillonite			1.2		
HCl/NaOH-treated bentonite	295 ± 1 K	Co(II) 20–200 mg L^{-1}	1.02	mg g^{-1}	45
Ion exchange resins	IRN77	298 ± 1 K	75.63	mg g^{-1}	135
	SKN1		60.03		
Cr(III)					
Kaolin	303 K		1.13×10^{-3}	mmol g^{-1}	27
Acid-activated kaolinite			1.5		
ZrO-kaolinite			1.0		
TBA-kaolinite			0.9		
Tannin-immobilized activated clay	300 K		2.406	L g^{-1}	76
	310 K		2.670		
	320 K		2.687		
	330 K		3.113		
[3-(2-Aminoethylamino)propyl]trimethoxy-silane grafted sepiolite			2.042	$mg^{1-1/n}$ g^{-1} $L^{1/n}$	78
[3-(2-Aminoethylamino)propyl]trimethoxy-silane grafted acid-activated sepiolite			2.845		
Mercapto functionalized sepiolite	289.15 K	Pb(II) 0–80 mg L^{-1}	21.89 ± 1.97	mg g^{-1}	79
	299.15 K		22.90 ± 2.00		
	318.15 K		33.73 ± 1.28		
Zero-valent iron	298 K	Cr(VI) 60–100 mg L^{-1}	56.88	mg g^{-1}	62
Fe–Ni bimetallic nanoparticle			64.71		
Fe–Ni bimetallic-montmorillonite nanocomposite			69.13		

Table 2 (*Contd.*)

Metal cation/adsorbent	Experimental variables		Freundlich capacity (K_F)		Ref.
Hydrous TiO_2	288 K	pH 1.5	4.067	mg g^{-1}	255
	303 K		8.241		
	318 K		7.804		
Hydrous ZrO_2	298 K	pH 2.0	7.05	mg g^{-1}	91
	308 K		6.97		
	318 K		6.51		
	328 K		5.12		
	338 K		4.94		
Loamy sand soil			1078	$mg^{1-1/n}$ $L^{1/n}$ kg^{-1}	124
Cu(II)					
Local bentonite	293.15 K		5.77×10^{-4}	mol^{1-n} L^{n} g^{-1}	37
	313.15 K		6.33×10^{-4}		
	333.15 K		5.91×10^{-4}		
Kaolin	303 K		4.20×10^{-4}	mmol g^{-1}	27
Ball clay			7.16×10^{-3}		
Bentonite	303 K	Cu(II) 50–300 mg L^{-1}	19.54	mg g^{-1}	36
Bentonite	293 K	pH 3.0	1.020	mg g^{-1}	34
		pH 5.0	1.622		
		pH 7.0	5.755		
		pH 9.0	8.482		
Bentonite	303 K	pH 6.02	0.84	mg g^{-1}	58
	323 K		2.87		
Bentonite + goethite	303 K		1.00		
	323 K		2.76		
Bentonite + humic acid	303 K		1.92		
	323 K		3.13		
Bentonite + geothite + humic acid	303 K		1.38		
	323 K		2.11		
MgO coated bentonite	295.15 K	pH 6.0	8.93 ± 0.90	$mg^{1-1/n}$ L^{-1} g^{-1}	59
Kaolinite	303 K	Cu(II) 10–250 mg L^{-1}, pH 5.7	1.1	$mg^{1-1/n}$ $L^{1/n}$ g^{-1}	57
Acid-activated kaolinite			1.3		
Montmorillonite			9.2		
Acid-activated montmorillonite			12.4		
8-Hydroxy quinoline immobilized bentonite	293 K		34.78	L g^{-1}	70
	303 K		35.83		
	313 K		37.86		
	323 K		41.16		
2,2′-Dipyridyl immobilized bentonite	293 K	Cu(II) 92.5–200 mg L^{-1}, pH 5.7	11.20	L g^{-1}	72
	303 K		20.72		
	313 K		23.85		
	323 K		30.02		
Goethite	300 ± 1 K	Cu(II) 5–25 mg L^{-1}	2.227	L g^{-1}	113
Natural muscovite	293 K	Cu(II) 0–100 mg L^{-1}, pH 6.0	0.034	$mg^{1-1/n}$ $L^{1/n}$ g^{-1}	43
Chitosan–clay–magnetite composite	296 ± 2 K	pH 5.0	5.828	L g^{-1}	178
Iron oxide-immobilized sand	298 ± 1 K		0.487	mg g^{-1}	128
Amino functionalized silica gel (3-aminopropyltri-methoxysilane : silica = 0.1)			1.416	$mg^{1-1/n}$ $L^{1/n}$ g^{-1}	115
Amino functionalized silica gel (3-aminopropyltri-methoxysilane : silica = 0.2)			5.77		
Amino functionalized silica gel (3-aminopropyltri-methoxysilane : silica = 0.3)			17.132		
3-Aminopropyltriethoxysilane and glutaraldehyde coated Fe_3O_4	293 ± 1 K	pH 4.0	14.544	$mmol^{1-1/n}$ $L^{1/n}$ g^{-1}	107
Titanate nanotube	298 ± 1 K	Cu(II) 0.1–3.0 mmol L^{-1}	0.88	mmol g^{-1}	99
Silico-antimonate ion exchanger	298 ± 1 K		0.44	mmol g^{-1}	133
Electric furnace slag	293 K		0.44	$mg^{1-1/n}$ $L^{1/n}$ g^{-1}	137
	303 K		0.65		
	313 K		1.09		
Fe(III)					
Kaolinite	303 K	Fe(III) 10–250 mg L^{-1}, pH 3.0	1.3	$mg^{1-1/n}$ $L^{1/n}$ g^{-1}	52
Acid-activated kaolinite			1.7		

Table 2 (*Contd.*)

Metal cation/adsorbent	Experimental variables		Freundlich capacity (K_F)		Ref.
Montmorillonite			5.2		
Acid-activated montmorillonite			6.4		
ZrO-kaolinite	303 K	Fe(III) 10–250 mg L^{-1}, pH 3.0	1.0	$mg^{1-1/n}\ L^{1/n}\ g^{-1}$	49
ZrO-montmorillonite			1.4		
Chitosan–attapulgite composites	298 K		7.402	$mg\ g^{-1}$	132
	308 K		12.23		
	318 K		13.77		
Hg(II)					
Hybrid mesoporous alumina-silicate sieve	303 ± 2 K	Hg(II) 2–16 mg L^{-1}	18.95	$mg\ g^{-1}$	80
Dithiocarbamate chelating resin	298 K	Hg(II) 1–25 mmol L^{-1}	1.158	$mmol\ L^{-1}$	136
Mn(II)					
Montmorillonite K 10	298 K		0.31	$mg\ g^{-1}$	33
Brazilian bentonite			0.85		
Ni(II)					
Kaolin	303 K		5.11×10^{-5}	$mmol\ g^{-1}$	27
Ball clay			5.62×10^{-3}		
Kaolinite	303 K	Ni(II) 10–250 mg L^{-1}, pH 5.7	1.1	$mg^{1-1/n}\ L^{1/n}\ g^{-1}$	51
Acid-activated kaolinite			1.5		
Montmorillonite			4.5		
Acid-activated montmorillonite			6.0		
ZrO-kaolinite	303 K	Ni(II) 10–250 mg L^{-1}, pH 5.7	0.8	$mg^{1-1/n}\ L^{1/n}\ g^{-1}$	49
ZrO-montmorillonite			1.3		
Bentonite	293 K	pH 5.0	2.326	$L\ g^{-1}$	61
Bentonite/iron oxides (5 : 1 at 20 °C)			6.730		
Montmorillonite K10	298 K		1.000	$mg^{1-1/n}\ L^{1/n}\ g^{-1}$	74
3-Mercaptopropyltrimethoxy-silane modified montmorillonite K10			0.410		
Mg-mesoporous alumina	298 ± 1 K	Ni(II) 5–30 mg L^{-1}	16.62	$mg\ g^{-1}$	260
Na-attapulgite	291.15 K	pH 6.0 ± 0.1	0.0026	$mol^{1-n}\ L^{n}\ g^{-1}$	42
	313.15 K		0.0011		
	333.15 K		0.0011		
Hydrous TiO_2	288 ± 1 K	Ni(II) 10–150 mg L^{-1}, pH 5.0 ± 1	7.69	$mg\ g^{-1}$	259
	303 ± 1 K		8.34		
	318 ± 1 K		11.93		
	328 ± 1 K		13.06		
Silico-antimonate ion exchanger	298 ± 1 K		0.93	$mmol\ g^{-1}$	133
Dimethylglyoxime treated clinoptilolite	293 K		0.138	$L\ g^{-1}$	87
	313 K		0.128		
	333 K		0.114		
Pb(II)					
Local bentonite	293.13	pH 5.2 ± 0.2	3.03×10^{-3}	$mol^{1-n}\ L^{n}\ g^{-1}$	32
	323.13		5.11×10^{-3}		
	343.13		9.06×10^{-3}		
Turkish kaolinite	293 K	pH 6.0	0.58	$mg\ g^{-1}$	31
Turkish kaolinite	293 K	pH 5.0	0.175	$L\ g^{-1}$	30
Kaolin	303 K		7.73×10^{-5}	$mmol\ g^{-1}$	27
Ball clay			4.01×10^{-3}		
Montmorillonite	298 K	pH 6.0	15.06	$L\ g^{-1}$	40
Na-bentonite	298 K	Pb(II) 1.45×10^{-5} to 1.74×10^{-4} mol L^{-1}	3.61×10^{-2}	$mol^{1-1/n}\ L^{n}\ g^{-1}$	38
	318 K		2.57×10^{-2}		
	338 K		8.89×10^{-3}		
Montmorillonite–illite	310 K	Pb(II) 100 mg L^{-1}	9.115	$L\ g^{-1}$	251
		Pb(II) 150 mg L^{-1}	19 150		
		Pb(II) 200 mg L^{-1}	19.600		
Acid-activated kaolinite	303 K	Pb(II) 10–250 mg L^{-1}, pH 5.7	0.55	$mg^{1-1/n}\ L^{1/n}\ g^{-1}$	54
Acid-activated montmorillonite			13.30		
Kaolinite	303 K		0.808	$mg^{1-1/n}\ L^{1n}\ g^{-1}$	44
Aluminium sulphate modified kaolinite			6.94		

Table 2 (*Contd.*)

Metal cation/adsorbent	Experimental variables		Freundlich capacity (K_F)		Ref.
Kaolinite	303 K	Pb(II) 10–250 mg L^{-1}, pH 5.7	0.37	$mg^{1-1/n}\ L^{1/n}\ g^{-1}$	53
ZrO-kaolinite			0.34		
TBA-kaolinite			0.31		
Montmorillonite			7.32		
ZrO-montmorillonite			2.01		
TBA-montmorillonite			1.36		
8-Hydroxy quinoline-immobilized bentonite			58.73	$L\ g^{-1}$	71
	303 K		71.84		
	313 K		78.13		
	323 K		91.91		
Clay–poly(methoxyethyl)acrylamide composite	293 K	Pb(II) 100–300 mg L^{-1}	3.30×10^{-3}	$L\ g^{-1}$	75
	303 K		3.71×10^{-3}		
	313 K		3.75×10^{-3}		
	323 K		3.23×10^{-3}		
Natural muscovite	293 K	Pb(II) 0–100 mg L^{-1}, pH 6.0	0.096	$mg^{1-1/n}\ L^{1n}\ g^{-1}$	43
Mordenite	293 K	Pb(II) 20–100 mg L^{-1}, pH 6.0	0.509	$mg^{1-1/n}\ L^{1n}\ g^{-1}$	186
	303 K		1.080		
	313 K		1.137		
	323 K		1.211		
Natural apatite			0.131	$L\ mmol^{-1}$	121
Synthetic hydroxyapatite			0.487		
N-Methylimidazole anchored activated palygorskite	283 K		51.94	$mg\ g^{-1}$	212
	298 K		112.17		
	313 K		122.73		
Thiol-functionalized silica	298 K	Pb(II) 20–250 mg L^{-1}	63.99 ± 3.92	$L\ g^{-1}$	117
Activated alumina	303 K	pH 5.0	4.34	$mg^{1-1/n}\ L^{1/n}\ g^{-1}$	111
Hydrous MnO_2	298 K	pH 3.2–3.5	1.625	$mmol^{1-n}\ L^{n}\ g^{-1}$	96
NiO	303 K	Pb(II) 100–600 mg L^{-1}	35.46	$mg\ g^{-1}$	94
ZnO			0.152	$mg\ g^{-1}$	93
Fe_3O_4	298 K	pH 5.5	0.128	$mmol^{1-1/n}\ L^{1n}\ g^{-1}$	101
	313 K		0.145		
	328 K		0.167		
TiO_2/SiO_2 binary mixed oxide	298 K	pH 6.0	1.18	$mol^{1-1/n}\ L^{1n}\ g^{-1}$	98
	308 K		2.46		
	325 K		0.13		
Mg_2Al LDH	303.15 K	Pb(II) 5–23 mg L^{-1}, pH 5.7 ± 0.01	19.76	$mg\ g^{-1}$	119
	323.15 K		23.31		
	343.15 K		30.91		
River sand	298 ± 2 K		15.4 ± 6.9	$mmol\ g^{-1}$	125
Sand	293 K		0.28 ± 0.19	$mmol\ g^{-1}$	126
	303 K		0.63 ± 0.09		
	313 K		5.30 ± 3.61		
	323 K		5.10 ± 1.28		
Iron oxide-immobilized sand	298 ± 1 K		0.785	$mg\ g^{-1}$	128
Loamy sand soil			387.1	$mg^{1-1/n}\ L^{1/n}\ kg^{-1}$	124
Titanate nanotube	298 ± 1 K	Pb(II) 0.1–3.0 mmol L^{-1}	1.22	$mmol\ g^{-1}$	80
Electric furnace slag	293 K		0.57	$mg^{1-1/n}\ L^{1n}\ g^{-1}$	137
	303 K		0.93		
	313 K		1.82		
Dithiocarbamate chelating resin	298 K	Pb(II) 1–25 mmol L^{-1}	0.588	$mmol\ L^{-1}$	136
Zn(II)					
Kaolin	303 K		1.07×10^{-3}	$mmol\ g^{-1}$	27
Ball clay			5.32×10^{-3}		
Bentonite	293 K	pH 3.0	1.100	$mg\ g^{-1}$	34
		pH 5.0	1.732		
		pH 7.0	10.063		
		pH 9.0	12.320		
HCl/NaOH-treated bentonite	295 ± 1 K	Zn(II) 20–200 mg L^{-1}	71.22	$mg\ g^{-1}$	45
Hydrous MnO_2	298 K	pH 3.5–4.0	1.002	$mmol^{1-n}\ L^{n}\ g^{-1}$	96
Silico-antimonate ion exchanger	298 ± 1 K		0.47	$mmol\ g^{-1}$	133

its small ionic radius and higher ionic charge. For the divalent metal ions, a broad relationship between relative affinity and the tendency to hydrolyze was shown to determine their selectivity sequence. The results are also in general agreement with the CEC of 11.3 mmol per 100 g for kaolin and 14.9 mmol per 100 g for ballclay as reported by the authors.

The adsorption process of Cr(III) on kaolinite was influenced by solution pH, ionic strength and temperature.[28] The kaolinite surface in water had a net negative surface charge at natural pH with an isoelectric point at ~pH 2.35. Similar work was reported by Arias and Sen[29] for Zn(II) removal by kaolin with K_F of 1.61 mg g^{-1}. Sari *et al.*[30] proposed that Pb(II) ions from water were held by ionisable surface groups located at the edges of Turkish kaolinite and had K_F of 0.175 L g^{-1} at 293 K.

A local clay material consisting of 59.46% SiO_2 and 14.92% Al_2O_3 had K_F of 0.54 and 0.58 mg g^{-1} respectively for Cr(III) and Pb(II).[31]

The maximum K_F for Pb(II) on a local bentonite[32] was 9.06 × 10^{-3} mol^{1-n} L^n g^{-1} at 343.15 K and it was suggested that pH of the medium determined whether inner-sphere complexation or chemisorption was the mechanism by which Pb(II) was held to Na-bentonite.

Natural Brazilian bentonite (NT-25) had much larger Freundlich capacity[33] than the commercial montmorillonite, K10 (NT-25: Cd(II) 1.74 mg g^{-1}; Mn(II) 0.85 mg g^{-1}; K10: Cd(II) 0.42 mg g^{-1}; Mn(II) 0.31 mg g^{-1}). Hard Lewis acids and bases tend to form outer-sphere complexes and their adsorption capacity occurs mostly in surfaces with an excess of negative charge. Brazilian bentonite was also shown to have a larger CEC (74.8 mmol per 100 g) compared to K10 montmorillonite (45.1 mmol per 100 g).

Natural bentonite had K_F of 0.46 to 3.83 mg g^{-1}, 1.02 to 8.48 mg g^{-1} and 1.10 to 12.32 mg g^{-1} in the pH range of 3.0 to 9.0 respectively for Co(II), Cu(II) and Zn(II).[34] The surface charge density turns more negative at high pH taking up more of the cations. The CEC of bentonite was shown to be pH dependent with values of 45.50 mmol per 100 g (pH 5.0), 51.85 mmol per 100 g (pH 6.35) and 62.40 mmol per 100 g (pH 8.0). The adsorption capacity is attributed to ion-exchange reactions in the micropores of the mineral at comparatively high pH. This was also the case with Zn(II) adsorption on bentonite[35] with Freundlich capacity of 1.46 mg g^{-1} at 303 K. In another work on bentonite clay, Karapinar and Donat[36] found the Freundlich capacities for Cd(II) and Cu(II) to be 46.56 and 19.54 mg g^{-1} respectively.

Freundlich capacity of Na-bentonite for Cu(II)[37] varied from 5.77 × 10^{-4} to 5.91 × 10^{-4} mol^{1-n} L^n g^{-1} in the temperature range, 293.15 to 333.15 K and Cu(II) ions were held through ion exchange with H^+/Na^+ of the surface at low pH. At pH > 6.5, Cu(II) species present are $Cu(OH)_2$, $Cu(OH)^+$ and $Cu(OH)_2^{2+}$ that bind to negatively charged sites of Na-bentonite surface. It was also found that Na-bentonite had a higher Freundlich capacity for Pb(II) (K_F: 3.61 × 10^{-2} to 8.89 × 10^{-3} mol^{1-n} L^n g^{-1} in the temperature range, 298 to 338 K) than raw bentonite.[38] These differences were due to favourable properties of higher cation exchange capacity (91 mmol per 100 g), better dispersibility and better thermostability. Pb(II) adsorption on Na-bentonite was dominated by ion exchange or outer-sphere surface complexation at low pH, and by inner-sphere surface complexation at high pH.

Natural bentonite–Zn(II) interactions had higher Freundlich capacity than bentonite–Cu(II) (Zn(II): 16.22 mg g^{-1}, Cu(II) 8.71 mg g^{-1}).[39] While exchangeable cations present in bentonite surface participated in ion-exchange type adsorption, higher ionic potential of Zn(II) compared to Cd(II), must have helped it to bind strongly with the clay surface.

Zhang and Hou[40] suggested that adsorption capacity of montmorillonite (CEC 73.16 mmol per 100 g) for Pb(II) (K_F: 15.06 L g^{-1}) arose partly from chemical binding occurring at surface hydroxyl groups and partly from electrostatic interactions with the permanent negatively charged sites on montmorillonite.

Thermal or chemical treatments were also used to enhance adsorption capacity of clay. Thus, the material obtained by treatment (900 °C + sodium acetate + acetic acid + sodium nitrate) of a local clay had better adsorption capacity for Cd(II), Pb(II) and Zn(II).[41]

Strong surface complexation was suggested to be responsible for adsorption of Ni(II) on Na-attapulgite with K_F varying from 2.6 × 10^{-3} to 1× 10^{-3} mol^{1-n} L^n g^{-1} in the temperature range of 291.15 to 333.15 K.[42]

Natural muscovite[43] adsorbed As(III), As(V), Cd(II), Cu(II) and Pb(II) with Freundlich capacities of 0.03, 0.20, 0.01, 0.03 and 0.10 $mg^{1-1/n}$ $L^{1/n}$ g^{-1} respectively at 293 K. The overall adsorption capacity was influenced by impurities such as quartz and undetermined minerals present on the natural muscovite. Muscovite has a low surface area and a very low CEC (0.28 mmol per 100 g) compared to most other natural minerals explaining its low adsorption capacities.

2.1.2. Modified clays. Freundlich capacities of kaolinite modified with 25% (w/w) aluminium sulphate and of raw kaolinite were 6.94 and 0.81 $mg^{1-1/n}$ $L^{1/n}$ g^{-1} for Pb(II).[44] The large difference was attributed to higher CEC of the modified kaolinite (23.6 mmol per 100 g) compared to original kaolinite (9.5 mmol per 100 g).

When bentonite (CEC 51.20 mmol per 100 g) was modified by treating with HCl and subsequently with NaOH, Freundlich capacities for Co(II) and Zn(II) were 1.02 and 71.22 mg L^{-1} respectively.[45] The modification, according to the authors, opened up more macro and micro pores in the clay mineral that helped in removing more metal ions.

Clay mineral based adsorbents (kaolinite, montmorillonite, ZrO-kaolinite, ZrO-montmorillonite, acid-activated kaolinite and acid-activated montmorillonite) were shown to have excellent adsorption properties for Cd(II), Co(II), Cu(II), Cr(VI), Fe(III), Ni(II), and Pb(II).[46–57] The montmorillonite-based adsorbents possessed higher adsorption capacity (Cd(II): 1.2 to 12.9, Co(II): 1.1 to 6.0, Cu(II): 1.1 to 12.4, Cr(VI): 1.0 to 1.5, Fe(III): 1.3 to 6.4, Ni(II): 1.1 to 6.0, Pb(II): 0.4 to 13.3 $mg^{1-1/n}$ $L^{1/n}$ g^{-1}) (Fig. 1–6). The raw montmorillonite was almost five times as effective in adsorbing metal ions as kaolinite. The introduction of Zr(hydr) oxide did not improve the adsorption capacity of either montmorillonite or kaolinite. The poly(hydroxo zirconium) ions might have masked the negatively charged sites and blocked the

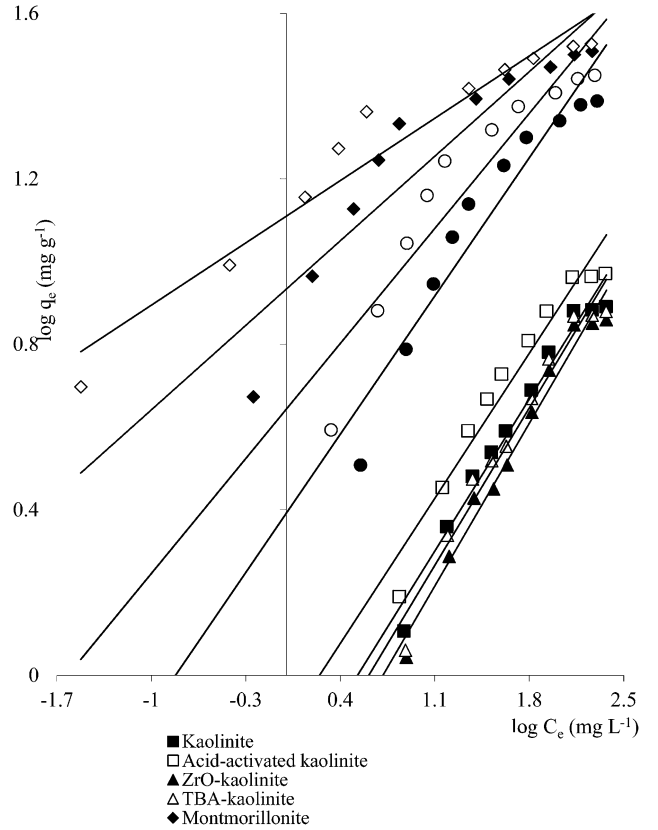

Fig. 1 Freundlich plots for Cd(II) adsorption on clay minerals (clay mineral 2.0 g L^{-1}, Cd(II) 10–250 mg L^{-1}, pH 5.5, time 240 min, temperature 303 K).

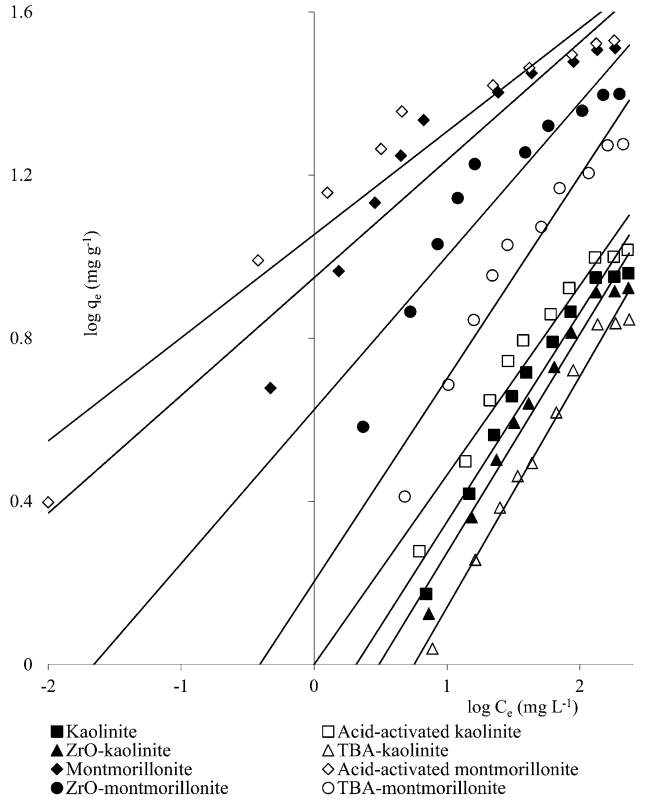

Fig. 2 Freundlich plots for Pb(II) adsorption on clay minerals (clay mineral 2.0 g L^{-1}, Pb(II) 10–250 mg L^{-1}, pH 5.7, time 180 min, temperature 303 K).

pores. Acid activation, however, enhanced the adsorption capacity of the clay minerals through increase in surface area as well as pore volume. The results were in conformity with the CEC values measured by the authors (kaolinite: 11.3 mmol per 100 g, ZrO-kaolinite: 10.2 mmol per 100 g, acid-activated kaolinite: 22.0 mmol per 100 g) compared to their montmorillonite counterparts (montmorillonite: 153.0 mmol per 100 g, ZrO-montmorillonite: 73.2 mmol per 100 g, acid-activated montmorillonite: 341.0 mmol per 100 g).

Adsorption of Cd(II) and Cu(II) at 303 and 323 K on natural and modified bentonite (B) [modified with goethite (G), humic acid (H) and binary mixture of goethite/humic acid (G + H)][58] showed that the humic acid modified species had the highest Freundlich capacity [for *e.g.*, at 323 K, K_F for Cd–B + H: 2.82, Cd–B + G + H: 2.65, Cd–B + G: 1.08, Cd–B: 2.40 mg g^{-1}; K_F for Cu–B + H: 3.13, Cu–B + G + H: 2.11, Cu–B + G: 2.76, Cu–B: 2.87 mg g^{-1}]. Modification with either goethite or humic acid might have introduced some new sites onto bentonite. Humic acid created strong complexing sites on bentonite that could take up more metal ions. These results were reflected in the increased CEC values [B: 95 mmol per 100 g, B + G: 105.32 mmol per 100 g, B + H: 120.4 mmol per 100 g, B + G + H: 125.8 mmol per 100 g].

K_F (8.93 ± 0.90 $mg^{1-1/n}$ $L^{1/n}$ g^{-1}) of MgO-coated bentonite for Cu(II) removal was much higher than that of the raw clay.[59] The higher adsorption was suggested to be due to the coordinative environments of Cu(II) ions and surface hydroxyl groups in a hydrated surface. MgO could have acted as a stabilizing buffer, which minimized metal solubility and avoided redissolution. Mixed Fe, Mg (hydr)oxides coated bentonite composite had Freundlich capacity of 35.19 $mg^{1-1/n}$ $L^{3/n}$ g^{-1} for Pb(II) with ion-exchange of Mg(II) by Pb(II) being the dominant process.[60]

Freundlich capacities for natural bentonite and bentonite/iron oxide composite of Ni(II)[61] were 2.33 and 6.73 L g^{-1} respectively at 293 K. The increased specific surface area and pore volume of composites compared to the natural bentonite suggested formation of agglomerated structures from precipitated nanosized iron oxides on adsorbent surface responsible for higher removal of Ni(II).

Fe–Ni bimetallic-montmorillonite nanocomposites possessed higher Freundlich adsorption capacity (69.13 mg g^{-1}) compared to zero-valent iron (56.88 mg g^{-1}) and Fe–Ni bimetallic nanoparticles (64.71 mg g^{-1}) for removal of Cr(VI).[62] Adsorption and reduction of Cr(VI) to Cr(III) occurred simultaneously and the authors suggested existence of a facile electron transfer from nanoparticle to the adsorbed Cr(VI) species resulting in faster reduction. Strong ionic interactions between Cr(VI) and composite surface were shown to occur through pore diffusion enhancing adsorption–desorption dynamics.

Use of different metal cations for pillaring on clays influences the Freundlich adsorption capacity. Tomul[63] has shown that Cd(II) adsorption on Fe pillared bentonite (0.451 L g^{-1}),

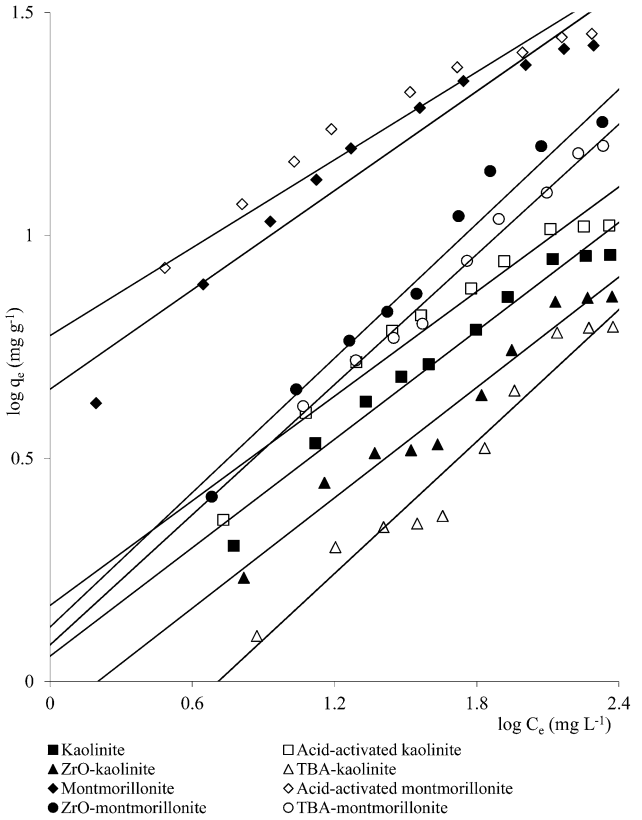

Fig. 3 Freundlich plots for Ni(II) adsorption on clay minerals (clay mineral 2.0 g L^{-1}, Ni(II) 10–250 mg L^{-1}, pH 5.7, time 180 min, temperature 303 K).

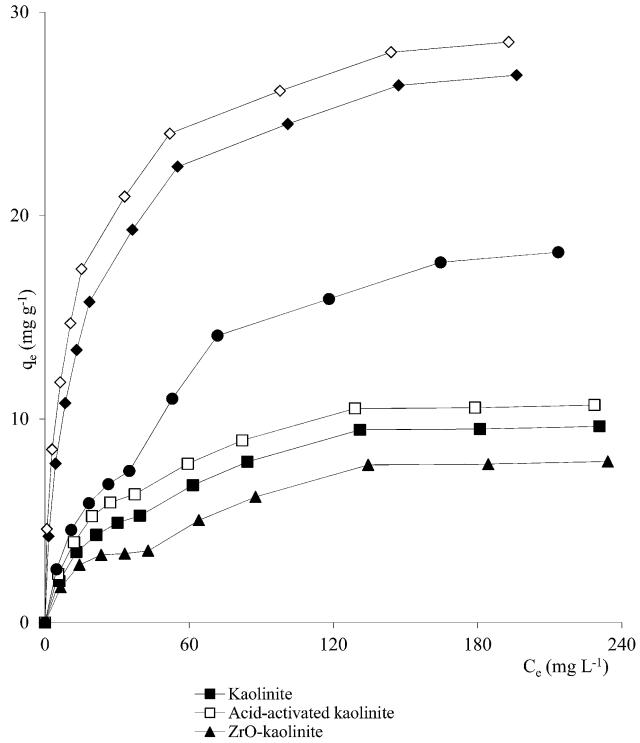

Fig. 4 Plots of q_e *vs.* C_e for Co(II) adsorption on clay minerals (clay mineral 2.0 g L^{-1}, Co(II) 10–250 mg L^{-1}, pH 5.8, time 240 min, temperature 303 K).

Fe/Cr pillared bentonite (0.347 L g^{-1}) and Cr pillared bentonite (0.264 L g^{-1}) had different adsorption capacities at 298 K. Since pore structure and surface properties of an adsorbent have a significant effect on the adsorption process, and the distribution of pores affects the efficiency and selectivity of adsorption, Fe pillared bentonite, Fe/Cr pillared bentonite and Cr pillared bentonite differ in their adsorption capacities due to differences in pore distribution.

Yan *et al.*[64] have shown that the Freundlich adsorption capacities of (i) acid-activated Al_{13}-pillared Na^+-montmorillonite (Al_{13}-PAAMt), (ii) Al_{13}-pillared Na^+-montmorillonite (Al_{13}-PMt) and (iii) Na^+-montmorillonite (Na^+-Mt) with respect to Cd(II) were in the order of (i) > (ii) > (iii). The uptake of Cd(II) was influenced by the changes in basal spacing, specific surface area and total pore volume due to intercalation with inorganic polyoxycations and also acid treatment.

In a significant earlier work, Jobstmann and Singh[26] found the Freundlich adsorption capacities of natural montmorillonite (3775.5 μM^{1-n} kg^{-1} L^n) for Cd(II) to be almost one order higher than that of hydroxy-aluminium-interlayered-montmorillonite (507.0 μM^{1-n} kg^{-1} L^n). The pillared clay had $n < 1$ suggesting the presence of energetically non-uniform sites while the unpillared montmorillonite had n close to 1 (0.85) that showed that the surface could be considered as nearly homogeneous. According to the authors, Cd(II) occupied both permanent charge sites and broken bond AlOH sites and the

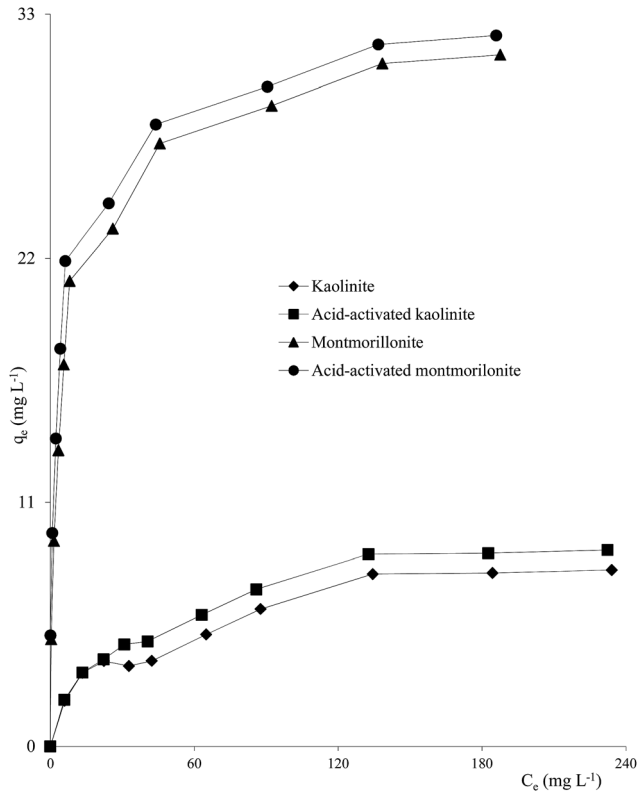

Fig. 5 Plots of q_e *vs.* C_e for Cu(II) adsorption on clay minerals (clay mineral 2.0 g L^{-1}, Cu(II) 10–250 mg L^{-1}, pH 5.7, time 360 min, temperature 303 K).

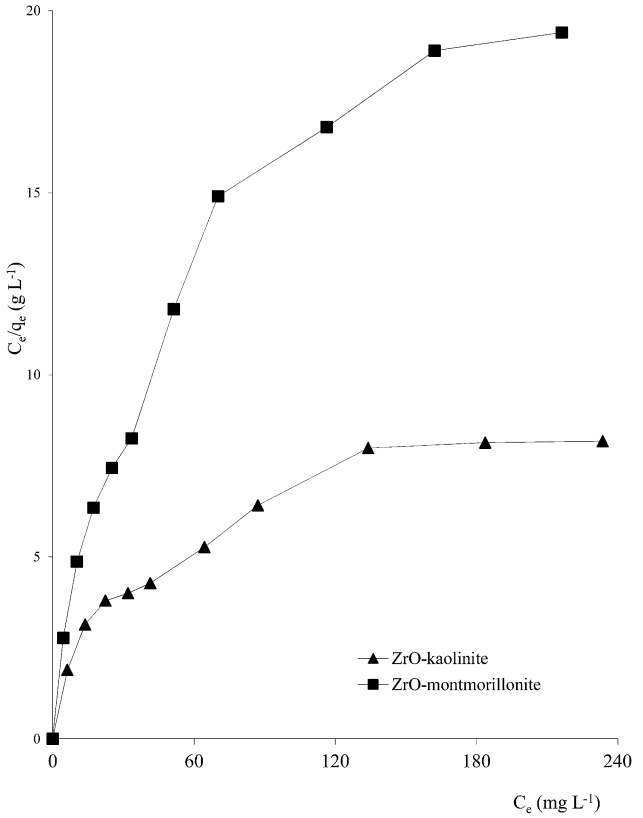

Fig. 6 Plots of q_e *vs.* C_e for Fe(III) adsorption on clay minerals (clay mineral 2.0 g L^{-1}, Fe(III) 10–250 mg L^{-1}, pH 3.0, time 300 min, temperature 303 K).

higher adsorption capacity of the natural montmorillonite was due to Cd(II) being more effectively adsorbed at the interlayer sites rather than inside the pores. Moreover, the CEC of pillared montmorillonite (64.5 mmol per 100 g) was ~33% lower than the unpillared montmorillonite (96.6 mmol per 100 g).

Fe-montmorillonite had almost 4 times as large Freundlich capacity for Cd(II) (K_F: 16.9 L g^{-1}) than that of Ca-montmorillonite (parent clay, K_F: 3.90 L g^{-1}).[65] The higher value was correlated to large interlayer spacing in Fe-montmorillonite. Even when humic acid was used to modify Ca-montmorillonite, Freundlich adsorption capacity for Cd(II), Cu(II) and Cr(III) was higher than that of the raw clay, but the increase was now around 25% only.[66] Humic acid introduced multiple functional groups to the clay mineral while at the same time blocking some of the pores and therefore, the increase in adsorption capacity was much below the expected value.

2.1.3. Organo-functionalized clay. Poly(hydroxo aluminium)- and cetyltrimethyl-ammonium-modified montmorillonite had Freundlich capacity of 1.47×10^3 L mol^{-1} for Cr(III).[67]

The preferential removal of As(V) over As(III) was observed by Su *et al.*[68] with octadecyl benzyl dimethyl ammonium-modified bentonite as the adsorbent when the Freundlich capacity for As(V) was more than 4 times that for As(III). At pH < 9.0, the predominant form of As(III) in aqueous solution is H_3AsO_3 such that anion exchange could not be the mechanism for As(III) removal. Whatever As(III) is removed is through a physical adsorption process involving Si–O and Al–O groups at the edges of the particles.

A number of metal ions [Cd(II), Cr(VI), Ni(II), Pb(II)] was adsorbed on the clay minerals, kaolinite and montmorillonite, as well as on tetrabutylammonium (TBA)-kaolinite and TBA-montmorillonite[47,53,55,69] with the Freundlich capacities in a broad range of values (Cd(II): 0.32 to 2.21, Cr(VI): 0.9 to 1.1, Ni(II): 3.4 to 1.13, Pb(II): 0.37 to 1.36 $mg^{1-1/n}$ $L^{1/n}$ g^{-1}). As already pointed out, introduction of TBA might have blocked the pores leaving no scope for increasing the adsorption capacities (Fig. 1–3). The modified clays had lower CEC than the respective parent clays (kaolinite: 11.3 mmol per 100 g, TBA-kaolinite: mmol per 100 g, montmorillonite: 153.0 mmol per 100 g, TBA-montmorillonite: mmol per 100 g).

Bentonite with 8-hydroxy quinoline immobilized on its surface had Freundlich capacity for Cu(II)[70] of 34.78 to 41.16 L g^{-1} and for Pb(II)[71] of 58.73 to 91.91 L g^{-1} in the temperature range, 293 to 323 K. The FTIR intensities of C–C and C–N ring stretching vibrations were shown to increase after adsorption of Cu(II) or Pb(II). Another material obtained by immobilizing 2,2′-dipyridyl on bentonite gave K_F for Cu(II) adsorption of 11.20 to 30.02 L g^{-1} in the temperature interval, 293 to 323 K (n 0.127 to 0.281).[72] C–C and C–N ring stretching (skeletal) FTIR bands were observed after Cu(II) adsorption.

Dodecylamine modified sodium montmorillonite yielded a Cr(VI) Freundlich capacity[73] of 3.27 $mg^{1-1/n}$ g^{-1} $L^{1/n}$. The negatively charged hydrogentetraoxochromate ($HCrO_4^-$) and the protonated dodecylamine could have interacted *via* an electrostatic force of attraction in the clay matrix.

Carvalho *et al.*[74] reported Freundlich capacities for adsorption of Ni(II) from water on montmorillonite K10 and modified montmorillonite K10 (modified with 3-mercaptopropyltrimethoxysilane) as 1.00 and 0.41 $mg^{1-1/n}$ $L^{1/n}$ g^{-1} respectively at 298 K.

Şölener *et al.*[75] measured K_F of clay–poly(methoxyethyl) acrylamide composite for Pb(II) from 3.30×10^{-3} L g^{-1} (293 K) to 3.75×10^{-3} L g^{-1} (313 K) which decreased to 3.23×10^{-3} L g^{-1} (at 323 K). The interactions occurred through olefinic double bond, carbonyl and amine groups, *etc.*

In adsorption of Cr(VI) on tannin-immobilized activated clay,[76] K_F increased from 2.41 to 3.11 L g^{-1} when the solution temperature was increased from 300 to 330 K. It was suggested that Cr(VI) anions were partly reduced to Cr(III) which were adsorbed as cations.

Adsorption capacity of sepiolite was boosted after acid activation and surface functionalization with mercaptosilane with respect to Cr(VI) uptake.[77] The modified sepiolite had higher content of silanol groups, which resulted in a higher adsorption capacity. The same group of workers[78] reported Cr(VI) adsorption from water on natural and acid-activated sepiolites, functionalized by covalent grafting [3-(2-aminoethylamino)propyl] trimethoxy-silane from water. The Freundlich capacities were 2.042 and 2.845 $mg^{1-1/n}$ g^{-1} $L^{1/n}$ respectively. The electrostatic attraction of anionic Cr(VI) species by protonated amine groups and the formation of hydrogen bonds between the CrO_4^{2-} species and the non-protonated amine groups were possible mechanisms of metal ion removal at pH 2.0. Adsorption of Pb(II)

on mercapto functionalized sepiolite was facilitated by the formation of bidentate complexation with mercapto groups besides monodentate complexation, as suggested by Liang *et al.*[79] The increase of reaction temperature from 289.15 to 318.15 K boosted the Freundlich capacity from 21.89 ± 1.97 to 33.73 ± 1.28 mg g^{-1}.

2.1.4. Zeolites. A hybrid mesoporous aluminosilicate sieve (prepared with fly ash and impregnated with zeolite A precursors) had Hg(II) Freundlich capacity[80] of 18.95 mg g^{-1} and it was suggested that electrostatic interaction and ion-exchange were the key factors controlling adsorption.

Freundlich capacity of natural zeolite (clinoptilolite) for Fe(III) was higher (0.376 mg g^{-1}) compared to Zn(II) (0.015 mg g^{-1}) and Mn(II) (0.035 mg g^{-1}).[81] The surface charge imbalance created by substitution of Si^{4+} by Al^{3+} was balanced by exchangeable cations. Similarly, natural zeolitic volcanic tuff yielded Freundlich capacities of 2.88, 2.50 and 2.07 mg g^{-1} for 293, 313 and 333 K respectively for Pb(II) adsorption.[82]

In another work, natural zeolite showed higher Freundlich capacity for Pb(II) (K_F: 59.56 L mg^{-1}) than for Cu(II) (K_F: 9.08 L mg^{-1}) at 303 K.[83]

NaA and NaX zeolites contain mineral impurities in the form of Ca, Mg, Fe and K and when these materials are used as adsorbents for Zn(II), the impurities interfere in the exchange of Zn(II) with Na(I).[84] NaA and NaX have small particles size and higher internal surface area allowing Zn(II) cations to access and diffuse into the framework structure. This has resulted in high K_F of 85.54 and 77.24 L g^{-1} respectively for NaA and NaX.

Argun[85] reported decrease in K_F of clinoptilolite for Ni(II) adsorption from 0.68 to 0.53 mg g^{-1} when the temperature changed from 293 to 333 K.

Aluminium-loaded Shirasu-zeolite (Al-SZP) had a reasonable Freundlich capacity of 0.122 mmol g^{-1} for As(V) and adsorption intensity of 0.13.[86] The adsorption capacity of the material was better than activated alumina. The adsorption of As(V) onto Al-SZP proceeded from the formation of aluminum hydroxide on the surface, followed by the replacement of the hydroxide anion by As(V) in aqueous media.

Ni(II) adsorption by both ion-exchange and complexation processes on dimethylglyoxime treated clinoptilolite yielded Freundlich capacities in the range of 0.138 to 0.114 L g^{-1} (temperature 293 to 333 K).[87]

Adsorption of Cu(II) on humic acid immobilized-cetylpyridinium bromide-modified zeolite[88] followed ion exchange in the internal zeolite channels.

Freundlich capacity for Cd(II) removal on zeolite-based geopolymer (synthesized from coal fly ash)[89] was 6.603 L g^{-1}. The adsorbent was fully coated with hydroxyl compounds that penetrated into the porous network structure that played a role in the adsorption process.

Three different minerals, vermiculite, zeolite and pumice were used for adsorption of Cd(II) from water.[90] K_F had values of 0.69, 0.65 and 0.55 L g^{-1} for vermiculite, zeolite, and pumice respectively. Increasing amount of adsorption was shown to modify the adsorbent characteristics making chemical interactions as the dominant process. Zeolite and vermiculite adsorbed Cd(II) to a larger extent compared to pumice in line with the CEC values of the materials (CEC 170 mmol per 100 g, 100 mmol per 100 g and 30 mmol per 100 g for zeolite, vermiculite and pumice, respectively) and the adsorption percentage was higher at the lowest Cd(II) concentration.

2.1.5. Oxides and modified oxides. Different oxides had been used for metal uptake. Freundlich capacity of $ZrO_2 \cdot nH_2O$ for Cr(VI) decreased from 7.05 to 4.94 mg g^{-1} in the temperature range of 298 to 338 K.[91] The larger specific surface area of the material makes it a good adsorbent for Cr(VI).

In a comparative study, Sheela *et al.*[92] found that nano ZnO had Freundlich capacity in the order of Zn(II) (K_F: 2.234 mg g^{-1}), Cd(II) (11.77 mg g^{-1}) and Hg(II) (17.32 mg g^{-1}). It was suggested that, during the possible ion exchange process, metal cations moved through either the pores of ZnO mass or through channels of the crystal lattice. Moreover they might replace exchangeable cations, mainly surface hydroxyl groups. The interaction between nano ZnO and Pb(II) yielded Freundlich capacity of 0.152 mg g^{-1}, the larger surface area of the adsorbent might play some role in the uptake process.[93]

NiO nanoparticles had a preferential uptake of Pb(II) (K_F: 34.45 mg g^{-1}) over Cd(II) (K_F: 6.61 mg g^{-1}) attributed to lower pH of hydrolysis of Pb(II).[94]

With Al_2O_3 as the adsorbent,[95] Cd(II) cations were shown to bind to the surface through specific adsorption on (Al–OH), resulting in the formation of monodenate or bidenate complexes with Al–O^-. Freundlich capacities for Cd(II), Pb(II) and Zn(II) adsorption on hydrous MnO_2 were 1.38, 1.63 and 1.00 $mmol^{1-n}$ L^n g^{-1} respectively at 298 K.[96] An ion-exchange mechanism was proposed in which release of H^+ was accompanied by Cd(II) and Pb(II) uptake.

Chen *et al.*[97] found that the Freundlich capacities of Cd(II) adsorption on nano TiO_2 and humic acid-modified TiO_2 were influenced by solution pH [pH 5.0: K_F (5.22 ± 0.8) × 10^{-2} $\mu g^{1-1/n}$ $L^{1/n}$ g^{-1} for TiO_2 and (5.73 ± 0.8) × 10^{-2} $\mu g^{1-1/n}$ $L^{1/n}$ g^{-1} for HA–TiO_2; pH 7.0: (7.31 ± 2.5) × 10^{-2} $\mu g^{1-1/n}$ $L^{1/n}$ g^{-1} and (5.33 ± 2.5) × 10^{-2} $\mu g^{1-1/n}$ $L^{1/n}$ g^{-1} for TiO_2 and HA–TiO_2 respectively and at pH 9.0: (4.09 ± 0.6) × 10^{-2} $\mu g^{1-1/n}$ $L^{1/n}$ g^{-1} and (9.90 ± 2.77) × 10^{-2} $\mu g^{1-1/n}$ $L^{1/n}$ g^{-1} for TiO_2 and HA–TiO_2 respectively]. The humic acid modification increased the adsorption capacity due to smaller aggregation sizes and better dispersion of nano particles in the presence of HA. Aliphatic chains constitute the basic structure for HA fractions on modified TiO_2, and they might form net, stretch, or spongy structures below pH 7.0, but condensed at pH > 7.0. Therefore, with increasing pH, the number of available adsorption sites for Cd(II) increase. The adsorption ability of modified TiO_2 was stronger than that of the unmodified TiO_2 in weak acid and weak base solutions. It was suggested that the surface charges of HA–TiO_2 might change quickly than those of TiO_2 at pH 7 giving a lower Freundlich capacity for HA–TiO_2 than TiO_2.

Pb(II) adsorbed on nano TiO_2–SiO_2 with Freundlich capacities of 1.18 to 2.46 $mol^{1-1/n}$ $L^{1/n}$ g^{-1} in the temperature range of 298 to 308 K and decreased to 0.13 $mol^{1-1/n}$ $L^{1/n}$ g^{-1} at 325 K.[98] It was proposed that Pb(II) bonded with TiO_2–SiO_2 surface *via* surface oxygen atoms and proton release.

Liu *et al.*[99] used titanate nanotubes for removal of a few metal ions with Freundlich capacities of 1.22 mmol g^{-1} (Pb(II)),

0.92 mmol g^{-1} (Cd(II)), 0.88 mmol g^{-1} (Cu(II)) and 0.87 mmol g^{-1} (Cr(III)). It was suggested that adsorption of metal ions by the adsorbent could be possible by –OH and –ONa located in titanate interlaminations. The adsorption mechanism followed ion-exchange between H^+/Na^+ and metal ions.

Freundlich capacity for Se(IV) adsorption on iron oxide was more than that on silicon oxide.[100] K_F decreased from 1.09 to 0.34 $mg^{1-1/n}\ L^{1/n}\ mg^{-1}$ and 0.90 to 0.46 $mg^{1-1/n}\ L^{1/n}\ mg^{-1}$ for iron oxide and silicon oxide respectively (at 303 to 323 K). Se(IV) binding to the oxides were through electrostatic and inner-sphere complexation. Several inner-sphere complexes could be formed at the surface of ferric oxide: monodentate (≡S–O–Se(O)OH, ≡S–O–Se(O)O^- or ≡S–O–Se(O−)$_2$OH), bidentate (≡S–O)$_2$–SeO and tridentate (≡S–O)$_3$–SeOH.

Freundlich capacity of Fe_3O_4 nanoadsorbents for Pb(II) removal[101] was in the range of 0.13 to 0.17 $mmol^{1-1/n}\ L^{1/n}\ mol^{-1}$ with increasing temperature (298 to 328 K) and endothermic interactions. As(V) anions as $H_2AsO_4^-$ were shown to have bound to Fe_3O_4 nanoparticles on positive charge sites of the surface yielding a Freundlich capacity of 1.238 $\mu g^{1-1/n}\ g^{-1/n}\ L^{1/n}$.[102]

Al_2O_3-supported iron oxide yielded Freundlich capacity of 6.15 to 11.15 for Pb(II) in the temperature range, 288 to 318 K.[103] The solid surface was shown to contain α-FeOOH that bound Pb(II).

Bimetallic nano-oxides, such as $MnFe_2O_4$ and $CoFe_2O_4$, had Freundlich adsorption capacities almost twice that of Fe_3O_4 for As(III) ($MnFe_2O_4$–As(III): 29.6 $mg^{1-1/n}\ L^{1/n}\ g^{-1}$, $CoFe_2O_4$–As(III): 36.9 $mg^{1-1/n}\ L^{1/n}\ g^{-1}$, Fe_3O_4–As(III): 15.9 $mg^{1-1/n}\ L^{1/n}\ g^{-1}$).[104] The O1s binding energies from XPS measurements were used to suggest that higher adsorption capacities of the bimetallic oxides for As(III) and As(V) compared to Fe_3O_4 were due to increase in the number of surface hydroxyl species.

Zhang *et al.*,[105] while using Ce doped Fe-oxide as an adsorbent for As(V), considered the surface as amphoteric with the presence of surface hydroxyl groups (M–OH). Higher As(V) removal at pH > 5.8 was suggested as due to specific adsorption of As(V) anions. The same group of authors[106] latter prepared a series of nanosized hydrated ferric oxide (HFO)-loaded polymeric hybrid adsorbents and showed that Freundlich adsorption capacity for As(V) was mainly dependent upon HFO loadings. Adsorbents with low HFO loadings exhibited better performance at relatively low solute levels, while those with higher HFO loadings displayed higher adsorption capacities at higher solute levels. However, large HFO loadings resulted in a dramatic decrease in As(VI) adsorption arising from blocking of the pores and difficult accessibility of the active sites.

Fe_3O_4 nanoparticles modified with 3-aminopropyltriethoxysilane and glutaraldehyde adsorbed Cu(II) from aqueous system[107] with Freundlich capacity of 14.544 $mmol^{1-1/n}\ L^{1/n}\ g^{-1}$.

Fe_3O_4 modified with cetyltrimethylammonium bromide was shown to possess higher uptake capacity for As(V) compared to pure Fe_3O_4.[108] CTA^+ present on the surface of Fe_3O_4 held As(V) anions forming CTA–As(V) complex.

Carboxymethyl-β-cyclodextrin polymer modified Fe_3O_4 nanoparticles had Freundlich capacities of 13.44 to 25.82 L g^{-1} for Pb(II), 0.426 to 17.64 L g^{-1} for Cd(II) and 0.755 to 2.39 L g^{-1} for Ni(II) at 298 K.[109] The polymer grafted on nanoparticles enhanced the adsorption capacity because of the complexing abilities of the multiple –OH and –COOH groups in polymer with metal cations. In a similar work, Tan *et al.*[110] used amino-functionalized Fe_3O_4 magnetic nano-particles for Pb(II) removal with Freundlich capacity 21.9 L g^{-1}.

Freundlich adsorption capacity for Cd(II) and Pb(II) on activated alumina was 4.34 and 3.82 $mg^{1-1/n}\ L^{1/n}\ g^{-1}$ respectively at 303 K.[111] A mechanism based on ion exchange inside the micropores was proposed in which the metal ions entered the pores and also the channels of the lattice where they replaced the exchangeable cations. Pore diffusion was fast and was retarded only when the cations had to move through the smaller channels.

Freundlich capacity was slightly greater for protonated mesoporous alumina compared to aminated alumina for Cu(II) while the reverse was true in case of adsorption intensity (0.48 and 0.53) at 298 K.[112] Cu(II) ions were exchanged for aminated and protonated groups of compounds present in the material.

Large surface area of goethite ensured comparatively large Freundlich capacities of 2.140 and 2.227 L g^{-1}, respectively for adsorption of Cd(II) and Cu(II).[113]

Granados-Correa *et al.*[114] measured Cd(II) K_F of 0.11 and 0.07 $mg^{1-1/n}\ L^{1/n}\ g^{-1}$ respectively for bohemite and goethite. Bohemite has higher surface area and larger number of functional groups than goethite, which explains the higher uptake. Cd(II) was proposed as having directed chemical bond to the surface, implying a specific adsorption mechanism.

Manu *et al.*[115] used three different functionalized silica samples (prepared with 3-aminopropyltrimethoxysilane (APTMS)) with different APTMS : silica ratio (w/w) to adsorb Cu(II) from water. K_F increased from 1.416 to 17.132 $mg^{1-1/n}\ L^{1/n}\ g^{-1}$ with increasing APTMA : silica ratio. Increase in the concentration of amino groups on the surface of silica resulted in an increase in affinity for Cu(II).

Freundlich adsorption capacity on amino functionalized mesoporous silica (NH_2-MCM-41) followed the order Cd(II) > Ni(II) > Pb(II) at 298 K.[116] Introduction of amine groups into MCM-41 gave much higher adsorption capacity for Ni(II) and Cd(II). The metal cations were bound to the surface *via* N-atoms of primary amine groups through complex formation. In a similar work, it was found that thiol-functionalized silica adsorbed Cd(II) and Pb(II) with Freundlich capacity of 25.65 ± 1.43 and 63.99 ± 3.92 L mg^{-1} respectively at 298 K.117 In this case, cation binding involved two or more –SH groups. Both monodentate and bidentate complexation with thiol groups was proposed.

2.1.6. Other inorganic solids. Tannin-immobilized calcined hydrotalcite had higher Freundlich capacity for Cu(II) than for Zn(II) and Cd(II).[118] Cu(II) with smaller ionic radius was shown to diffuse rapidly into the pores leading to its higher uptake.

Surface –OH groups in Mg_2Al layered double hydroxides were responsible for large K_F of 19.76 to 30.91 $mg^{1-1/n}\ L^n\ g^{-1}$ for Pb(II) in the temperature range of 303.15 to 343.15 K.[119]

Nano hydroxyapatite had a large Freundlich capacity for Pb(II) (282.308 mg g^{-1}) compared to that for Cd(II) (122.854 mg g^{-1}) and Ni(II) (9.806 mg g^{-1}).[120] The preferred adsorption of

Pb(II) was justified on the basis of smaller hydrated radius of Pb(II). Synthetic hydroxyapatite also had a large Pb(II) Freundlich capacity (K_F: 0.487 L mmol^{-1}) compared to that of natural apatite (K_F: 0.131 L mmol^{-1}).[121]

Tourmaline (a natural hydrous silicate of CEC, 384 mmol per 100 g) was shown to bind Pb(II) through surface electropolar forces[122] arising from electric dipoles on the surface and yielded K_F of 0.53 L mg^{-1}.

Wang *et al.*[123] showed that K_F values of loess soil for Cd(II) increased from 3.80 to 4.87 mg g^{-1} in the temperature range, 278 to 318 K and Cd(II) ions were held to soil surface by formation of $CdSiO_3$ with aluminium silicate minerals. The Freundlich intensity factor, n, was very small (n = 0.14 to 0.20) indicating largely heterogeneous energy distribution in the soil surface. The CEC of the loess soil was 11.2 mmol per 100 g, but influence of temperature on CEC was not indicated.

Cr(VI) and Pb(II) adsorption was suggested to have occurred through hydroxyl groups on the surface and edges of soil particles on a loamy sandy soil with Freundlich capacity of 1078.0 and 387.1 L$^{1/n}$ mg kg^{-1} mg$^{-1/n}$ respectively.[124]

Ahmed *et al.*[125] used river sand for Pb(II) adsorption with Freundlich capacity and intensity of 15.4 ± 6.9 mmol g^{-1} and 0.71 ± 0.01, respectively (adsorbent 100 mg, stirring speed 700 rpm, temperature 298 ± 2 K). A similar investigation was reported where beach sand was used as adsorbent for Pb(II)[126] with K_F of 0.28 ± 0.19 mmol g^{-1} (n= 0.39 ± 0.09) to 5.10 ± 1.28 mmol g^{-1} (n= 0.67 ± 0.06) at 293 to 323 K. Beach sand was also used for Zn(II) removal (K_F: 0.49 ± 0.05 mmol g^{-1}).[127] The sand contained calcite, quartz and aragonite as the main constituents. The presence of negative sites in these minerals in the form of carbonates and oxides provided affinity for the positively charged metal ions in aqueous solutions. Iron-oxide nanoparticle-immobilized sand was used for removal of Cd(II), Cu(II) and Pb(II) with Freundlich capacities of 0.18, 0.49 and 0.78 mg g^{-1} respectively.[128] It was suggested that Cu(II) adsorption followed ion-exchange as well as inner-sphere surface complexation, while Cd(II) and Pb(II) were held through ion-exchange and electrostatic attraction. Exothermic adsorption of Cr(VI) on acid activated river sand had Freundlich capacity of 0.17 to 0.10 mg g^{-1} in the temperature range of 298 to 308 K.[129]

Hydroxyapatite–chitosan composite preferentially adsorbed Pb(II) (4.039 mg$^{1-1/n}$ L$^{1/n}$ g^{-1}) compared to Co(II) (2.619 mg$^{1-1/n}$ L$^{1/n}$ g^{-1}) and Ni(II) (1.577 mg$^{1-1/n}$ L$^{1/n}$ g^{-1}). The presence of amino and hydroxyl groups in chitosan served as the active sites for adsorption.[130]

Chitosan–clay–magnetite composites were used for Cu(II) and As(V) removal[131] with higher uptake for Cu(II) (K_F for Cu(II): 5.828 L g^{-1} and As(V): 0.282 L g^{-1}). The clay had a large surface area for incorporating nano-magnetite and chitosan while preventing particle agglomeration, and therefore, had better adsorption capacity.

Chitosan–attapulgite composites were shown to be a better adsorbent for Fe(III) (K_F: 7.40 to 13.77 mg g^{-1} at 298 to 318 K) than Cr(III) (K_F: 4.31 to 13.62 mg g^{-1} at 298 to 318 K).[132] The synergistic effect of broadened pores and electrostatic interactions between composites and the metal ions was suggested to have an important role.

The silico-antimonate ion exchanger had K_F of 0.79, 0.44, 0.93 and 0.47 0.44 mmol g^{-1} respectively for Cd(II), Cu(II), Ni(II) and Zn(II) from water (adsorbent 10.0 g L^{-1}, metal ions 5 × 10^{-2} to 10^{-4} M, pH 2.0, 298 K).[133] The interactions were essentially those between a Lewis base and a Lewis acid. The interactions of the metal ions with the hydrated Si(IV) antimonate, increased with an increase in the ionic radii and the order of selectivity for the metal ions was Ni(II) > Cd(II) > Zn(II) > Cu(II). When Fe(III)–titanate ion exchanger was used for Cd(II) and Zn(II) adsorption,[134] Freundlich capacities were 3.98 × 10^{-3} and 7.97 × 10^{-3} mol$^{1-1/n}$ L$^{1/n}$ g^{-1} respectively at 298 K. The small radius of dehydrated Zn(II) increased the mobility and the packing density of Zn(II) compared to Cd(II), facilitating the greater uptake of Zn(II).

Co(II) adsorption on two ion exchange resins (IRN77 and SKN1) had Freundlich capacities of 75.63 and 60.03 mg g^{-1}.[135]

Shaaban *et al.*[136] reported that Hg(II) (1.158 mmol L^{-1}) was more preferably removed by dithiocarbamate chelating resin in comparison to Cd(II) (0.831 mmol L^{-1}) and Pb(II) (0.588 mmol L^{-1}). Through the study of surface morphology, it was observed that chelating resin before adsorption had least packed structure with many pores or cavities in the surface, which facilitated mass transfer of metal ions to the adsorbent.

Increase in K_F from 0.44 to1.09 and 0.57 to 1.82 L$^{1/n}$ g^{-1} mg$^{1-1/n}$ for Cu(II) and Pb(II) on electric furnace slag was observed in the temperature interval of 293 to 313 K.[137] The mixture of calcium-ferrite phases [$CaO \cdot Fe_2O_3$, $CaO \cdot 2Fe_2O_3$, $CaO \cdot 7Fe_2O_3$] and calcium-manganese-silicates phase [$(Ca, Mn)_2 \cdot SiO_4$, $CaO \cdot MgO \cdot SiO_2$] on the surface of the slag was suggested as being responsible for the cation uptake.

Activated red mud had a small K_F for As(III) of 0.37 L μmol^{-1} while the values for As(V) were 5.93 to 63.27 L μmol^{-1}.[138] The adsorbent was shown to have highly porous aggregates of much finer particles with large number of adsorption sites.

Gupta *et al.*[139] used a carbon slurry (fertilizer industry waste) for Cr(VI) uptake and reported K_F values in the range of 1.09 to 1.02 mg g^{-1}. The adsorbent contained constituents such as C (78.93%), O (19.41%), Al (1.16%) and F (0.49%). The organic content generally imparted porosity to the adsorbent. The large surface of the slurry enhanced the metal uptake capacity.

Freundlich capacity of Cd(II) on waste material from boron enrichment process was higher than Zn(II) removal (Cd(II): 1.75, Zn(II) 1.44 mg g^{-1}).[140] The authors reported that buexite ($NaCaB_5O_9 \cdot 8H_2O$) was the major phase of the adsorbent, where Ca was reduced significantly after adsorption of Cd(II) and Zn(II), suggesting ion exchange occurring between Ca^{2+} and Cd(II)/Zn(II).

2.2. Langmuir isotherm and its applications

Langmuir model[141] was originally developed to describe gas adsorption onto activated carbon. It is the most straightforward non-linear isotherm based on the assumptions that (i) the adsorbent surface has energetically uniform sites for adsorbate ions, atoms and molecules, (ii) no adsorbate–adsorbate interactions are present, (iii) the same mechanism is followed throughout the process, and (iii) at the maximum adsorption, the surface is covered with only a monolayer.

Langmuir model was derived by following mass action, kinetic, or statistical thermodynamic approaches. The isotherm refers to homogeneous adsorption, where each interacting molecule carries constant enthalpy and activation energy.[142] Moreover, it is assumed that no transmigration of the adsorbate in the plane of the surface occurs during the interaction process.[3,143]

Langmuir isotherm equation is based on evaluating the fractional surface coverage, θ

$$\theta = q_e/q_m = bC_e/(1 + bC_e) \quad (3)$$

where q_m is the quantity of adsorbate required to form a single monolayer on unit mass of the solid, popularly known as the Langmuir capacity, q_e is the amount adsorbed at equilibrium on unit mass of the solid, C_e is the concentration of gas or solute remaining unadsorbed at equilibrium, and b is Langmuir coefficient related to the adsorption equilibrium constant. Eqn (3) is usually written in the simplified form:

$$C_e/q_e = (1/bq_m) + (1/q_m)C_e \quad (4)$$

Plots of C_e/q_e *vs.* C_e are utilized to obtain the values of q_m and b.

Langmuir capacities provide a useful and convenient method to compare the adsorption capacities of similar or different types of solids. Because of the ease of application, almost every work on adsorption reports on Langmuir isotherm and the two coefficients, q_m and b. The Langmuir capacities for adsorption of metal ions on some inorganic adsorbents are given in Table 3. A selection of recent literature on application of Langmuir isotherm is discussed below.

2.2.1. Clays. Clay minerals have been used extensively as adsorbents in aqueous medium for removing a large number of different contaminants. One of the most common 1 : 1 layered minerals, kaolinite was shown to have Cr(III) adsorption capacity of 4.43×10^{-5} to 4.98×10^{-5} mol g^{-1} in the temperature range of 303 to 323 K and 4.40×10^{-5} to 5.83×10^{-5} mol g^{-1} when the ionic strength was varied from 1×10^{-3} to 1×10^{-1} mol L^{-1}.[28] The ionic strength influenced the coulombic interactions between the charged surface and the metal ions through a number of counter ions in the diffuse layer. This affected the charge development on the clay mineral surface and uptake of Cr(III) increased. Adsorption of Cr(III) and Pb(II) on Turkish kaolinite had Langmuir capacities of 21.55 and 18.08 mg g^{-1} respectively at 293 K.[31] Another Turkish kaolinite possessed q_m of 31.75 mg g^{-1} for Pb(II).[30]

For adsorption of a number of cations, Cd(II), Cr(III), Cu(II), Pb(II), Zn(II) and Ni(II) at 303 K, Chantawong *et al.*[27] measured the Langmuir capacity of Thai kaolin to be 6.71×10^{-3}, 3.49×10^{-2}, 12.00×10^{-3}, 3.18×10^{-3} and 2.79×10^{-2} mmol g^{-1}, and of ball clay to be 2.10×10^{-2}, 6.90×10^{-2}, 2.50×10^{-2}, 1.70×10^{-2}, 4.40×10^{-2} and 7.00×10^{-3} mmol g^{-1} respectively. Kaolin was shown to have a preference for Cr(III) than to the softer Lewis acids, Cu(II), Cd(II), Ni(II), Pb(II) and Zn(II). This indicated the main adsorption sites on kaolin to be having Lewis base characteristics. Ballclay, whose main constituent was illite (2 : 1 type) had excess negative charge due to isomorphous substitution in tetrahedral and octahedral sheets resulting in formation of outer-sphere complexes. The adsorption sites exhibited relatively hard Lewis base characteristics and had highest adsorption for Cr(III). In another work, Langmuir capacity of ball clay (SiO_2 53.70%, Al_2O_3 31.31%, moisture 10.03%) for Cd(II) was found to be 27.27 mg g^{-1}.[144] It was suggested that silanol [≡Si–OH, =Si–$(OH)_2$ and ≡S–$(OH)_3$] and alumina [≡Al–OH and =Al–$(OH)_2$] groups were involved in adsorption of Cd(II).

Zn(II) was shown to adsorb in the micropores of bentonite through an ion-exchange mechanism at pH 6.64 with a Langmuir capacity of 68.49 mg g^{-1} at 303 K.[35] On the other hand, natural bentonite had Langmuir capacity of 12.38 to 15.92, 6.78 to 16.86 and 15.67 to 17.07 mg g^{-1} respectively for Cu(II), Co(II) and Zn(II) in a pH range of 3.0 to 9.0 at 293 K.[34] The metal cations prefer to bind to the mineral surface at higher solution pH when the surface developed negative charge. In another work, bentonite was shown to have Cu(II) and Cd(II) Langmuir capacities of 12.5×10^{-2} and 6.80×10^{-2} mmol g^{-1} respectively at 303 K.[36] The reported adsorption capacities, however, have wide variance even for similar mineral. Thus, bentonite was shown to have a very large Langmuir capacity for Cu(II) of 909 mg g^{-1}.[145] It was proposed that Cu(II) had attached to bentonite *via* complexation with surface hydroxyl groups and predominantly by cation exchange at the negatively charged surface of the crystallites. Pb(II) Langmuir capacity on natural bentonite increased from 107.0 to 120.0 mg g^{-1} in the temperature range, 293 to 333 K.[146]

Langmuir capacity of Na-bentonite has been measured as 9.73×10^{-5} to 1.08×10^{-4} mol g^{-1} in the temperature range of 293.15 to 333.15 K for Cu(II)[37] adsorption by ion exchange with H^+/Na^+, 17.88 mg g^{-1} for Cd(II),[147] and 2.31×10^{-4} to 3.10×10^{-4} mol g^{-1} (298 to 338 K) for Pb(II).[38]

Brazilian bentonite (NT-25) had higher Langmuir capacity of 11.2 and 6.0 mg g^{-1} for Cd(II) and Mn(II) compared to K10 montmorillonite (Cd(II): 6.3 mg g^{-1}, Mn(II): 4.8 mg g^{-1}) at 298 K.[33] Cation-exchange with sites located on (001) basal planes of the clays was shown to be responsible for fast uptake of the cations leading to formation of inner-sphere surface complexes. Chinese bentonite had Langmuir capacity of 1.15×10^{-4} to 1.64×10^{-4} mol g^{-1} for Pb(II) at temperatures, 293.15 to 343.15 K.[32] The interactions were shown to be energy-intensive.

Veli and Alyüz[39] showed that higher ionic potential of Zn(II) was responsible for bentonite taking up twice as much Zn(II) (q_m: 80.64 mg g^{-1}) than Cu(II) (q_m: 44.84 mg g^{-1}).

Surface complexation between Cu(II) and negatively charged SiO^- and AlO^- on the edges of spent activated clay was shown to be mostly responsible for Cu(II) uptake (q_m: 10.9 to 13.2 mg g^{-1} for pH 5.0 to 6.0; q_m: 9.5 to 12.8 mg g^{-1} at 277 to 323 K).[148] In a similar work, Weng *et al.*[149] showed that spent activated clay had Cr(VI) Langmuir capacity of 0.74 to 0.59 mg g^{-1} (pH: 2.0 to 4.0), 0.74 to 1.42 mg g^{-1} (277 to 313 K) and 0.95 to 0.47 mg g^{-1} (ionic strength: 0.005 to 0.1 M). The adverse effect of ionic strength was due partly to the competition between ClO_4^- and $HCrO_4^-$ for $Si–OH^+$ and $Al–OH^+$ adsorption sites.

Langmuir capacity of calcined bentonite for Ni(II) increased from 2.875 to 3.893 mg g^{-1} in the temperature range of 293 to 348 K.[150]

Table 3 Langmuir capacities for adsorption of metal ions on some inorganic adsorbents

Metal cation/adsorbent	Experimental variables		Langmuir capacity (q_m)		Ref.
As(III)					
Octadecyl benzyl dimethyl ammonium modified bentonite	306 K		0.82	mg g^{-1}	68
Natural muscovite	293 K	As(III) 0–100 mg L^{-1}, pH 6.0	0.330	mg g^{-1}	43
Hematite		pH 7.3	$(9.3 \pm 0.2) \times 10^{-6}$	mol m^{-2}	211
Magnetite		pH 6.5	$(3.1 \pm 0.1) \times 10^{-6}$		
Goethite		pH 7.5	$(2.5 \pm 0.1) \times 10^{-6}$		
Fe modified beidellite	298 K	As(III) 250–5000 μg L^{-1}	789.9	μg g^{-1}	181
	308 K		808.4		
	318 K		834.0		
Fe–Ce modified zeolite	298 K		476.6		
	308 K		499.3		
	318 K		540.5		
Fe modified sepiolite	298 K		477.3		
	308 K		490.7		
	318 K		512.3		
$Fe(NO_3)_3$ modified zeolite		As(III) 0–70 μM	40.48	μmol L^{-1}	187
Polymetallic sea nodule		As(III) 0.2 mg L^{-1}	0.69	mg g^{-1}	222
		As(III) 0.15 mg L^{-1}	0.58		
		As(III) 0.1 mg L^{-1}	0.31		
$MnFe_2O_4$	293 K	pH 7.0	93.8	mg g^{-1}	104
$CoFe_2O_4$			100.3		
Fe_3O_4			49.8		
Sand	293 K	As(III) 100–800 μg L^{-1}, pH 7.5	5.63	μg g^{-1}	216
Iron oxide-coated sand			28.57		
Activated red mud	296 ± 1 K	As(III) 2.04–156.66 μM, pH 6.8 ± 0.1	7.22	mmol g^{-1}	138
As(V)					
Octadecyl benzyl dimethyl ammonium modified bentonite	306 K		1.48	mg g^{-1}	68
Natural muscovite	293 K	As(V) 0–100 mg L^{-1}, pH 6.0	0.791	mg g^{-1}	43
Laterite	305 K	As(V) 0.5–4 mg L^{-1}, pH 5.5	0.149	mg g^{-1}	208
		As(V) 4.0–20 mg L^{-1}, pH 5.5	0.306		
		As(V) 0.2–4 mg L^{-1}, pH 7.0	0.140		
		As(V) 4.0–20 mg L^{-1}, pH 7.0	0.240		
		As(V) 0.2–20 mg L^{-1}, pH 5.5	0.507		
	293 K	As(V) 0.5–4 mg L^{-1}, pH 7.0	0.130		
		As(V) 4.0–20 mg L^{-1}, pH 7.0	0.220		
	315 K	As(V) 0.5–5 mg L^{-1}, pH 5.5	0.238		
		As(V) 5.0–20 mg L^{-1}, pH 5.5	0.569		
		As(V) 0.5–4 mg L^{-1}, pH 7.0	0.156		
		As(V) 4.0–20 mg L^{-1}, pH 7.0	0.275		
		As(V) 0.5–20 mg L^{-1}, pH 5.5	0.565		
Hematite		pH 7.3	$(2.9 \pm 0.5) \times 10^{-5}$	mol m^{-2}	211
Magnetite		pH 6.5	$(3.8 \pm 0.2) \times 10^{-6}$		
Goethite		pH 7.5	$(3.0 \pm 0.2) \times 10^{-6}$		
Iron oxide-coated perlite	303 K	pH 6.5–7.0	0.39	mg g^{-1}	161
Fe modified beydellite	298 K	As(III) 250–5000 μg L^{-1}	794.3	μg g^{-1}	181
	308 K		817.6		
	318 K		841.0		
Fe–Ce modified zeolite	298 K		542.3		
	308 K		547.3		
	318 K		533.4		
Fe modified sepiolite	298 K		515.7		
	308 K		538.8		
	318 K		558.0		
Fe_3O_4			0.35	mmol g^{-1}	201
CeO_2			0.45		
Fe–Ce bimetal oxide			2.00		
$MnFe_2O_4$	293 K	pH 3.0	90.4	mg g^{-1}	104
$CoFe_2O_4$			73.8		
Fe_3O_4			44.1		
Ce(IV)-doped iron oxide	293 K		70.4	mg g^{-1}	105

Table 3 (*Contd.*)

Metal cation/adsorbent	Experimental variables		Langmuir capacity (q_m)		Ref.
Cetyltrimethylammonium bromide modified Fe_3O_4	293 K	As(v) 100 μg L^{-1} to 7 mg L^{-1}	13.21	mg g^{-1}	108
Phosphonic acid modified silica polyamine composite		pH 4.0	98.00	mg g^{-1}	191
		pH 6.0	55.00		
Chitosan–clay–magnetite composite	296 ± 2 K	pH 5.0	6.5	mg g^{-1}	178
LDH intercalated by Cl^-		As(VI) 0.02–1.0 mmol L^{-1}	322.58	mmol kg^{-1}	203
Gibbsite			51.55		
Polymetallic sea nodule		As(v) 0.24 mg L^{-1}	2.85	mg g^{-1}	222
		As(v) 0.16 mg L^{-1}	1.47		
		As(v) 0.1 mg L^{-1}	10.2		
Activated red mud	288 K	As(v) 5.74–182.57 μM, pH 7.0 ± 0.1	25.91	mmol g^{-1}	138
	293 K	As(v) 7.70–136.50 μM, pH 7.0 ± 0.1	28.90		
	296 ± 1 K	As(v) 2.0–151.87 μM, pH 7.0 ± 0.1	39.84		
	323 K	As(v) 6.91–152.18 μM, pH 7.0 ± 0.1	40.98		
	296 ± 1 K	As(v) 7.03–220.85 μM, pH 4.5 ± 0.1	102.00		
Cd(II)					
Kaolin	303 K		6.71×10^{-3}	mmol g^{-1}	27
Ball clay			2.10×10^{-2}		
Bentonite	303 K	Cd(II) 50–300 mg L^{-1}	6.80×10^{2}	mmol g^{-1}	36
Montmorillonite K 10	298 K		6.30	mg g^{-1}	33
Brazilian bentonite			11.20		
Acid-activated kaolinite	303 K	pH 5.5	11.70	mg g^{-1}	46
Acid-activated montmorillonite			33.20		
Sepiolite	293 ± 1 K		0.388	meq g^{-1}	151
Fe-montmorillonite	298 K	pH 5.0	25.70	mg g^{-1}	65
Phosphate-immobilized Zr-pillared bentonite		pH 6.0	50.07	mg g^{-1}	159
Montmorillonite	293 K		21.90	μM kg^{-1}	26
Hydroxy-Al interlayered montmorillonite			2.50		
Na^+-montmorillonite		pH 6.5	0.125	mmol kg^{-1}	64
Acid-activated Na^+-montmorillonite			0.139		
Al_{13}-pillared acid-activated Na^+-montmorillonite			0.163		
Bentonite	293 K	pH 5.0	61.35	mg g^{-1}	61
Bentonite/iron oxides (5 : 1 at 20 °C)			63.29		
Bentonite/iron oxides (1 : 1 at 85 °C)			48.78		
Fe-pillared bentonite		Cd(II) 0.178–5.34 mmol L^{-1}	0.773	mmol g^{-1}	63
Fe/Cr-pillared bentonite			0.633		
Cr-pillared bentonite			0.423		
Montmorillonite	298 K	pH 5.0	11.868	mg g^{-1}	66
Humic acid modified Ca-montmorillonite			14.148		
Montmorillonite	295 K	pH 5.0	8.06	mg g^{-1}	163
Sodium dodecyl sulphate-montmorillonite			11.67		
Hydroxy-alumino-silicate-montmorillonite			14.36		
Kaolinite	303 K	pH 5.5	6.78	mg g^{-1}	47
ZrO-kaolinite			5.27		
TBA-kaolinite			6.31		
Montmorillonite			30.67		
ZrO-montmorillonite			36.63		
TBA-montmorillonite			43.47		
Bentonite	303 K	pH 6.02	7.73	mg g^{-1}	58
	323 K		11.26		
Bentonite + goethite	303 K		9.56		
	323 K		12.34		
Bentonite + humic acid	303 K		9.90		
	323 K		15.92		
Bentonite + geothite + humic acid	303 K		10.09		
	323 K		16.00		
Vermiculite	298 K	Cd(II) 0–500 μM	143.00	μmol g^{-1}	90
Zeolite			118.00		
Pumice			47.00		
Natural muscovite	293 K	Cd(II) 0–100 mg L^{-1}, pH 6.0	0.750	mg g^{-1}	43

Table 3 (*Contd.*)

Metal cation/adsorbent	Experimental variables		Langmuir capacity (q_m)		Ref.
Phosphate	298 ± 1 K		7.54	mg g^{-1}	209
Ca-deficient hydroxyapatite		Cd(II) 10–30 mg L^{-1}	23.04	mg g^{-1}	177
N-2-Hydroxypropyl trimethyl ammonium chloride chitosan modified bentonite	293 K		22.23	mg g^{-1}	169
Zeolite-based geopolymer	—	—	26.246	mg g^{-1}	89
Tannin immobilised calcined hydrotalcite	303 K	pH 6.0	78.9	mg g^{-1}	118
	313 K		81.9		
	323 K		91.5		
	333 K		101.7		
Mixed oxide [0.5 M SiO_2–0.5 M $Fe(OH)_3$]	303 K	pH 5.0	9.81×10^{-2}	mmol g^{-1}	199
	313 K		10.23×10^{-2}		
	323 K		10.64×10^{-2}		
SiO_2	288 K	Cd(II) 8.89×10^{-2} to 88.9×10^{-2} mmol L^{-1}	0.033	mmol g^{-1}	198
	298 K		0.036		
	308 K		0.039		
	318 K		0.043		
$Fe(OH)_3$	288 K		0.086		
	298 K		0.089		
	308 K		0.091		
	318 K		0.094		
Mixed oxide [0.5 M SiO_2–0.5 M $Fe(OH)_3$]	288 K		0.101		
	298 K		0.103		
	308 K		0.107		
	318 K		0.112		
Thiol-functionalized silica	298 K	Cd(II) 20–250 mg L^{-1}	33.72 ± 1.23	mg g^{-1}	117
Amino functionalized MCM-41		Cd(II) 10–70 mg L^{-1}	18.25	mg g^{-1}	116
Poly(ethyleneimine)–silica gel		pH 5.0–6.0	38.46	mg g^{-1}	192
Glutaraldehyde crosslinked poly(ethyleneimine)–silica gel			29.26		
Nano zerovalent iron	285 K	Cd(II) 25–450 mg L^{-1}	714.3	mg g^{-1}	218
	297 K		769.2		
	307 K		714.3		
Boehmite (γ-AlOOH)	298 K	Cd(II) 50 mg L^{-1}, pH 6.0	3.552	mg g^{-1}	114
Goethite (γ-FeOOH)			5.276		
Iron oxide-immobilized sand	298 ± 1 K		0.528	mg g^{-1}	128
Loess soils	278 K	Cd(II) 25–150 mg L^{-1}	6.68	mg g^{-1}	123
	288 K		7.03		
	298 K		8.17		
	308 K		8.90		
	318 K		9.37		
Hydrous MnO_2	298 K	pH 3.5–4.0	12.49	mmol g^{-1}	96
NiO	303 K	Cd(II) 100–600 mg L^{-1}	625.0	mg g^{-1}	94
Al_2O_3	303 K	pH 6.7	89.28	mg g^{-1}	95
Activated alumina	303 K	pH 5.0	35.06	mg g^{-1}	111
Titanate nanotube	298 ± 1 K	Cd(II) 0.1–3.0 mmol L^{-1}	2.13	mmol g^{-1}	99
Fly ash	303 K		1.24	mg g^{-1}	231
	313 K		1.64		
	323 K		2.00		
Vanadium mine tailing	303 K		3.52	mg g^{-1}	223
	313 K		4.49		
	323 K		8.83		
Clarified sludge	303 ± 0.5 K	pH 5.0	36.23	mg g^{-1}	240
Dithiocarbamate chelating resin	298 K	Cd(II) 1–25 mmol L^{-1}	2.15	mmol g^{-1}	136
Co(II)					
Kaolinite	303 K	pH 5.8	11.2	mg g^{-1}	50
Acid-activated kaolinite			12.1		
Montmorillonite			28.6		
Acid-activated montmorillonite			29.7		
Bentonite	293 K	pH 3.0	6.775	mg g^{-1}	34
		pH 5.0	8.467		
		pH 7.0	9.911		
		pH 9.0	16.863		

Table 3 (*Contd.*)

Metal cation/adsorbent	Experimental variables		Langmuir capacity (q_m)		Ref.
HCl/NaOH-treated bentonite	295 ± 1 K	Co(II) 20–200 mg L^{-1}	138.17	mg g^{-1}	45
Phosphate-immobilized Zr-pillared bentonite		pH 6.0	47.81	mg g^{-1}	159
Humic acid-immobilized-amine modified polyacrylamide–bentonite composite	303 K	pH 8.0	106.21	mg g^{-1}	168
Smectite	298 ± 1 K	pH 5.0	$(13.9 \pm 0.1) \times 10^3$	mmol g^{-1}	167
Aluminum pillared/3-mercap-topropyltrimethoxysilane organofunctionalized smectite			$(23.8 \pm 0.1) \times 10^3$		
Zirconium pillared/3-mercap-topropyltrimethoxysilane organofunctionalized smectites			$(25.8 \pm 0.2) \times 10^3$		
ZrO-kaolinite	303 K	Co(II) 10–250 mg L^{-1}, pH 5.7	9.0	mg g^{-1}	49
ZrO-montmorillonite			22.3		
TBA-kaolinite	303 K	Co(II) 10–250 mg L^{-1}, pH 5.7	8.4	mg g^{-1}	164
TBA-montmorillonite			19.7		
NiO	303 K	pH 7.5	8.13×10^{-5}	mol g^{-1}	195
	308 K		8.48×10^{-5}		
	313 K		8.69×10^{-5}		
	323 K		8.93×10^{-5}		
	303 ± 1 K	pH 7.0	6.41×10^{-5}		
		pH 7.5	8.13×10^{-5}		
		pH 8.0	11.27×10^{-5}		
		pH 8.5	17.61×10^{-5}		
$Mg(OH)_2$	298 K	Co(II) 3–135 mg L^{-1}	95.24	mg g^{-1}	196
	308 K		117.65		
	318 K		125.00		
Clinoptilolite	303 K	Co(II) 100–400 mg L^{-1}	244.13	mg g^{-1}	182
Cancrinite-type zeolite	298 ± 2.1 K		1.532	mmol g^{-1}	185
Ion exchange resins IRN77	298 ± 1 K		86.17	mg g^{-1}	135
SKN1			69.44		
Cr(III)					
Kaolinite	303 K	pH 5.5, ionic strength 1×10^{-3}	4.40×10^{-5}	mol g^{-1}	28
			4.47×10^{-5}		
			4.98×10^{-5}		
	313 K	pH 5.5, ionic strength 1×10^{-3}	4.40×10^{-5}		
	323 K				
	303 K				
		pH 5.5, ionic strength 1×10^{-2}	4.51×10^{-5}		
		pH 5.5, ionic strength 1×10^{-1}	5.83×10^{-5}		
	303 K	pH 4.5	3.86×10^{-5}		
		pH 5.0	4.09×10^{-5}		
		pH 5.5	6.62×10^{-5}		
		pH 6.0	4.34×10^{-5}		
Turkish kaolinite	293 K	pH 6.0	21.55	mg g^{-1}	31
Kaolin	303 K		3.49×10^{-2}	mmol g^{-1}	27
Ball clay			6.90×10^{-2}		
Montmorillonite	295 K	pH 5.0	11.00	mg g^{-1}	163
Sodium dodecyl sulphate-montmorillonite			13.28		
Hydroxy-alumino-silicate-montmorillonite			14.83		
Montmorillonite	298 K	pH 5.0	12.443	mg g^{-1}	66
Humic acid modified Ca-montmorillonite			15.657		
Al-/cetyl trimethyl ammonium-modified montmorillonite			2.28×10^4	mol g^{-1}	67
Ca-montmorillonite	298 K	pH 5.0	12.443	mg g^{-1}	65
Humic acid modified Ca-montmorillonite			15.657		
Vermiculite	298 K	Adsorbent 1.25 g L^{-1}	46.95	mg g^{-1}	153
Sepiolite	293 ± 1 K	Adsorbent 2.5–25 g L^{-1}	0.534	meq g^{-1}	151
Chitosan–attapulgite composites	298 K		27.03	mg g^{-1}	132
	308 K		46.08		
	318 K		65.36		

Table 3 (*Contd.*)

Metal cation/adsorbent	Experimental variables		Langmuir capacity (q_m)		Ref.
Hydrous TiO_2	288 K	pH 5.0	14.03	mg g^{-1}	255
	303 K		17.73		
	318 K		17.45		
Titanate nanotube	298 ± 1 K	Cr(III) 0.1–3.0 mmol L^{-1}	1.37	mmol g^{-1}	80
Vanadium mine tailing	303 K		16.23	mg g^{-1}	223
	313 K		19.33		
	323 K		28.27		
Bagasse fly ash	303 K		4.35	mg g^{-1}	229
	313 K		4.30		
	323 K		4.25		
Cr(VI)					
Turkish vermiculite	293 K	pH 1.5	87.7	mg g^{-1}	250
Kaolinite	303 K	Cr(VI), 10–250 mg L^{-1}, pH 4.6	11.60	mg g^{-1}	55
Acid-activated kaolinite			13.90		
ZrO-kaolinite			10.90		
TBA-kaolinite			10.60		
Alkyl ammonium surfactant bentonite (2.38 : 1 clay–surfactant (w/w) ratio	291 K		8.36	mg g^{-1}	165
			13.57		
Alkyl ammonium surfactant bentonite (4.75 : 1 clay–surfactant (w/w) ratio)	310 K		8.51		
			14.64		
Spent activated clay	277 K	pH 2.0	0.743	mg g^{-1}	149
		pH 2.5	0.589		
		pH 3.0	0.502		
		pH 3.5	0.427		
		pH 4.0	0.331		
	287 K	pH 2.0	0.756		
		pH 2.5	0.618		
		pH 3.0	0.518		
		pH 3.5	0.436		
		pH 4.0	0.327		
	297 K	pH 2.0	0.957		
		pH 2.5	0.621		
		pH 3.0	0.526		
		pH 3.5	0.482		
		pH 4.0	0.331		
	313 K	pH 2.0	1.422		
		pH 2.5	0.649		
		pH 3.0	0.557		
		pH 3.5	0.548		
		pH 4.0	0.334		
Tannin-immobilized activated clay	300 K		18.34	mg g^{-1}	76
	310 K		20.12		
	320 K		21.19		
	330 K		24.09		
[3-(2-Aminoethylamino)propyl trimethoxy-silane] grafted natural sepiolite	298 K	Cr(VI) 10–250 mg L^{-1}	52.99	mg g^{-1}	78
[3-(2-Aminoethylamino)propyl trimethoxy-silane] grafted acid-activated sepiolite			80.84		
Activated alumina		pH 3.0	25.57	mg g^{-1}	239
Fuller's earth			23.58		
Dolomite	293 K	pH 2.0	10.010	mg g^{-1}	205
	303 K		8.385		
	313 K		6.654		
	333 K		5.609		
Hexa decyl trimethyl ammonium-zeolite	288 K	pH 6.0	5.07	mg g^{-1}	188
	281 K	pH 8.0	3.10		
	283 K	pH 10.0	0.21		

Table 3 (*Contd.*)

Metal cation/adsorbent	Experimental variables		Langmuir capacity (q_m)		Ref.
Dodecyl benzyl dimethyl ammonium-rectorite	299 K	pH 6.0	0.97	mg g^{-1}	215
Hexadecyl trimethyl ammonium-rectorite			2.39		
Octadecyl trimethyl ammonium-rectorite			3.57		
Hydrous TiO_2	288 K	pH 1.5	10.83	mg g^{-1}	255
	303 K		20.00		
	318 K		26.81		
Hydrous ZrO_2	298	pH 2.0	61.00	mg g^{-1}	91
	308		61.00		
	318		63.00		
	328		64.00		
	338		66.00		
Montmorillonite-supported magnetite	298 ± 2 K		13.88	mg g^{-1}	219
Magnetite	298 ± 2 K		20.16	mg g^{-1}	220
Commercial magnetite			13.72		
Diatomite-supported magnetite			12.31		
Loamy sand soil			1570.00	mg kg^{-1}	124
Zero-valent iron	298 K	Cr(VI) 60–100 mg L^{-1}	76.92	mg g^{-1}	62
Fe–Ni bimetallic nanoparticle			100.00		
Fe–Ni bimetallic-montmorillonite nanocomposite			100.00		
Red mud	300 K	pH 2.0	4.36×10^{-4}	mol g^{-1}	237
	313 K		4.15×10^{-4}		
	323 K		4.05×10^{-4}		
Fly ash		pH 3.0	23.86	mg g^{-1}	239
Clarified sludge			26.31		
Fly ash			1.379	mg g^{-1}	235
Fly ash impregnated with Al			1.820		
Fly ash impregnated with Fe			1.667		
Cu(II)					
Kaolinite	293 K		14.89	mg g^{-1}	249
	303 K		16.75		
	313 K		16.79		
Kaolin	303 K		12.00×10^{-3}	mmol g^{-1}	27
Ball clay			2.50×10^{-2}		
Local bentonite	293 K		909	mg g^{-1}	145
Local bentonite	293.15 K		9.73×10^{-5}	mol g^{-1}	37
	313.15 K		9.65×10^{-5}		
	333.15 K		1.08×10^{-5}		
Local montmorillonite			30.994	mg g^{-1}	252
Cankiri bentonite	296 K		44.84	mg g^{-1}	39
Bentonite	293 K	pH 3.0	12.376	mg g^{-1}	34
		pH 5.0	14.104		
		pH 7.0	12.547		
		pH 9.0	15.924		
Bentonite	303 K	Cu(II) 50–300 mg L^{-1}	12.5×10^{2}	mmol g^{-1}	36
Na-bentonite	298 K		17.877	mg g^{-1}	147
Natural kaolinite	298 ± 1 K		6.2 ± 0.2	mmol g^{-1}	154
Urea-intercalated kaolinite			8.5 ± 0.1		
Urea intercalated/delaminated kaolinite			9.6 ± 0.2		
Kaolinite	303 K	Cu(II) 10–250 mg L^{-1}, pH 5.7	9.2	mg g^{-1}	57
Acid-activated kaolinite			10.1		
Montmorillonite			31.8		
Acid-activated montmorillonite			32.3		
Montmorillonite	298 K	pH 5.0	12.633	mg g^{-1}	66
Humic acid modified Ca-montmorillonite			15.254		
Bentonite		Cu(II) 200–700 mg L^{-1}	149.25	mg g^{-1}	160
Phosphate-modified bentonite			158.73		
Sulphate-modified bentonite			166.67		
MgO coated bentonite	295.15 K	pH 6.0	58.44 ± 0.46	mg g^{-1}	59

Table 3 (*Contd.*)

Metal cation/adsorbent	Experimental variables		Langmuir capacity (q_m)		Ref.
Ca-montmorillonite	298 K	pH 5.0	12.443	mg g^{-1}	66
Humic acid modified Ca-montmorillonite			15.657		
Montmorillonite	295 K	pH 5.0	10.09	mg g^{-1}	163
Sodium dodecyl sulphate-montmorillonite			12.27		
Hydroxy-alumino-silicate-montmorillonite			14.51		
Sodium dodecyl sulfate montmorillonite		Cu(II) 4.5–45 mmol	254.1	mmol kg^{-1}	171
Smectite	298 ± 1 K	pH 5.0	$(15.7 \pm 0.1) \times 10^3$	mmol g^{-1}	167
Aluminum pillared/3-mercapto propyltrimethoxysilane organofunctionalized smectite			$(28.2 \pm 0.1) \times 10^3$		
Zirconium pillared and 3-mercapto propyltrimethoxy-silane organofunctionalized smectite			$(29.4 \pm 0.1) \times 10^3$		
ZrO-kaolinite	303 K	Cu(II) 10–250 mg L^{-1}, pH 5.7	3.0	mg g^{-1}	56
TBA-kaolinite			3.2		
ZrO-montmorillonite			7.1		
TBA-montmorillonite			27.3		
Bentonite	303 K	pH 6.02	9.72	mg g^{-1}	58
	323 K		11.29		
Bentonite + goethite	303 K		9.90		
	323 K		13.91		
Bentonite + humic acid	303 K		10.33		
	323 K		16.13		
Bentonite + geothite + humic acid	303 K		10.03		
	323 K		16.42		
8-Hydroxy Quinoline immobilized bentonite	293 K		51.12	mg g^{-1}	70
	303 K		51.56		
	313 K		55.04		
	323 K		56.55		
2,2′-Dipyridyl immobilized bentonite	293 K	Cu(II) 92.5–200 mg L^{-1}, pH 5.7	49.44	mg g^{-1}	72
	303 K		50.33		
	313 K		54.01		
	323 K		54.07		
Chitosan immobilized bentonite		Cu(II) 50–500 mg L^{-1}, pH 4.0	21.552	mg g^{-1}	176
Humic acid-immobilized-amine modified polyacrylamide–bentonite composite	303 K	pH 8.0	96.15	mg g^{-1}	168
Bentonite	293 ± 2 K	pH 5.0	11.36	mg g^{-1}	177
		pH 6.2	29.43		
Bentonite–polyacrylamide composite		pH 5.0	19.89		
		pH 6.2	32.81		
Chitosan–clay–magnetite composite	296 ± 2 K	pH 5.0	14.30	mg g^{-1}	178
Vermiculite	298 K	Adsorbent 1.25 g L^{-1}	43.67	mg g^{-1}	153
Natural muscovite	293 K	Cu(II) 0–100 mg L^{-1}, pH 6.0	0.618	mg g^{-1}	43
Local zeolite			0.128	mmol g^{-1}	180
Local clay			0.098		
Local diatomite			0.047		
Spent activated clay	300 K	pH 5.0 ± 0.1	10.9	mg g^{-1}	148
		pH 5.5 ± 0.1	11.5		
		pH 6.0 ± 0.1	13.2		
Tannin immobilized calcined hydrotalcite	303 K	pH 6.0	81.4	mg g^{-1}	118
	313 K		84.4		
	323 K		94.7		
	333 K		103.5		
Iron oxide-immobilized sand	298 ± 1 K		1.265	mg g^{-1}	128
Natural zeolite tuff	303 K	pH 5.0	23.3	mg g^{-1}	83
Clinoptilolite	303 K	Cu(II) 100–400 mg L^{-1}	141.12	mg g^{-1}	182
Humic acid-immobilized cetylpyridinium-zeolite	298 K		19.8	mg g^{-1}	88
	303 K		20.5		
	318 K		21.5		

Table 3 (*Contd.*)

Metal cation/adsorbent	Experimental variables		Langmuir capacity (q_m)		Ref.
Cancrinite-type zeolite	298 ± 2.1 K		2.081	mmol g^{-1}	185
N-[3-(Trimethoxysilyl)propyl]-ethylenediamine grafted silica	293 K		0.182	mmol g^{-1}	193
Amino functionalized silica gel (3-aminopropyltri-methoxysilane : silica = 0.1)			0.485	mmol g^{-1}	115
Amino functionalized silica gel (3-aminopropyltri-methoxysilane : silica = 0.2)			0.500		
Amino functionalized silica gel (3-aminopropyltri-methoxysilane : silica = 0.3)			0.850		
Aminated mesoporous alumina	298 ± 1 K		7.09	mg g^{-1}	112
Protonated mesoporous alumina			8.55		
3-Aminopropyltriethoxysilane/glutaraldehyde coated Fe_3O_4	293 ± 1 K	pH 4.0	61.07	mg g^{-1}	107
Titanate nanotube	298 ± 1 K	Cu(II) 0.1–3.0 mmol L^{-1}	1.92	mmol g^{-1}	99
Powered limestone	298 K		0.29	mg g^{-1}	226
Vanadium mine tailing	303 K		5.36	mg g^{-1}	223
	313 K		8.75		
	323 K		14.96		
Bagasse fly ash	303 K		2.26	mg g^{-1}	230
	313 K		2.34		
	323 K		2.36		
Fly ash	303 K		5.71	mg g^{-1}	232
	313 K		5.67		
	323 K		5.56		
Pit coal fly ash	277 K		4.594	mg g^{-1}	233
	291 K		4.715		
	333 K		7.613		
Electric furnace slag	293 K		32.68	mg g^{-1}	137
	303 K		36.36		
	313 K		39.22		
Fe(III)					
Kaolinite	303 K	Fe(III) 10–250 mg L^{-1}, pH 3.0	11.2	mg g^{-1}	52
Acid-activated kaolinite			12.1		
Montmorillonite			28.9		
Acid-activated montmorillonite			30.0		
ZrO-kaolinite	303 K	Fe(III) 10–250 mg L^{-1}, pH 3.0	9.7	mg g^{-1}	49
ZrO-montmorillonite			23.8		
TBA-kaolinite	303 K	Fe(II) 10–250 mg L^{-1}, pH 3.0	9.3	mg g^{-1}	164
TBA-montmorillonite			22.6		
Chitosan–attapulgite composites	298 K		36.76	mg g^{-1}	132
	308 K		47.17		
	318 K		62.50		
Hg(II)					
Phosphate-immobilized Zr-pillared bentonite		pH 6.0	50.98	mg g^{-1}	159
Montmorillonite	298.15 ± 0.2 K	pH 3.0	1.23 ± 0.12	mmol g^{-1}	173
Dimethyl sulfoxide/3-aminopropyl-triethoxysilane intercalated montmorillonite			1.56 ± 0.12		
Pyridine/3-aminopropyl-triethoxysilane intercalated montmorillonite			1.77 ± 0.12		
Hybrid mesoporous aluminosilicate sieve	303 ± 2 K	Hg(II) 2–16 mg L^{-1}, pH 6.0	20.66	mg g^{-1}	80
Silica gel-based hybrid composite (heterogeneous synthesis)	288 K	Hg(II) 1×10^3 to 5×10^3 mol L^{-1}	0.56	mg g^{-1}	194
	298 K		0.72		
	308 K		0.90		
Silica gel-based hybrid composite (homogeneous synthesis)	288 K		0.57		
	298 K		0.58		
	308 K		0.74		

Table 3 (*Contd.*)

Metal cation/adsorbent	Experimental variables		Langmuir capacity (q_m)		Ref.
Dithiocarbamate chelating resin	298 K	Hg(II) 1–25 mmol L^{-1}	2.45	mmol g^{-1}	136
Mn(II)					
Montmorillonite K 10	298 K		4.80	mg g^{-1}	33
			6.00		
Brazilian bentonite					
Sepiolite	293 ± 1 K	Adsorbent 2.5–25 g L^{-1}	0.247	meq g^{-1}	151
Clinoptilolite	303 K	Mn(II) 100–400 mg L^{-1}	76.78	mg g^{-1}	182
Natural nontronite	298 ± 1 K	Mn(II) 0.125–2.5 mmol L^{-1}	13.015	mmol g^{-1}	179
3-Aminopropyltriethoxy-silane modified nontronite			23.256		
Ni(II)					
Local bentonite	293 K		2.875	mg g^{-1}	150
	313 K		3.072		
	323 K		3.047		
	348 K		3.893		
Ball clay	303 K		7.00×10^{-3}	mmol g^{-1}	27
Na-bentonite	298 K		13.966	mg g^{-1}	147
Chitosan immobilized bentonite		Ni(II) 50–500 mg L^{-1}, pH 4.0	15.823	mg g^{-1}	176
Kaolinite	303 K	Ni(II) 10–250 mg L^{-1}, pH 5.7	10.4	mg g^{-1}	51
Acid-activated kaolinite			11.9		
Montmorillonite			28.4		
Acid-activated montmorillonite			29.5		
ZrO-kaolinite	303 K	Ni(II) 10–250 mg L^{-1}, pH 5.7	8.8	mg g^{-1}	49
ZrO-montmorillonite			22.0		
TBA-kaolinite	303 K	Ni(II) 10–250 mg L^{-1}, pH 5.7	8.4	mg g^{-1}	164
TBA-montmorillonite			19.7		
Montmorillonite K10	298 K		2.10	mg g^{-1}	74
3-Mercaptopropyl-trimethoxysilane-modified montmorillonite K10			4.73		
Na-attapulgite	291.15	pH 6.0 ± 0.1	9.42×10^{-5}	mol g^{-1}	42
	313.15		9.78×10^{-5}		
	333.15		1.05×10^{-5}		
Mg-mesoporous alumina	298 ± 1 K	Ni(II) 5–30 mg L^{-1}	22.32	mg g^{-1}	260
Poly(ethyleneimine)–silica gel		pH 5.0–6.0	28.25	mg g^{-1}	192
Glutaraldehyde crosslinked poly(ethyleneimine)–silica gel			18.62		
Amino functionalized MCM-41		Ni(II) 10–70 mg L^{-1}	12.36	mg g^{-1}	116
Cancrinite-type zeolite	298 ± 2.1 K		1.532	mmol g^{-1}	185
Clinoptilolite	293 K		3.28	mg g^{-1}	85
	313 K		2.97		
	333 K		2.65		
Dimethylglyoxime treated clinoptilolite	293 K		0.96	mmol g^{-1}	87
	313 K		0.18		
	333 K		0.13		
Hydrous TiO_2	288 ± 1 K	Ni(II) 10–150 mg L^{-1}, pH 5.0 ± 1	19.18	mg g^{-1}	259
	303 ± 1 K		22.07		
	318 ± 1 K		23.24		
	328 ± 1 K		26.47		
Fly ash	303 K		1.12	mg g^{-1}	231
	313 K		1.35		
	323 K		1.70		
Pb(II)					
Local bentonite	293.13	pH 5.2 ± 0.2	1.15×10^{-4}	mol g^{-1}	32
	323.13		1.46×10^{-4}		
	343.13		1.64×10^{-4}		
Turkish kaolinite	293 K	pH 6.0	21.55	mg g^{-1}	31
Turkish kaolinite	293 K	pH 5.0	31.75	mg g^{-1}	30
Kaolin	303 K		3.18×10^{-3}	mmol g^{-1}	27
Ball clay			1.70×10^{-2}		

Table 3 (*Contd.*)

Metal cation/adsorbent	Experimental variables		Langmuir capacity (q_m)		Ref.
Montmorillonite	298 K	pH 6.0	57.0	mg g^{-1}	40
Na-bentonite	298 K	Pb(II) 1.45×10^{-5} to 1.74×10^{-4} mol L^{-1}	2.31×10^{-4}	mol g^{-1}	38
	318 K		2.52×10^{-4}		
	338 K		3.10×10^{-4}		
Natural bentonite	293 K		107.00	mg g^{-1}	146
	313 K		110.00		
	333 K		120.00		
Acid-activated kaolinite	303 K	Pb(II) 10–250 mg L^{-1}, pH 5.7	12.33	mg g^{-1}	54
Acid-activated montmorillonite			31.35		
Natural kaolinite	298 ± 1 K		6.3 ± 0.2	mmol g^{-1}	154
Urea-intercalated kaolinite			9.6 ± 0.1		
Urea intercalated and delaminated kaolinite			9.9 ± 0.2		
Kaolinite	303 K		4.73	mg g^{-1}	44
Aluminium sulphate modified kaolinite			32.2		
Kaolinite	303 K	Pb(II) 10–250 mg L^{-1}, pH 5.7	11.52	mg g^{-1}	53
ZrO-kaolinite			9.01		
TBA-kaolinite			5.44		
Montmorillonite			31.05		
ZrO-montmorillonite			31.44		
TBA-montmorillonite			30.67		
Kaolinite	295 ± 1 K	Pb(II) 50–400 mg L^{-1}	13.32	mg g^{-1}	162
Acid treated kaolinite			51.60		
NaOH/3-chloropropyl-triethoxysilane modified kaolinite			54.35		
Natural smectite	298 ± 0.2 K	pH 55.0 mg L^{-1}, pH 5.0	8.857	mmol g^{-1}	175
Al-pillared 3-amino-propyltriethoxysilane organofunctionalized smectite			9.831		
Ti-pillared 3-amino-propytriethoxysilane organofunctionalized smectite			9.546		
Cr-pillared 3-amino-propyltriethoxysilane organofunctionalized smectite			9.278		
Zr-pillared 3-amino-propyltriethoxysilane organofunctionalized smectite			9.347		
Chitosan immobilized bentonite		Pb(II) 50–500 mg L^{-1}, pH 4.0	26.385	mg g^{-1}	176
8-Hydroxy quinoline-immobilized bentonite	293 K	Pb(II) 100–300 mg L^{-1}	139.08	mg g^{-1}	71
	303 K		139.48		
	313 K		141.43		
	323 K		142.94		
Montmorillonite–illite	310 K	Pb(II) 100 mg L^{-1}	54.122	mg g^{-1}	252
		Pb(II) 150 mg L^{-1}	54.517		
		Pb(II) 200 mg L^{-1}	56.768		
Mercapto functionalized sepiolite	289.15 K	Pb(II) 0–180 mg L^{-1}	67.62 ± 5.71	mg g^{-1}	79
	299.15 K		95.50 ± 6.78		
	318.15 K		95.63 ± 6.31		
Clay–poly(methoxyethyl)acrylamide composite	293 K	Pb(II) 100–300 mg L^{-1}	3.46×10^{-4}	mol g^{-1}	75
	303 K		3.58×10^{-4}		
	313 K		3.85×10^{-4}		
	323 K		3.91×10^{-4}		
Vermiculite	283 K	Pb(II) 20–200 mg L^{-1}	86.96	mg g^{-1}	152
	308 K		94.61		
	333 K		104.50		
	353 K		109.90		
Palygorskite	293.15 K	pH 5.0 ± 0.1	8.4×10^{-5}	mol g^{-1}	207
	313.15 K		1.0×10^{-4}		
Mordenite	293 K	Pb(II) 20–100 mg L^{-1}, pH 6.0	13.95	mg g^{-1}	186
	303 K		18.55		
	313 K		21.56		
	323 K		24.48		
Natural muscovite	293 K	Pb(II) 0–100 mg L^{-1}, pH 6.0	0.630	mg g^{-1}	43

Table 3 (*Contd.*)

Metal cation/adsorbent	Experimental variables		Langmuir capacity (q_m)		Ref.
Francolite	303 K		1208.00	mg g^{-1}	206
	313 K		543.10		
	323 K		345.13		
	333 K		128.90		
Tourmaline			200	mg g^{-1}	122
Natural nontronite	298 ± 1 K	Pb(II) 0.125–2.500 mmol L^{-1}	13.329	mmol g^{-1}	179
3-Aminopropyltriethoxysilane modified nontronite			24.799		
N-Methylimidazole anchored activated palygorskite	283 K		714.29	mg g^{-1}	212
	298 K		680.27		
	313 K		666.67		
Ca-deficient hydroxyapatite		Pb(II) 10–30 mg L^{-1}	19.96	mg g^{-1}	210
Natural apatite			0.400	mmol g^{-1}	121
Synthetic hydroxyapatite			0.442		
Mg_2Al LDH	303.15 K	Pb(II) 5–23 mg L^{-1}, pH 5.7 ± 0.01	66.16	mg g^{-1}	119
	323.15 K		69.23		
	343.15 K		75.18		
Loamy sand soil			2168.00	mg kg^{-1}	124
Amino functionalized MCM-41		Pb(II) 10–70 mg L^{-1}	57.74	mg g^{-1}	116
Clinoptilolite	293 K	pH 2.0	71.94	mg g^{-1}	183
		pH 3.0	109.89		
		pH 4.0	117.64		
		pH 5.0	111.11		
		pH 6.0	108.69		
		pH 7.0	92.59		
		315–500 μm	144.92		
		500–800 μm	138.88		
		800–1000 μm	128.20		
		1000–1600 μm	121.95		
		100 rpm	149.25		
		150 rpm	156.25		
		175 rpm	166.66		
		225 rpm	172.41		
	298 K		120.48		
	313 K		169.49		
	318 K		181.81		
	343 K		185.18		
Cancrinite-type zeolite	298 ± 2.1 K		2.130	mmol g^{-1}	185
Natural zeolite tuff	303 K	pH 5.0	78.6	mg g^{-1}	83
Activated alumina	303 K	pH 5.0	83.33	mg g^{-1}	111
Hydrous MnO_2	298 K	pH 3.2–3.5	15.78	mmol g^{-1}	96
NiO	303 K	Pb(II) 100–600 mg L^{-1}	909.0	mg g^{-1}	94
Fe_3O_4	298 K	pH 5.5	0.14	mmol g^{-1}	101
	313 K		0.15		
	328 K		0.17		
Al_2O_3-supported iron oxide	288 K	Pb(II) 0.1–0.8 mM	0.096	mmol g^{-1}	103
	308 K		0.110		
	318 K		0.140		
TiO_2/SiO_2 binary mixed oxide	298 K	pH 6.0	97.46	μmol g^{-1}	98
	308 K		169.77		
	325 K		203.25		
Poly(ethyleneimine)–silica gel		pH 5.0–6.0	82.64	mg g^{-1}	192
Glutaraldehyde crosslinked poly(ethyleneimine)–silica gel			50.76		
Thiol-functionalized silica	298 K	Pb(II) 20–250 mg L^{-1}	117.51 ± 5.16	mg g^{-1}	117
N-[3-(Trimethoxysilyl)propyl]-ethylenediamine grafted silica	293 K		0.057	mmol g^{-1}	193
Sand	293 K		22.90 ± 0.27	μmol g^{-1}	126
	303 K		21.60 ± 0.01		
	313 K		21.50 ± 0.20		
	323 K		26.80 ± 0.39		
Iron oxide-immobilized sand	298 ± 1 K		2.088	mg g^{-1}	128

Table 3 (*Contd.*)

Metal cation/adsorbent	Experimental variables		Langmuir capacity (q_m)		Ref.
Titanate nanotubes	70 W	Pb(II) 2–200 mg g^{-1}	1000	mg g^{-1}	221
	400 W		2000		
	700 W		1769		
Titanate nanotube	298 ± 1 K	Pb(II) 0.1–3.0 mmol L^{-1}	2.64	mmol g^{-1}	99
Talc	293 K		7.994		228
	303 K		6.146		
	313 K		6.305		
	323 K		5.359		
	333 K		4.724		
	343 K		4.255		
Red mud	300	pH 2.0	3.44×10^{-4}	mol g^{-1}	237
	313		3.39×10^{-4}		
	323		3.23×10^{-4}		
Bagasse fly ash	303		2.50	mg g^{-1}	229
	313		2.30		
	323		2.10		
Vanadium mine tailing	303 K		20.73	mg g^{-1}	223
	313 K		24.43		
	323 K		46.31		
Blast furnace sludge	298 K		227.00	mg g^{-1}	238
	318 K		161.00		
Blast furnace dust	298 K		142.00		
	318 K		111.00		
Blast furnace slag	298 K		125.00		
	318 K		91.00		
Electric furnace slag	293 K		33.78	mg g^{-1}	137
	303 K		35.84		
	313 K		37.04		
Dithiocarbamate chelating resin	298 K	Cd(II) 1–25 mmol L^{-1}	2.15	mmol g^{-1}	136
Se(IV)					
Iron oxide	303 K	Se(IV) 10–50 mg L^{-1}, pH ~4.0 ± 0.5	8.47	mg g^{-1}	100
	313 K		7.30		
	323 K		6.52		
Silicon oxide	303 K		7.06		
	313 K		6.38		
	323 K		4.58		
Zn(II)					
Cankiri bentonite	296 K		80.64	mg g^{-1}	39
Kaolin	303 K		2.79×10^{-2}	mmol g^{-1}	27
Ball clay			4.40×10^{-2}		
Acid washed kaolin	303 K		250	mg g^{-1}	29
Bentonite	293 K	pH 3.0	15.674	mg g^{-1}	34
		pH 5.0	21.097		
		pH 7.0	15.060		
		pH 9.0	17.065		
Bentonite	303 K	Zn(II) 10–90 mg L^{-1}	68.49	mg g^{-1}	35
Bentonite		Zn(II) 200–700 mg L^{-1}	98.04	mg g^{-1}	160
Phosphate-modified bentonite			104.17		
Sulphate-modified bentonite			111.11		
Bentonite	293 K	pH 5.0	36.63	mg g^{-1}	61
Bentonite/iron oxides (5 : 1 at 20 °C)			29.67		
Bentonite/iron oxides (1 : 1 at 85 °C)			14.10		
Local clay 1	298 ± 1 K	Zn(II) 50 mg L^{-1}, pH 5.0	1.007	mmol g^{-1}	175
Al/Zr pillared local clay 1 (calcined at 723 K)			1.119		
Al/Ti pillared local clay 1 (calcined at 723 K)			1.217		
Al/Zr pillared local clay 1 (calcined at 873 K)			1.501		
Al/Ti pillared local clay 1 (calcined at 873 K)			1.547		
Local clay 2			0.934		
Al/Zr pillared local clay 2 (calcined at 723 K)			1.151		
Al/Ti pillared local clay 2 (calcined at 723 K)			1.578		
Al/Zr pillared local clay 2 (calcined at 873 K)			1.587		

Table 3 (*Contd.*)

Metal cation/adsorbent	Experimental variables		Langmuir capacity (q_m)		Ref.
Al/Ti pillared local clay 2 (calcined at 873 K)			1.567		
HCl/NaOH-treated bentonite	295 ± 1 K	Zn(II) 20–200 mg L^{-1}	138.17	mg g^{-1}	45
Sodium dodecylsulfate-montmorillonite		Zn(II) 4.5–45 mmol	202.9	mmol kg^{-1}	171
Humic acid-immobilized-amine modified polyacrylamide–bentonite composite	303 K	pH 8.0	52.93	mg g^{-1}	168
Tannin immobilised calcined hydrotalcite	303 K	pH 6.0	78.9	mg g^{-1}	118
	313 K		81.9		
	323 K		91.5		
	333 K		101.7		
Natural nontronite	298 ± 1 K	Zn(II) 0.125–2.5 mmol L^{-1}	12.269	mmol g^{-1}	179
3-Aminopropyltriethoxysilane modified nontronite			23.098		
NaA zeolite	298 K	Zn(II) 100 mg L^{-1}, pH 6.0	118.906	mg g^{-1}	84
NaX zeolite			106.382		
Clinoptilolite	303 K	Zn(II) 100–400 mg L^{-1}	133.85	mg g^{-1}	182
Cancrinite-type zeolite	298 ± 2.1 K		1.532	mmol g^{-1}	185
Clinoptilolite		Zn(II) 50–500 mg L^{-1}	21.20	mg g^{-1}	184
NaCl treated clinoptilolite (at 20 °C)			20.80		
NaCl treated clinoptilolite (at 70 °C)			22.20		
HCl treated clinoptilolite			17.90		
Phosphate	298 ± 1 K		10.32	mg g^{-1}	209
Francolite	303 K		126.70	mg g^{-1}	206
Diatomite	298 K		27.247	mg g^{-1}	256
	303 K		27.777		
	313 K		37.375		
MnO_2 modified diatomite	298 K		16.339		
	303 K		14.598		
	313 K		22.026		
	323 K		51.41		
	333 K		38.45		
Hydrous MnO_2	298 K	pH 3.5–4.0	0.833	mmol g^{-1}	96
Chinese loess soil	288 K		70.80	mg g^{-1}	202
	298 K		70.20		
	308 K		75.20		
	318 K		83.20		
Sand	303 ± 2 K		169 ± 0.2	μmol g^{-1}	127
Poly(ethyleneimine)–silica gel		pH 5.0–6.0	52.08	mg g^{-1}	192
glutaraldehyde crosslinked poly(ethyleneimine)–silica gel			32.79		
Bagasse fly ash	303 K		2.34	mg g^{-1}	230
	313 K		2.45		
	323 K		2.54		
Pit coal fly ash	277 K		4.105	mg g^{-1}	233
	291 K		5.753		
	333 K		7.655		
Powdered marble waste	298 K	Zn(II) 100–300 mg L^{-1}	175.13	mg g^{-1}	227

Natural sepiolite had highest uptake of Cr(III) (0.53 mg g^{-1}) followed by Cd(II) (0.39 mg g^{-1}) and Mn(II) (0.25 mg g^{-1}) at 293 K.[151] The interactions were shown to occur through ion-exchange, complex formation and surface adsorption mechanisms. Liu *et al.*[152] reported endothermic interactions of Pb(II) with vermiculite when the Langmuir capacity varied from 86.96 to 109.50 mg g^{-1} (283 to 353 K). The increased adsorption at higher temperature was attributed to the increase in the number of active sites (Si–OH and Al–OH) as well as to decrease in the adsorption activation energy. In a similar work, vermiculite was shown to have preference for Cr(III) (q_m: 46.95 mg g^{-1}) over Cu(II) (q_m: 43.67 mg g^{-1}).[153] Vermiculite could adsorb metal ions through cation exchange at the planar sites, resulting from the interactions between metal ions and negative permanent charge forming outer-sphere complexes, and also through the formation of inner-sphere complexes through Si–O– and Al–O– groups at the clay particle edges. The comparatively smaller Cr(III) could compete faster for exchange sites than Cu(II).

Interactions of muscovite with As(III), As(V), Cd(II), Cu(II) and Pb(II) yielded Langmuir capacities of 0.33 mg g^{-1} (b: 0.027 L mg^{-1}), 0.79 mg g^{-1} (b: 0.172 L mg^{-1}), 0.75 mg g^{-1}

(b: 0.005 L mg^{-1}), 0.62 mg g^{-1} (b: 0.028 L mg^{-1}) and 0.63 mg g^{-1} (b: 0.054 L mg^{-1}) respectively at 293 K.[43] The mechanism suggested was formation of inner-sphere complexes of As(III), As(V), Cu(II), and Pb(II), and outer-sphere complex of Cd(II).

2.2.2. Modified clays. Most of the recent works involved modified clays as adsorbents. Thermally and chemically treated clays have better pore distribution and uniform particle size which give them higher adsorption capacity compared to the parent clay. This was shown for a local clay mixture (montmorillonite, chlorite, palygorskite, illite, and kaolinite) with respect to adsorption of Cd(II), Pb(II) and Zn(II).[41]

Kaolinite intercalated with urea followed by dealumination showed better adsorption of Cu(II) (kaolinite 6.2 ± 0.2 mmol g^{-1}, urea-intercalated kaolinite 8.5 ± 0.1 mmol g^{-1}, urea intercalated/delaminated kaolinite 9.6 ± 0.2 mmol g^{-1}) and Pb(II) (kaolinite 6.3 ± 0.2 mmol g^{-1}, urea-intercalated kaolinite 9.6 ± 0.1 mmol g^{-1}, urea intercalated/delaminated kaolinite 9.9 ± 0.2 mmol g^{-1}).[154] It is suggested that the inner-sphere interactions particularly at the edge sites of kaolinite dominated the outer-sphere ones. Further, adsorption on intercalated surface is governed by the microenvironment around each site, composed of basic centers, created by hydration.

Acid activated clays have improved Langmuir capacity for Pb(II) over the raw clays[155] [q_m for raw green clay 25.44 mg g^{-1}, H_2SO_4 activated green clay 40.75 mg g^{-1}; raw red clay: 17.84 mg g^{-1}; H_2SO_4 activated red clay 27.15 mg g^{-1}; b: 0.018 to 0.074 L mg^{-1}]. The acid activated clays showed increase in specific surface area, total pore volume, internal porosity and pore size compared to untreated clay. Pb(II) was shown to interact with Si–OH groups on the surface.

Similarly, acid-activated kaolinite (Cd(II) 11.70 mg g^{-1}, Co(II) 12.10 mg g^{-1}, Cu(II) 10.10 mg g^{-1}, Cr(VI) 13.90 mg g^{-1}, Ni(II) 11.90 mg g^{-1}, Pb(II) 12.33 mg g^{-1}, Fe(III) 12.10 mg g^{-1}) and montmorillonite (Cd(II) 33.20 mg g^{-1}, Co(II) 29.70 mg g^{-1}, Cu(II) 32.30 mg g^{-1}, Ni(II) 29.50 mg g^{-1}, Pb(II) 31.35 mg g^{-1}, Fe(III) 30.00 mg g^{-1}) have enhanced Langmuir capacities for a group of metal ions.[46,50–52,54,55,57] The process of acid activation could have removed mineral impurities from the surface with partial dissolution of the external layers. This might be a contributing factor in increased adsorption capacity after acid activation (Fig. 7–11).

Bentonite modified with aqueous HCl followed by soaking in NaOH had Langmuir capacity of 138.17 and 202.63 mg g^{-1} respectively for Co(II) and Zn(II)[45] (b for Co(II) 2.39 × 10^{-3} L mg^{-1} and Zn(II) 0.61 L mg^{-1}). The cations were held to the clay surface either by proton exchange or surface reaction due to high surface charge developed from the treatments.

A homogeneous mixture of china clay and fly ash had very similar As(III) adsorption capacities at 303 K (0.39 mg g^{-1}, b = 1.590 L mg^{-1}) and 323 K (0.40 mg g^{-1}, b = 5.548 L mg^{-1}).[156] It shows that the active surface area for As(III) uptake did not change much in the temperature range.

Na^+-montmorillonite showed progressively higher Langmuir capacity for Cd(II) after Al_{13}-pillaring and acid activation (q_m: 0.125, 0.139, and 0.163 mmol kg^{-1}, b: 2.582, 2.899 and 5.483 L mmol^{-1}, respectively).[64] The b values were in the range of 2.582 to 5.483 L mmol^{-1}. It was shown that intercalation followed by

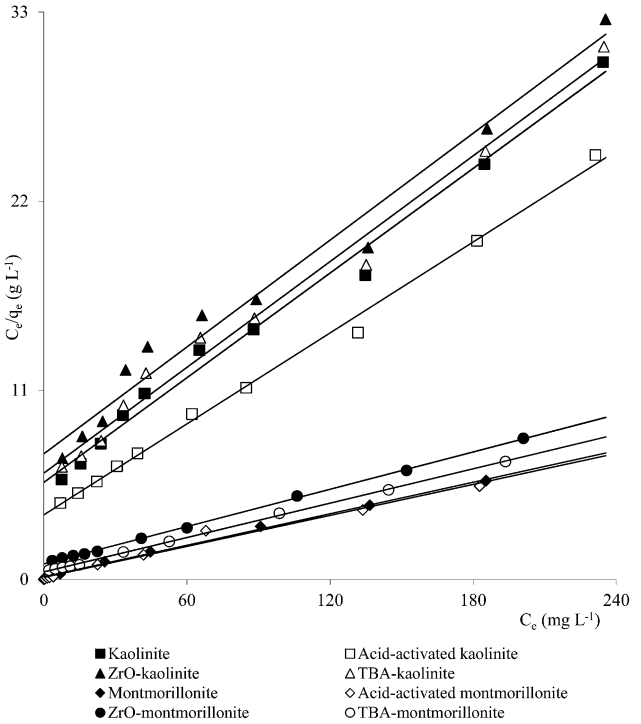

Fig. 7 Langmuir plots for Cd(II) adsorption on clay minerals (clay mineral 2.0 g L^{-1}, Cd(II) 10–250 mg L^{-1}, pH 5.5, time 240 min, temperature 303 K).

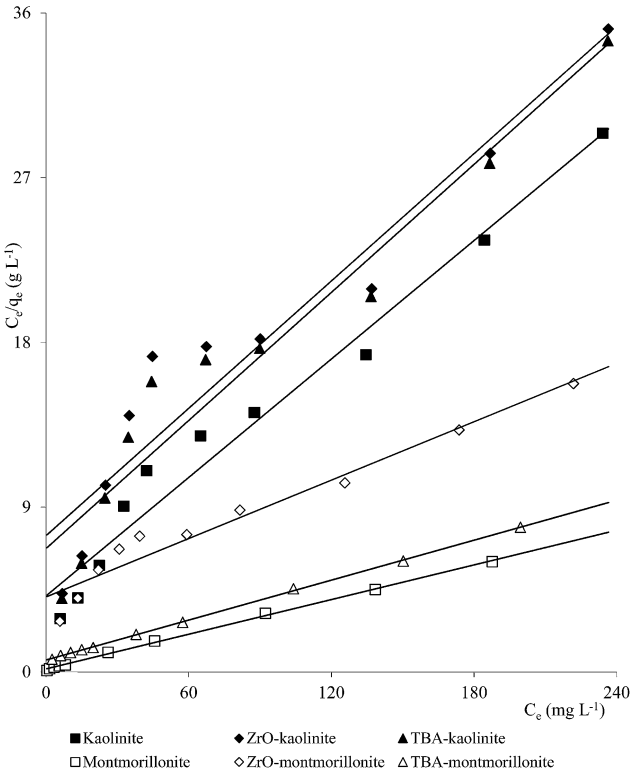

Fig. 8 Langmuir plots for Cu(II) adsorption on clay minerals (clay mineral 2.0 g L^{-1}, Cu(II) 10–250 mg L^{-1}, pH 5.7, time 360 min, temperature 303 K).

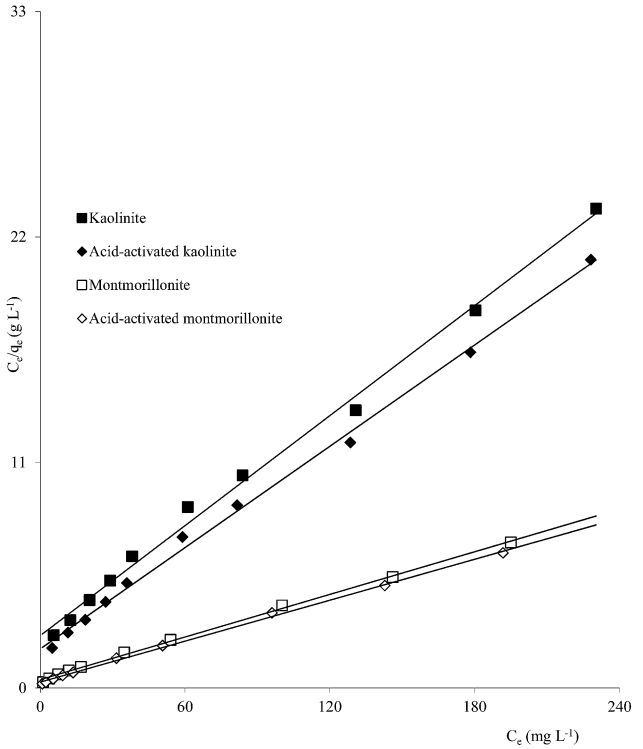

Fig. 9 Langmuir plots for Fe(III) adsorption on clay minerals (clay mineral 2.0 g L^{-1}, Fe(III) 10–250 mg L^{-1}, pH 3.0, time 300 min, temperature 303 K).

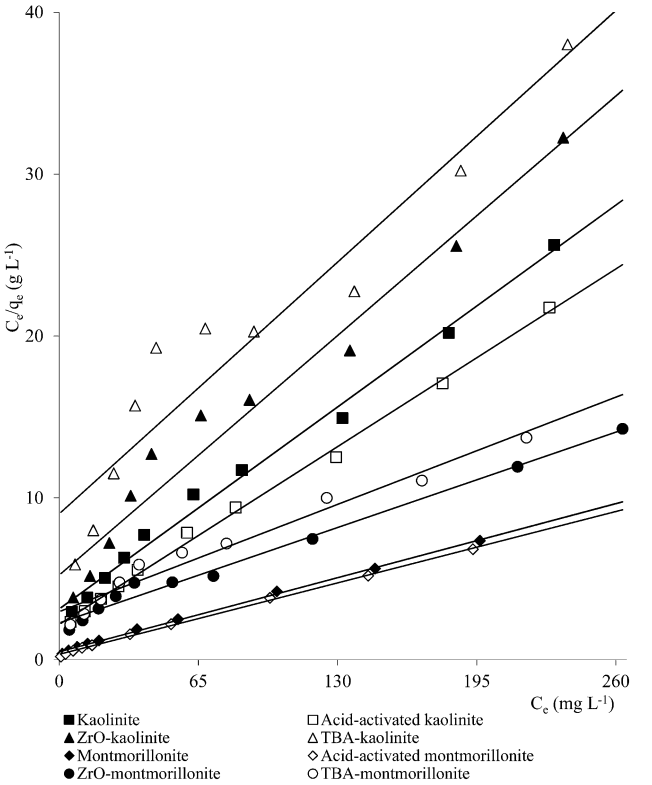

Fig. 11 Langmuir plots for Ni(II) adsorption on clay minerals (clay mineral 2.0 g L^{-1}, Ni(II) 10–250 mg L^{-1}, pH 5.7, time 180 min, temperature 303 K).

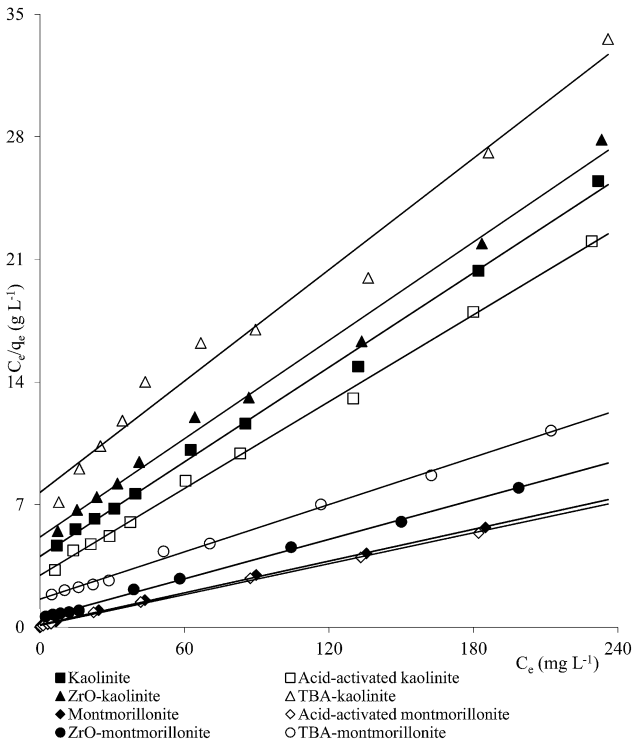

Fig. 10 Langmuir plots for Pb(II) adsorption on clay minerals (clay mineral 2.0 g L^{-1}, Pb(II) 10–250 mg L^{-1}, pH 5.7, time 180 min, temperature 303 K).

acid treatment increased the basal spacing, specific surface area and total pore volume of the materials resulting in higher uptake of Cd(II). Similarly, Cd(II) was preferably adsorbed on carbon modified aluminum-pillared montmorillonite compared to the unpillared form.[157]

Al/Ti and Al/Zr-pillared clays, calcined at 723 and 873 K for 2 h, had Zn(II) adsorption capacities of 3.178 to 4.162 mg g^{-1} at pH 5.0 and temperature 298 ± 1 K.[158] The chemisorption process was controlled by positioning and amount of hydroxyl groups in outer regions of the materials, as in lamellae borders or central structures.

Tomul[63] reported higher Cd(II) adsorption on Fe-pillared bentonite (0.77 L $mmol^{-1}$) than Fe/Cr pillared bentonite (0.63 L $mmol^{-1}$) and Cr pillared bentonite (0.42 L $mmol^{-1}$). The variations were shown to be due to the differences in pore size distribution.

MgO coated bentonite had Cu(II) Langmuir capacity of 58.44 ± 0.46 mg g^{-1} (b: 0.22 ± 0.13 L mg^{-1}).[59] MgO was shown to act as a buffering stabilizer that minimized the solubility of Cu(II) cations avoiding their redissolution.

Cation-exchange and outer sphere surface complexation had mainly contributed to Pb(II) adsorption (q_m: 95.88 mg g^{-1} at pH 4.0 ± 0.1, b: 9.00 L g^{-1}) on Fe, Mg (hydr)oxides coated bentonite composite in acidic pH.[60]

Phosphate-immobilized zirconium pillared bentonite had q_m of 50.98, 50.07 and 47.81 mg g^{-1} respectively for Hg(II), Cd(II) and Co(II)[159] and it was shown that the adsorption was

dependent on the ionic radii of the hydrated metal ions [b for Hg(II): 0.306 L g^{-1}, Cd(II): 0.195 L g^{-1}, Co(II): 0.180 L g^{-1}].

Introduction of inorganic functional groups, sulphate and phosphate, into bentonite resulted in improved Cu(II) and Zn(II) uptake (q_m Cu(II): 149.25, 158.73 and 166.69 mg g^{-1} ($b = 4.10 \times 10^{-3}$, 4.61×10^{-3} and 6.18×10^{-3} L g^{-1}); Zn(II): 98.04, 104.17 and 111.11 mg g^{-1} ($b = 6.59 \times 10^{-3}$, 7.50×10^{-3} and 8.07×10^{-3} L g^{-1}) for raw, sulphate- and phosphate-modified bentonite respectively).[160] The modified clay had enhanced CEC with the anions creating additional adsorption sites on the bentonite surface (Bentonite 95 ± 0.2 mmol per 100 g, sulphate modified bentonite 109 ± 0.2 mmol per 100 g, phosphate modified bentonite 118 ± 0.3 mmol per 100 g). The differences in the degree of hydration of Cu(II) and Zn(II) were reflected in the adsorption capacity values and it was shown that Cu(II) had easier access to the silicate surface than Zn(II).

In a similar work, kaolinite modified with 25% (w/w) aluminium sulphate, was observed to have ~7 times larger Langmuir capacity (32.2 mg g^{-1}) than the raw kaolinite (4.73 mg g^{-1}) for Pb(II).[44] It was proposed that the kaolinite layers were affected by the treatment creating a large number of micro-sized particles and bigger specific surface area. In addition, aluminium sulphate improved the ion exchange capacity of the clay mineral. There was, also consequent variation in Langmuir equilibrium constant [b: 3.00×10^{-2} L mg^{-1} and 5.04×10^{-2} L mg^{-1} for kaolinite and modified kaolinite].

Nano-sized iron oxide-coated perlite had Langmuir capacity of 0.39 mg g^{-1} (b: 44.84 L mg^{-1}) for As(v) oxyanions ($H_2AsO_4^-$ and $HAsO_4^{2-}$) at pH 4.0–7.0, the anions being held through coulombic interaction.[161]

The pillaring did not always lead to enhanced adsorption. Jobstmann and Singh[26] found that montmorillonite adsorbed more Cd(II) (q_m: 21.9 μM kg^{-1}, b: 0.22 L μM^{-1}) than hydroxy-aluminium-interlayered montmorillonite (q_m: 2.5 μM kg^{-1}, b: 0.21 L μM^{-1}) at 293 K. The CEC of montmorillonite decreased by ~30% after pillaring and this was shown to be the reason for decreased adsorption. Cd(II) was held by electrostatic attraction on raw montmorillonite, but a chemisorptive mechanism was proposed for the pillared montmorillonite.

When kaolinite and montmorillonite were modified by incorporation of ZrO into the interlayer space, the Langmuir capacity of the modified materials actually decreased [kaolinite (mg g^{-1}): Cu(II) 9.20 to 3.00, Cd(II) 6.78 to 5.27, Co(II) 11.20 to 9.00, Pb(II) 11.50 to 9.01, Ni(II) 10.40 to 8.80, Fe(III) 11.20 to 9.70, Cr(VI) 11.60 to 10.90; montmorillonite (mg g^{-1}): Cu(II) 31.80 to 7.10, Cd(II) 30.67 to 36.63, Co(II) 28.60 to 22.30, Pb(II) 31.05 to 31.44, Ni(II) 28.40 to 22.0, Fe(III) 28.90 to 23.80].[47,49,53,55,56] It was suggested that there was a net reduction in the number of available adsorption sites due to introduction of ZrO into the clay minerals (Fig. 7. Fig. 8, Fig. 10 and Fig. 11).

2.2.3. Organo-functionalized clays. Clays modified with various treatments had better Langmuir capacity for Pb(II) [H_2SO_4-kaolinite: q_m = 51.597 mg g^{-1} and (H_2SO_4 + 3-chloropropyltriethoxysilane + NaOH)-kaolinite: q_m = 54.351 mg g^{-1}] than the raw kaolinite (q_m = 13.320 mg g^{-1}).[162] It was found that kaolinite with 3-chloropropyltriethoxysilane had higher SiO_2/Al_2O_3 ratio and surface area than the raw kaolinite. The raw kaolinite possessed CEC of 8.7 mmol per 100 g, which increased to 12.7 mmol per 100 g for 3-chloropropyltriethoxysilane treated kaolinite, however the CEC decreased to 7.2 mmol per 100 g after acid treatment. Yun *et al.*[163] used montmorillonite (Mt) and modified montmorillonite (hydroxy-alumino-silicate montmorillonite, HAS-Mt and sodium dodecylsulfate montmorillonite, SDS-Mt) for adsorption of Cd(II), Cr(III) and Cu(II). The pillaring of the clay improved adsorption (Mt–Cu: 10.09 mg g^{-1}, Mt–Cd: 8.06 mg g^{-1}, Mt–Cr: 11.00 mg g^{-1}; HAS-Mt–Cu: 12.27 mg g^{-1}, HAS-Mt–Cd: 11.76 mg g^{-1}; HAS-Mt–Cr: 13.28 mg g^{-1}; SDS-Mt–Cu: 14.51 mg g^{-1}, SDS-Mt–Cr: 14.83 mg g^{-1}). It was found that the lamellar structure of pillared montmorillonite had a larger basal spacing than the raw montmorillonite allowing more metal ions to enter. The very small ionic radius of Cr(III) created a strong electrical field leading to strong adsorption, while this did not hold good for the bigger Cd(II) cations.

Introduction of TBA (tetrabutylammonium) ions into the interlayer space of kaolinite and montmorillonite was shown to result in an actual decrease in the Langmuir capacity with respect to a number of metal ions [kaolinite (mg g^{-1}): Cu(II) 9.20 to 3.20, Cd(II) 6.78 to 6.31, Co(II) 11.20 to 8.40, Pb(II) 11.50 to 5.44, Ni(II) 10.40 to 8.40, Fe(III) 11.20 to 9.30, Cr(VI) 11.60 to 10.60; montmorillonite (mg g^{-1}): Cu(II) 31.80 to 27.30, Cd(II) 30.67 to 43.47, Co(II) 28.60 to 19.70, Pb(II) 31.05 to 30.67, Ni(II) 28.40 to 19.70, Fe(III) 28.90 to 22.60].[47,53,55,56,164] The results indicated that introduction of different groups onto clay structure could be utilized to selectively block certain metal ions from being adsorbed on the surface (Fig. 7, Fig. 8, Fig. 10 and Fig. 11).

Organo-clays synthesized from bentonite with alkyl ammonium surfactant [di(hydrogenated tallow) dimethylammonium chloride (~75%) having 2-propanol (~14%) and water (~11%) as impurities] showed that adsorption of Cr(VI) was higher when bentonite was modified with a higher surfactant dose.[165] Higher surfactant loading increased the number of cationic adsorption sites and hence, the Langmuir capacity for Cr(VI) [2.38 : 1 clay–surfactant (w/w) ratio: q_m = 8.36 mg g^{-1}, b = 0.0136 L mg^{-1} (291 K) and q_m = 8.51 mg g^{-1}, b = 0.0093 L mg^{-1} (310 K); 4.75 : 1 clay–surfactant (w/w) ratio: q_m = 13.57 mg g^{-1}, b = 0.1325 L mg^{-1} (291 K) and q_m = 14.64 mg g^{-1}, b = 0.0922 L mg^{-1} (310 K)]. The probable mechanism involved electrostatic attraction between $Cr_2O_7^{2-}$ anions and positively charged sites developed in the organoclays through surfactant modification.

Montmorillonite modified with poly(hydroxo aluminium) and cetyltrimethyl-ammonium bromide[67] had Langmuir capacity of 2.28×10^{-4} mol g^{-1} for Cr(III) ($b = 1.65 \times 10^4$ L mol^{-1}). It was proposed that an excess of CTMA cations on the external surface of the modified clay could reverse the surface charge thereby favoring adsorption of Cr(III).

Langmuir capacity for Cr(VI) on smectite and 2-aminomethylpyridine modified smectite was 1.16 ± 0.12 and 1.87 ± 0.11 mmol g^{-1} at 298 ± 1 K respectively.[166] The free pair of electrons on N atoms functioned as good Lewis base and might be responsible for preferential uptake of metal ions by the modified smectites.

Natural and modified smectite (pillared with Al and Zr polyoxycations followed by organofunctionalization with

3-mercaptopropyltrimethoxysilane) adsorbed Cu(II) more than Co(II).[167] Langmuir capacities for Co(II) and Cu(II) adsorption were in the order of Zr/3-mercaptopropyl-trimethoxysilane-smectite [Co(II): $(25.8 \pm 0.2) \times 10^3$, Cu(II): $(29.4 \pm 0.1) \times 10^3$ mmol g^{-1}] > Al/3-mercaptopropyl-trimethoxysilane-smectite [Co(II): $(23.8 \pm 0.1) \times 10^3$, Cu(II): $(28.3 \pm 0.1) \times 10^3$ mmol g^{-1}] > natural smectite [Co(II): $(13.9 \pm 0.1) \times 10^3$, Cu(II): $(15.7 \pm 0.1) \times 10^3$ mmol g^{-1}] at 298 ± 1 K. The adsorption capacity of the modified clays depended on the nature of the complex formed on the surface and also on the affinity of the divalent metal cations to the attached ligand. Langmuir capacities showed that the sulfur donor atoms attached to the inorganic backbone had strong affinity for Cu(II).

Humic acid-immobilized-amine-modified polyacrylamide–bentonite composites had Langmuir capacities of 106.21, 96.15 and 52.93 mg g^{-1} at 303 K for Co(II), Cu(II) and Zn(II) respectively.[168] Humic acid had negative charge that enhanced the adsorption of metal cations through electrostatic interactions and/or complexation reactions. The intensity of adsorption (b) also followed the same order as Langmuir capacities *i.e.* Co(II): 1.32 L mg^{-1} > Cu(II): 0.21 L mg^{-1} > Zn(II): 0.03 L mg^{-1}.

Bentonite modified with *N*-2-hydroxypropyl trimethyl ammonium chloride chitosan yielded q_m and b as 22.23 mg g^{-1} and 0.178 L g^{-1} for Cd(II) adsorption.[169] The adsorption mechanism was based on chelation of Cd(II) with –OH and $-NH_2$ in the surface of modified-bentonite. Cation exchange between Cd(II) and modified-bentonite was also shown to play some role in the adsorption process.

Activated clay with tannin-immobilized on it adsorbed Cr(VI) with Langmuir capacities of 18.34 to 24.09 mg g^{-1} (b = 0.033 to 0.040 L mg^{-1}) at 300 to 330 K.[76] Adsorption mechanism suggested was esterification reaction with phenolic groups of tannin and anionic Cr(VI) species and also through partial reduction of Cr(VI) to Cr(III) followed by ion exchange in acidic medium.

Cr(VI) adsorption on a number of organo-clays [hexadecylpyridinium (HDPy)-, hexadecyl-trimethylammonium (HDTMA)-, and benzethonium (BE)-montmorillonite and vermiculite] showed higher Langmuir capacities for the organo-vermiculites (0.28–0.71 mol kg^{-1}) than the organo-montmorillonites (0.23–0.37 mol kg^{-1}) which might be due to larger basal spacing in the former.[170] The adsorption mechanism was Cr(VI) anion exchange with Cl^-, generated from the organic salts used for modification and present in the structure of organo-clays in the form of ion pairs. It was shown that Cr(VI) anions were held to the interlayer sites more strongly than to the external surface.

Langmuir capacity of dodecylamine modified sodium montmorillonite for Cr(VI)[73] was 23.69 mg g^{-1} (b = 0.109 L mg^{-1}) at pH 2.5 with proposed interactions between the protonated amine and hydrogentetraoxochromate(VI) anion. Hydrogen bonding was also likely between the protonated nitrogen in the primary amine and the OH groups in the clay ($NH_3^+ \cdots OH$) surface.

Sodium dodecylsulfate-modified montmorillonite yielded Langmuir capacities of 254.1 mmol kg^{-1} (b = 0.46 L $mmol^{-1}$) and 202.9 mmol kg^{-1} (b = 0.47 L $mmol^{-1}$) for Cu(II) and Zn(II) uptake respectively.[171] The modified montmorillonite had a much larger surface area than the raw clay, and consequently larger adsorption capacity. Grafting of sodium dodecylsulfate to the clay interlayer space increased the negative charge on the clay surface which might have enhanced the adsorption capacity for cations. Sodium dodecyl sulphate-modified-Fe-pillared montmorillonite had Langmuir capacities of 13.2 to 20.2 mg g^{-1} for Co(II) and 11.0 to 18.7 mg g^{-1} for Cu(II).[172] The clay-composites had larger surface area but smaller mesopore volume and diameter compared to the host montmorillonite. The decrease in mesopore volume and diameter indicated that some of the pores might have been blocked by the pillaring process.

Bentonite with 8-hydroxy quinoline immobilized on its surface had q_m from 51.12 to 56.55 mg g^{-1} (b = 0.315 to 0.627 L mg^{-1}) for Cu(II)[70] and 139.08 to 142.94 mg g^{-1} (b = 0.103 to 0.307 L mg^{-1}) for Pb(II)[71] at 293 to 323 K. Adsorption occurred through silanol –OH groups. Adsorption of Cu(II) on 2,2′-dipyridyl immobilized bentonite followed a similar mechanism[72] with Langmuir capacity of 49.44 to 54.07 mg g^{-1} (b = 4.33×10^{-2} to 0.208 L mg^{-1}) at 293 to 323 K.

Montmorillonite intercalated with dimethyl sulfoxide/3-aminopropyltriethoxysilane ($M_{DS/ASP}$) and pyridine/3-aminopropyltriethoxysilane ($M_{P/ASP}$) showed higher Langmuir capacity for Hg(II) [$M_{P/ASP}$: 1.77 ± 0.12 mmol g^{-1}, $M_{DS/ASP}$: 1.56 ± 0.12 mmol g^{-1}; raw clay: 1.23 ± 0.12 mmol g^{-1}] at pH 3.0 after an interaction time of 360 min and temperature 298.15 ± 0.2 K.[173] Adsorption depended on the nature of the complex formed on the internal and external surface as well as on the affinity of Hg(II) for the organic part.

Adsorption of Ni(II) on montmorillonite K10 and 3-mercaptopropyltrimethoxy-silane-montmorillonite K10 had monolayer capacities of 2.10 mg g^{-1} (b = 0.010 L mg^{-1}) and 4.73 mg g^{-1} (b = 0.157 L mg^{-1}) at 298 K.[74] The thiol groups on the surface of the modified clays were shown to be responsible for enhanced retention of Ni(II).

Bentonite modified with octadecylbenzyldimethylammonium cations was more efficient in removing As(V) (q_m: 1.48 mg g^{-1}, b: 0.11 L mg^{-1}) than As(III) (q_m: 0.82 mg g^{-1}, b = 0.17 L mg^{-1}) at 306 ± 1 K.[68] It was proposed that As(V) was held through formation of outer-sphere complex *via* surface anion exchange while inner-sphere complex at Si–O and Al–O groups at particle edges led to As(III) adsorption.

Montmorillonite modified with 3-(2-aminoethylamino)propyltrimethoxysilane had higher Langmuir capacity[174] [Cd(II): 12.9, Pb(II): 13.8, Cu(II): 36.0 mmol kg^{-1}] than the ones modified with 3-amino-propyltriethoxysilane [Cd(II): 7.0, Pb(II): 9.7, Cu(II): 28.0 mmol kg^{-1}] and unmodified montmorillonite [Cd(II): 5.3, Pb(II): 7.5, Cu(II): 11.0 mmol kg^{-1}]. The amino-functionalization had created high affinity sites on the clay for holding metal cations. It was shown that the metal cations were bound in monodentate mode to the amino groups, resulting in enhanced binding efficiency.

Ca-montmorillonite modified with humic acid had higher Langmuir capacity for Cr(III) (q_m: 15.7 mg g^{-1}, b: 0.300 L mg^{-1}), Cu(III) (q_m: 15.3 mg g^{-1}, b: 0.029 L mg^{-1}) and Cd(II) (q_m: 14.1 mg g^{-1}, b: 0.030 L mg^{-1}) than the raw clay [Cr(III) q_m: 12.4 mg g^{-1}, b: 0.231 L mg^{-1}; Cu(II) q_m: 12.6 mg g^{-1}, b: 0.026 L mg^{-1}; Cd(II) q_m:

11.9 mg g^{-1}, *b*: 0.024 L mg^{-1}].[66] Humic acid introduced multiple functional groups to the clay surface and the cations complex with these more effectively.

Olu-Owolabi *et al.*[58] reported Cd(II) and Cu(II) Langmuir capacities in the order of goethite/humic acid-modified bentonite (Cd(II): 16.00 mg g^{-1}, Cu(II): 16.42 mg g^{-1}) > humic acid modified bentonite (Cd(II): 15.92 mg g^{-1}, Cu(II): 16.13 mg g^{-1}) > goethite modified bentonite (Cd(II): 12.34 mg g^{-1}, Cu(II): 13.91 mg g^{-1}) > raw clay (Cd(II): 11.26 mg g^{-1}, Cu(II): 11.29 mg g^{-1}) at 323 K. The modified bentonites had higher CEC than the raw clay. The empty d-orbital of Cu(II) was shown to be responsible for giving rise to better complexation between Cu(II) and –OH/COOH groups on the surface rather than the filled d-orbital of Cd(II). It was also suggested that adsorption of Cd(II) was more likely *via* 5s orbital instead of 4d orbital.

Smectite (S) pillared with $(Al_{13}O_4(OH)_{24}(H_2O)_{12}{}^{7+}$, $Ti(OC_2H_5)_4$, $Cr_3(OH)_4{}^{4+})$ and $ZrOCl_2 \cdot 8H_2O$, and organo-functionalized with 3-aminopropyltriethoxysilane (APS)[175] had larger Pb(II) Langmuir capacities [9.98 × 10^3 mg g^{-1} ($S_{Zr/APS}$), 9.37 × 10^3 mg g^{-1} ($S_{Cr/APS}$), 8.91 × 10^3 mg g^{-1} ($S_{Ti/APS}$), 7.83 × 10^3 mg g^{-1} ($S_{Al/APS}$)] than natural smectite [6.81 × 10^3 mg g^{-1}] at pH 5.0, temperature 298 ± 0.2 K. Chemical modification was shown to be responsible for making the clay more porous with Pb(II) ions easily entering into the clay structure and interacting with the reactive basic groups anchored in the intercalated smectite.

Very recently, natural and acid-activated sepiolites were functionalized by covalent grafting [3-(2-aminoethylamino) propyl]trimethoxy-silane and were successfully used for removal of Cr(VI) from water.[78] The differences in Langmuir adsorption capacities of organo-functionalized sepiolite (q_m = 52.99 mg g^{-1}, $b = 0.026$ L mg^{-1}) and acid-activated organo-functionalized sepiolite ($q_m = 80.84$ mg g^{-1}, $b = 0.028$ L mg^{-1}) at pH = 2.0 were explained on the basis of protonation of the amine groups and electrostatic attraction of Cr(VI) anionic species.

Pb(II) adsorbed on mercapto-functionalized sepiolite endothermically and the Langmuir capacity increased from 67.62 ± 5.71 to 95.63 ± 6.31 mg g^{-1} in the temperature range, 289.15 to 318.15 K.[79] It was shown that the metal ions were prone to stable complexation with ligands containing soft donor atoms. XPS analysis revealed that one Pb(II) ion reacted with two mercapto groups to form bidentate complex species.

Chitosan immobilized on bentonite showed preferential adsorption for Pb(II) (q_m: 26.385 mg g^{-1}, *b*: 9.974 L mg^{-1}) over Cu(II) (q_m: 21.552 mg g^{-1}, *b*: 0.073 L mg^{-1}) and Ni(II) (q_m: 15.823 mg g^{-1}, *b*: 0.039 L mg^{-1}).[176] Pb(II), being highly electronegative, interacted strongly with –OH and $–NH_2$ groups of modified clay compared to Cu(II) and Ni(II).

Bentonite–polyacrylamide composites had higher Langmuir capacity than the raw bentonite for Cu(II)[177] [Bentonite q_m: 29.43 mg g^{-1}; *b*: 0.45 L mg^{-1} at pH 6.2 and q_m: 19.89 mg g^{-1}, *b*: 0.66 L mg^{-1} at pH 5.0; Bentonite–polyacrylamide composites q_m: 32.81 mg g^{-1}, *b*: 0.19 L mg^{-1} at pH 6.2 and q_m: 19.89 mg g^{-1}, *b*: 0.46 L mg^{-1} at pH 5.0]. The increased adsorption capacity was linked to interactions between the lone pair electron of N on the composite surface and empty orbital of Cu(II).

Şölenera *et al.*[75] found that Langmuir capacity for Pb(II) adsorption on clay–poly(methoxyethyl)acrylamide composite varied from 3.46 × 10^{-4} mol g^{-1} (b = 4.13 × 10^3 L mol^{-1} at 293 K) to 3.91 × 10^{-4} mol g^{-1} ($b = 8.02 \times 10^3$ L mol^{-1} at 323 K). The presence of olefinic double bonds, carbonyl and amine groups played an active role to attach Pb(II) to the composite.

A novel chitosan–clay (heulandite)–magnetite composite was used for As(V) (q_m: 6.50 mg g^{-1}, *b*: 0.015 L mg^{-1}) and Cu(II) (q_m: 14.30 mg g^{-1}, *b*: 0.176 L mg^{-1}).[178] The nano-magnetite and chitosan provided additional adsorption sites on clay.

Pb(II), Mn(II) and Zn(II) from aqueous solution were taken up by natural and 3-aminopropyltriethoxysilane modified nontronite[179] with comparatively large adsorption capacities [Pb(II): 13.329 and 24.799 mmol g^{-1}; Mn(II): 13.015 and 23.256 mmol g^{-1}; Zn(II): 12.269 and 23.098 mmol g^{-1} for nontronite and modified nontronite respectively]. The OH groups anchored in the natural nontronite contributed to the adsorption capacity and the free pair of electrons on the C-atoms in the modified adsorbent definitely boosted the adsorption of metal cations. Besides, the modified adsorbent had larger CEC (126.8 mmol per 100 g) compared to the original (87.0 mmol per 100 g).

2.2.4. Zeolites. Natural zeolite was shown to possess higher Cu(II) Langmuir capacity (0.13 mmol g^{-1}) than clay (0.10 mmol g^{-1}) and diatomite (0.05 mmol g^{-1}).[180] Cu(II) was bound to the adsorbents by ion exchange with the exchangeable cations such as Ca(II), Mg(II), K(I) and Na(I). Langmuir monolayer capacities of natural beidellite, zeolite and sepiolite were respectively in the ranges of 794.3 to 841.0 μg g^{-1}, 542.3 to 553.4 μg g^{-1} and 515.7 to 558.0 μg g^{-1} for As(V), and 789.9 to 834.0 μg g^{-1}, 476.6 to 540.5 μg g^{-1} and 477.3 to 512.3 μg g^{-1} for As(III) at 298 to 318 K.[181]

Another natural zeolite, clinoptilolite adsorbed Co(II) more than Cu(II), Zn(II) and Mn(II) with Langmuir capacities of 244.13 (Co(II)), 141.12 (Cu(II)), 1333.85 (Zn(II)) and 76.78 (Mn(II)) mmol kg^{-1}.[182] It was suggested that the metal cations in the form of hexa aqua complex ions with six surrounding water molecules entered the zeolite channeled and since Co(II) possessed the least diameter among the metal ions, it adsorbed maximum, while Mn(II) had minimum adsorption due to its biggest diameter. Wang *et al.*[83] suggested ion-exchange mechanism for Cu(II) and Pb(II) adsorption on natural zeolite tuff with q_m of 23.3 and 78.6 mg g^{-1} respectively. In another work, Shavandi *et al.*[81] reported Langmuir capacity on clinoptilolite of 1.116 mg g^{-1} for Fe(III), 0.076 mg g^{-1} for Mn(II) and 0.015 mg g^{-1} for Zn(II). An exothermic interaction of natural zeolitic volcanic tuff with Pb(II) was reported by Karatas[82] with Langmuir capacities of 16.81, 14.71 and 13.99 mg g^{-1} for 293 K, 313 K and 333 K respectively for Pb(II) adsorption.

Influence of solution pH, temperature, stirring speed and particle size for Pb(II) adsorption on clinoptilolite was reported by Bektaş and Kara.[183] q_m varied from 71.94 to 92.59 mg g^{-1} (pH: 2.0 to 7.0), 120.48 to 185.18 mg g^{-1} (temperature: 298 to 343 K), 149.25 to 172.41 mg g^{-1}. It was explained that uptake of Pb(II) by clinoptilolite occurred by ion exchange and through physical adsorption when pH was <6.0. Increasing agitation speed reduced the film boundary layer surrounding clinoptilolite particles thus increasing the external film transfer coefficient and hence the rate of uptake.

Clinoptilolite treated with 2 M NaCl at 343 K possessed higher monolayer capacity for Zn(II) than the untreated and HCl

treated samples[184] [clinoptilolite: 21.1 mg g^{-1}, clinoptilolite treated with 2 M NaCl: 20.8 mg g^{-1}, clinoptilolite treated with 2 M NaCl at 343 K: 22.2 mg g^{-1}, clinoptilolite treated with 0.1 M HCl: 17.9 mg g^{-1}]. Conditioning of clinoptilolite with NaCl enhanced adsorption capacities as NaCl caused an increase in Na^+ and a decrease in Ca^{2+} concentrations in clinoptilolite, leading to an increase of the ratios Na^+/K^+ and Mg^{2+}/Ca^{2+}. Conditioning with NaCl solution might also have removed fine dust particles from the surface of clinoptilolite crystals.

Qiu and Zheng[185] synthesized a cancrinite-type zeolite from fly ash and found that it had Langmuir capacities of 2.13, 2.08, 1.53, 1.24 and 1.15 mmol g^{-1} for Pb(II), Cu(II), Ni(II), Co(II) and Zn(II) respectively. The small differences were shown to be due to size differences of the hexaaqua complex ions.

Nibou *et al.*[84] reported higher Langmuir capacity of NaA zeolite for Zn(II) than NaX zeolites (NaA: 118.91 mg g^{-1}, NaX: 106.38 mg g^{-1}) at 298 K. The zeolites contained mineral impurities such as Ca, Mg, Fe and K which could interfere in the exchange of Zn(II) with Na(I). In addition, NaA and NaX had small particles with average size of 4 and 3 μm and higher internal surface areas of 280 and 375 m^2 g^{-1} respectively which allowed Zn(II) cations to access and diffuse into the framework structures.

Langmuir capacities of mordenite for Pb(II) varied from 13.95 to 24.48 mg g^{-1} at 293 to 323 K.[186] Mordenite [$(Ca, Na_2, K_2)_4 Al_8Si_{40}O_{96}\cdot 28H_2O$] with an open structure of 8- and 12-membered rings (2.6 × 5.7 and 6.7 × 7.0 Å, respectively) provided easy access to Pb(II) cations for adsorption inside the channels.

Langmuir capacity of As(III) on $Fe(NO_3)_3$ modified zeolite was 40.48 μmol L^{-1} where Fe–OH groups on the adsorbent surface were proposed as the adsorption sites.[187] In a similar study, Javadian *et al.*[89] reported Langmuir capacity of zeolite-based geopolymer for Cd(II) of 26.246 mg g^{-1}. The removal mechanisms included not only adsorption but also reaction with the oxides of iron and aluminum on the surface of zeolite.

A comparative study was reported by Chao and Chen[131] for adsorption of Cd(II), Cu(II), Ni(II), Pb(II) and Zn(II) on NaY and hexadecyltrimethylammonium-NaY zeolites. The Langmuir capacities on NaY were in the order Pb(II) (671 mmol kg^{-1}) > Cd(II) (390 mmol kg^{-1}) > Zn(II) (354 mmol kg^{-1}) > Cu(II) (371 mmol kg^{-1}) > Ni(II) (331 mmol kg^{-1}). Ion exchange being the primary mechanism, the adsorption capacities depended on the ion radius with highest adsorption for Pb(II) and least for Ni(II). Adsorption of cations onto hexadecyltrimethylammonium-NaY occurred through both ion exchange and complexation reactions and/or surface precipitation and the adsorption capacities were in the order of Pb(II) (653 mmol kg^{-1}) > Cu(II) (388 mmol kg^{-1}) > Cd(II) (351 mmol kg^{-1}) > Zn(II) (318 mmol kg^{-1}) > Ni(II) (315 mmol kg^{-1}). The presence of the hexadecyltrimethylammonium units on zeolite surface had covered or blocked some of the pores, resulting in slight decreases in the apparent surface area and pore volume. But N atoms in hexadecyltrimethylammonium-ions led to greater adsorption of Cu(II) through complexation reactions. Functional groups containing N atoms could provide nonbonding electrons to coordinate with divalent metals and as Cu(II) possessed relatively higher ability to form such complexes, the adsorption capacity of modified zeolite toward Cu(II) was greater than that of the NaY zeolite.

Nezamzadeh-Ejhieh and Kabiri-Samani[87] reported exothermic interactions of Ni(II) with dimethylglyoxime treated clinoptilolite with q_m decreasing from 0.96 to 0.13 mmol g^{-1} (temperature 293 to 333 K). The authors suggested a complex formation between Ni(II) and dimethylglyoxime through the free electron pairs of nitrogen atoms. Langmuir capacity of hexadecyltrimethylammonium-modified clinoptilolite for Cr(VI) decreased several times (5.07 to 0.21 mg g^{-1}) when the temperature of adsorption was raised from 288 to 298 K.[188] $HCrO_4^-$ anions were shown to have bound to ammonium groups.

Langmuir capacities of humic acid immobilized-cetylpyridinium-modified zeolite for Cu(II) increased from 19.8 to 21.5 mg g^{-1} in the temperature range, 298 to 318 K.[88] Adsorption of Cu(II) took place *via* surface complexation with –COOH and ph–OH groups of immobilized humic acid molecules and also through ion exchange with the exchangeable cations in the internal zeolite channels.

2.2.5. Oxides and modified oxides. Adsorption of Cu(II) on protonated and aminated mesoporous alumina yielded Langmuir capacities of 8.55 and 7.09 mg g^{-1} (b: 0.31 and 0.25 L g^{-1}).[112] The interconnected pore system of mesoporous alumina could reduce transport limitations and enhanced the accessibility of the active sites and help in adsorption process. Langmuir capacities for Cd(II) and Pb(II) on activated alumina were 35.06 mg g^{-1} ($b = 0.139$ L mg^{-1}) and 83.33 mg g^{-1} ($b = 0.052$ L mg^{-1}) respectively at 303 K.[111] Langmuir capacity of mesoporous alumina for As(V) was 5.1 times more than that of commercial alumina (mesoporous alumina: 61.3, alumina: 12.1 mg g^{-1}).[189] $Al(OH)_3$ present on hydrated alumina surface at neutral pH could form either $H_2AsO_4^-$ or $HAsO_4^{2-}$ accompanied by release of OH.

Adsorption of Cd(II) on Al_2O_3 was proposed to be mostly specific adsorption on surface sites (Al–OH) accompanied by formation of monodenate or bidenate complexes with $Al–O^-$ with Langmuir capacity of 89.28 mg g^{-1} at 303 K.[95]

γ-Al_2O_3 [synthesized from $NaAlO_2$ by precipitation with H_2SO_4 at different temperatures (298 or 353 K) and at different pH (6.0, 7.0 or 8.0) subsequently calcined at 773 K] adsorbed Cd(II), Pb(II) and Zn(II)[190] with Langmuir capacities of Pb(II) (9.86 to 13.11 mg g^{-1}) > Cd(II) (5.34 to 8.24 mg g^{-1}) > Zn(II) (5.27 to 7.16 mg g^{-1}). The values were conforming to the decreasing order of the atomic radii: Pb (1.75 Å) > Cd (1.54 Å) > Zn (1.38 Å). Large ionic radius resulted in a weaker repulsion from the positively-charged alumina surface, favoring adsorption on larger pores.

Kailasam *et al.*[191] utilized phosphonic acid modified silica polyamine composite with successive immobilization by Zr(IV) for adsorption of As(V) and measured the Langmuir adsorption capacity of 98.0 mg g^{-1} (b: 0.016 l g^{-1} at pH 4.0) and 55.0 (b: 0.018 L g^{-1} at pH 6.0). Maximum adsorption at pH 4.0 corresponded with the predominant As(V) species, $H_2AsO_4^-$.

Amino-functionalized mesoporous silica (NH_2-MCM-41) showed preferential adsorption of Pb(II) over Cd(II) and Ni(II)[116] with q_m of 57.74 mg g^{-1} (b: 0.035 L mg^{-1}), 18.25 mg g^{-1}

(b: 0.253 L mg^{-1}) and 12.36 (b: 0.225 L mg^{-1}) mg g^{-1} respectively at 298 K.[116] Adsorption resulted in complex formation between metal ions and N atoms of NH_2 functional groups.

Organo-functionalized silica with 3-aminopropyltrimethoxysilane (APTMS) held Cu(II)[115] with Langmuir capacities of 0.485 to 0.850 mmol g^{-1} for different APTMA : silica ratio at 303 ± 2 K. Increasing the concentration of amino groups on the surface of silica resulted in an increased affinity towards Cu(II).

Poly(ethyleneimine) coated silica (silica/PEI) and silica/PEI crosslinked with glutaraldehyde (silica/PEI/GA) had shown large Langmuir capacities for Cd(II), Ni(II), Pb(II) and Zn(II)[192] [Pb(II): 50.76, 82.64 mg g^{-1}, Zn(II): 32.79, 52.08 mg g^{-1}, Ni(II): 18.62, 28.25 mg g^{-1}, Cd(II): 29.32, 38.46 mg g^{-1} for silica/PEI/GA and silica/PEI respectively]. Crosslinking with GA decreased the amount of available amine groups causing a decrease in metal ion uptake.

Thiol-functionalized silica yielded q_m of 117.51 ± 5.16 mg g^{-1} (b: 3.51 ± 0.88 L mg^{-1}) and 33.72 ± 1.23 mg g^{-1} (b: 2.49 ± 1.25 L mg^{-1}) respectively for Pb(II) and Cd(II) at 298 K.[117] Adsorption was through the formation of bidentate and monodentate complexes with thiol groups wherein it was suggested that the metal cations interacted with the highly electronegative S atoms on the surface and shifted the sulfur binding energies to less positive ranges compared to the binding energies of bound thiol groups.

N-[3-(Trimethoxysilyl)propyl]-ethylenediamine grafted silica was shown to be a better adsorbent for Cu(II) and Pb(II) than unmodified silica[193] [silica-Pb(II) q_m: 0.02 mmol g^{-1}, b: 5.09 L $mmol^{-1}$; silica-Cu(II) q_m: 0.04 mmol g^{-1}, b: 1.75 L $mmol^{-1}$; modified silica-Pb(II) q_m: 0.18 mmol g^{-1}, b: 9.10 L $mmol^{-1}$; modified silica-Cu(II) q_m: 0.26 mmol g^{-1}, b: 12.54 L $mmol^{-1}$ at 293 K]. Two novel silica gel-based hybrid composites (with amidoxime immobilized *via* sulfur-containing spacer arm) were effective Hg(II)-adsorbents[194] with q_m of 0.56 to 0.90 mg g^{-1} (composite I) and 0.57 to 0.74 mg g^{-1} (composite II) at 288 to 308 K. In the endothermic interactions, both sulfur and amidoxime present in the adsorbents were suggested to be responsible for chelating Hg(II).

Al_2O_3-supported iron oxide showed q_m for Pb(II) of 0.09 to 0.14 mmol g^{-1} (b: 17.5 to 48.13 mM^{-1}) at 288 to 318 K. The presence of α-FeOOH as well as large surface area might be responsible for Pb(II) uptake.[103]

Su *et al.*[96] observed the preferential adsorption of Hydrous MnO_2 could adsorb Pb(II), Cd(II) and Zn(II) in the order Pb(II) (1.58 mmol g^{-1}) > Cd(II) (1.25 mmol g^{-1}) > Zn(II) (0.83 mmol g^{-1}) at 298 K, the differences were explained on the basis of the relative softness of the metal cations, electrostatic interaction and inner-sphere complex formation.

Langmuir capacities of $ZrO_2 \cdot nH_2O$ for Cr(VI) increased from 61.0 to 66.0 mg g^{-1} (b: 0.43 to 0.67 L mg^{-1} at 298 to 338 K), indicating endothermic interactions.[91] The low solubility, high thermal stability, amphoteric character and good resistance to oxidizing agents facilitated the adsorbent to interact with Cr(VI).

Naeem *et al.*[195] reported Co(II) adsorption on NiO by an endothermic process with Langmuir capacities of 8.13×10^{-5} to 8.93×10^{-5} mol g^{-1} (at 303 to 323 K). The adsorption capacities increased from 6.41×10^{-5} to 17.61×10^{-5} mol g^{-1} in the pH range of 7.0 to 8.5. It was suggested that increase in hydroxyl ions would dissociate more protons from NiOH surface groups on NiO leaving the surface negatively charged for uptake of Co(II) cations. NiO nanoparticles were shown to possess large Cd(II) and Pb(II) Langmuir capacities of 625.0 mg g^{-1} (b: 1.734 L mg^{-1}) and 909.0 mg g^{-1} (b: 9.478 L mg^{-1}) respectively at 303 K.[94] It was suggested that, due to smaller hydrated ionic radii, Pb(II) moved faster than Cd(II) to the adsorption sites on NiO nanoparticles.

Langmuir capacities of ZnO followed the trend Hg(II) (q_m: 714 mg g^{-1}, b: 4.686 L mg^{-1}) > Cd(II) (q_m: 384.0 mg g^{-1}, b: 1.814 L mg^{-1}) > Zn(II) (q_m: 357.0 mg g^{-1}, b: 0.753 L mg^{-1}).[92] Again, due to smaller hydrated ionic radii, Hg(II) moved faster to the adsorption sites with fewer weakly bound water molecules. The higher electronegativity of Hg(II) (2.0) compared to the others attracted Hg(II) much more strongly to the potential adsorption sites on ZnO. Recently, Venkatesham *et al.*[93] have reported that the larger surface area of nano ZnO might play an important role for Pb(II) adsorption with $q_m = 26.11$ mg g^{-1} and $b = 0.004$ L g^{-1}.

Endothermic Langmuir capacity of Co(II) on $Mg(OH)_2$ varied from 95.24 to 125.00 mg g^{-1} at 298 to 318 K.[196] The scattering of small solid flakes on top of one another during adsorption was show to indicate formation of the adsorbed layer on the crystal surface and edges of $Mg(OH)_2$ particles.

Langmuir capacity for As(V) on Fe_3O_4 nanoparticles (prepared from waste red mud) was 400 μg g^{-1}. The interaction between positive charge of adsorbent surface and $H_2AsO_4^-$ species might be responsible for As(V) removal process.[102] Adsorption of Pb(II) on Fe_3O_4 nanoadsorbents was shown to be electrostatic[101] with q_m of 0.14 to 0.17 mmol g^{-1} (b: 24.6 to 33.1 L $mmol^{-1}$ at 298 to 328 K).

As(V) adsorption on $CuFeO_4$ was influenced by solution pH and the Langmuir capacities varied from 45.66 to 15.06 mg g^{-1} in the pH range, 3.7 to 11.2 at 300 ± 1 K.[197] At lower pH (<7.3), the positively charged copper ferrite surface favoured adsorption of anionic As(V) species. At higher pH, negative charges on both adsorbent and adsorbate, led to electric repulsion and decreased the uptake of As(V).

Bimetal oxide magnetic nanomaterials, $MnFe_2O_4$ and $CoFe_2O_4$, adsorbed As(III) and As(V) more than Fe_3O_4 [q_m $MnFe_2O_4$: As(III) 93.8 mg g^{-1}, As(V) 90.4 mg g^{-1}; $CoFe_2O_4$: As(III) 100.3 mg g^{-1}, As(V) 73.8 mg g^{-1}; Fe_3O_4: As(III) 49.8 mg g^{-1}, As(V) 44.1 mg g^{-1}].[104] Adsorption occurred through replacement of OH groups on metal oxides with As(III) and As(V) forming monodentate, bidentate mononuclear and bidentate binuclear complexes. Replacement of Fe^{2+} with Mn^{2+} and Co^{2+} resulted in a significant increase in M–OH species in the magnetic nanomaterials.

Langmuir capacity of glutaraldehyde-3-aminopropyltriethoxysilane modified Fe_3O_4 nanoparticles for Cu(II) was 0.96 mmol g^{-1} at pH 4.0 (293 ± 1 K).[107] At low solution pH, protonation of –CH=N– (imine) groups of the adsorbent led to formation of $-CH{=}NH^+-$, causing electrostatic repulsion of Cu(II). At pH ≥ 4, the reaction was accompanied by an increase in the number of deprotonated imine groups (–CH=N–), thus, increasing the adsorption of Cu(II) cations.

Modification of Fe_3O_4 with cetyltrimethylammonium bromide (CTAB) enhanced As(V) adsorption capacity (q_m for

Fe_3O_4: 7.59 mg g^{-1}, Fe_3O_4@CTAB: 23.07 mg g^{-1}).[108] The positively charged CTA^+ on Fe_3O_4 surface could attract the negatively charged As(v) anions and CTA–As(v) complex was formed.

Modification of Fe_3O_4 nanoparticles with carboxymethyl-β-cyclodextrin polymer, Langmuir capacities for Pb(II), Cd(II) and Ni(II) were sufficiently boosted (Pb(II): 20.01 to 64.50 mg g^{-1}, Cd(II): 17.01 to 27.70 mg g^{-1}, Ni(II) 8.83 to 13.20 mg g^{-1}).[109] The multiple oxygen containing groups (–OH and –COOH) on the surface in the modified adsorbent supported complex formation with metal cations. Adsorption of Pb(II) on amino-functionalized Fe_3O_4 magnetic nano-particles yielded Langmuir capacity of 40.10 mg g^{-1}.[110]

Cd(II) adsorption on SiO_2, $Fe(OH)_3$ and an equimolar mixture (0.5 M SiO_2–0.5 M $Fe(OH)_3$)[198] was higher for the mixture (0.10–0.11 mmol g^{-1}) than either for $Fe(OH)_3$ (0.08–0.09 mmol g^{-1}) or SiO_2 (0.03–0.04 mmol g^{-1}) at 288–318 K. The increased adsorption of Cd(II) on the mixed oxide indicated that the surface groups, FeO^- and SiO^-, were involved in adsorption. When the mixed oxide was prepared by physical mixing or by sequential precipitation, the latter adsorbed more Cd(II) (q_m: 9.81 × 10^{-2} to 10.64 × 10^{-2} mmol g^{-1} at 303 to 323 K).[199] Formation of ternary complexes ($SOH + Cd^{2+} + H_3SiO_4^- \leftrightarrow SH_3SiO_4^- \cdot Cd^{2+} + OH^-$ where SOH was present on the adsorbent surface) might also be responsible for higher adsorption.

Pb(II) adsorption on nano TiO_2–SiO_2 showed Langmuir capacities of 97.46 to 203.25 μmol g^{-1} (*b*: 0.05 to 0.78 L μmol^{-1} at 298 to 325 K).[98] Preparation of the adsorbent by coprecipitation influenced properties like specific surface area, porosity, acidic sites, *etc.* of each component with additional influence on adsorption characteristics. Pb(II) may be bonded to adsorbent surface *via* surface oxygen atoms and proton release.

As(v) removal by a binary mixed oxide of iron and silicon was influenced by solution pH Langmuir capacities of 2.76 × 10^{-4} to 1.72 × 10^{-4} mol g^{-1} (pH 5.0 to 8.0) at 298 K.[200] The authors reported higher As(v) adsorption for uncalcined mixed oxide (27.60 × 10^{-5} mol g^{-1}) than for calcined samples (mixed oxide calcined at 573 K: 25.85 × 10^{-5} mol g^{-1} > mixed oxide calcined at 723 K: 9.98 × 10^{-5} mol g^{-1} > mixed oxide calcined at 1023 K: × 10^{-5} mol g^{-1}). It was shown that the small pores on the surface of mixed oxide particles disappear after heat treatment due to sintering resulting in surface area reduction. The authors suggested As(v) adsorption by displacement of the surface hydroxyl groups.

Langmuir capacity for As(v) on Ce doped Fe-oxide was 70.4 mg g^{-1} (*b*: 10.91 L mg^{-1}) at 293 K.[105] The adsorbent surface could be considered as amphoteric with surface hydroxyl groups (M–OH) playing an important role in As(v) adsorption.

As(v) adsorption on Fe–Ce bimetal oxide[201] yielded q_m of 2.0 mmol g^{-1} at 293 K significantly higher than that of Fe oxide (0.35 mmol g^{-1}) and of Ce oxide (0.45 mmol g^{-1}). It was suggested that As(v) anion replaced OH in Fe–OH by forming diprotonated monodentate mononuclear complexes. Ce could break magnetite structure of Fe(II)/Fe(III) system through oxidation of Fe^{2+} and to activate Fe atoms to form more Fe–OH.

2.2.6. Other inorganic solids. Tannin-immobilized calcined hydrotalcite showed endothermic interactions for Cd(II), Cu(II) and Zn(II) at 303 to 333 [q_m: Cd(II): 74.9 to 98.7 7 mg g^{-1}, Cu(II): 81.4 to 103.5 7 mg g^{-1}, Zn(II): 78.9 to 101.7 mg g^{-1}].[118] The modified hydrotalcite could react with metal cations through multiple mechanisms involving dispersive forces, diffusion, ion-exchange and complex formation.

Loess soil had good Langmuir capacities for Cd(II) of 6.68 to 9.37 mg g^{-1} at 278–318 K,[123] which was related to reactions between. Cd(II) and aluminum silicate to form $CdSiO_3$ and a surface complex, $CdAl_2(SiO_4)_2$. In another work, endothermic interactions of Zn(II) with Chinese loess soil showed larger Langmuir capacities of 70.8 to 83.2 mg g^{-1} (288–318 K).[202]

The clay mineral, illite (2 : 1 layered) constitutes about 70–90% of the loamy sand soil by weight and it has high net negative charge due to isomorphous substitution in the silica tetrahedra that creates ion-exchange sites. The hydroxyl groups, including SiOH and AlOH in the mineral edges were shown to be effective in adsorbing Cr(VI) and Pb(II) with monolayer capacities of 1570 and 2168 mg kg^{-1} respectively.[124]

Adsorption of As(v) on lithium/aluminum layered double hydroxide intercalated with chloride (Li/AlLDH-Cl) was shown to have a very large adsorption capacity (q_m: 322.58 mmol kg^{-1}) when compared to that of untreated gibbsite (51.55 mmol kg^{-1}).[203] Treatment with LiCl brought intercalation of Li cations into the host structure of $Al(OH)_3$ to form the layered double hydroxide. Li cations occupied the vacant octahedral holes within $Al(OH)_3$ and transformed $Al(OH)_3$ layers into active adsorption sites with high affinity for As(v).

Lignite (30–60 g) adsorbed Cu(II) from 4.045 to 2.625 mg g^{-1} (*b*: 0.038–0.056 L mg^{-1}).[204] Oxygen-containing groups like carboxyl (–COOH), alcoholic (–OH) and carbonyl (=C=O) acyed as the active centers of adsorption.

Exothermic adsorption of Cr(VI) on dolomite had q_m from 10.01 to 5.67 mg g^{-1} (*b*: 0.272 to 0.144 L mg^{-1} at 293–333 K) with OH^- and HCO_3^- groups playing the active role.[205]

Langmuir capacities for Pb(II) and Zn(II) on francolite decreased substantially with increasing temperature [Pb(II): 1208.00 to 128.90 mg g^{-1}, Zn(II): 126.70 to 38.45 mg g^{-1} at 303 to 333 K].[206] Adsorption was shown to be due to exchange of Ca^{2+} with Pb(II) and the larger ionic radius of Pb(II) favoured the ion exchange.

Adsorption of Pb(II) on palygorskite by an endothermic route had Langmuir capacities of 8.4 × 10^{-5} to 1.0 × 10^{-4} mol g^{-1} in the temperature range, 293.15 to 313.15 K.[207] It was shown that at higher temperature, a large number of =Al–OH and =XNa sites participated in adsorption.

Langmuir capacities of laterite for As(v) varied from 0.15 to 0.14 mg g^{-1} (pH 5.5 to 7.0), 0.13 to 0.28 mg g^{-1} (293 to 315 K) and 0.51 to 0.31 mg g^{-1} (ionic strength 0.01 to 0.00 mol L^{-1}).[208] The oxides present on the surface were shown to be responsible for As(v) adsorption. A low-grade phosphate was shown to have larger adsorption capacity for Zn(II) than Cd(II) [Zn(II): q_m 10.32 mg g^{-1}, *b*: 0.23 L mg^{-1}; Cd(II): q_m 7.54 mg g^{-1}, *b*: 0.20 L mg^{-1}] at 298 ± 1 K.[209] The results might have been affected by the larger size of Cd(II) compared to that of Zn(II).

Langmuir capacity of synthetic hydroxy apatite for Pb(II) was found to be marginally higher (0.44 mmol g^{-1}) than that of natural apatite (0.40 mmol g^{-1}).[121] Zhu *et al.*[210] used Ca-deficient

hydroxyapatite for Cd(II) and Pb(II) removal with Langmuir capacities of 23.04 and 19.93 mg g^{-1} respectively. Nano hydroxyapatite adsorbed Pb(II) (1000.00 mg g^{-1}) much more than Cd(II) (142.857 mg g^{-1}) and Ni(II) (40.00 mg g^{-1}). Hard Lewis bases like OH^- and PO_4^{3-} in the nano hydroxyapatite had higher affinity for Pb(II) (borderline hard Lewis acid) than for Cd(II) and Ni(II) (soft Lewis acids).

Tourmaline had Pb(II) Langmuir capacity of 200 mg g^{-1} (b: 0.01 L mg^{-1}).[122] Tourmaline acted as an electric dipole with small, separate electric fields and Pb(II) ions were held through electrostatic attraction. By crushing tourmaline into small particles, the cations in tourmaline (*e.g.* Mg^{2+}, Ca^{2+}, Na^+) became exposed along different directions of the crystal fracture and these were lost to water in a tourmaline suspension creating negative tourmaline surface ready for Pb(II).

Very high adsorption capacity for Cd(II) ($q_m = 434.78$ mg g^{-1}, $b = 0.077$ L mg^{-1}) and Cu(II) ($q_m = 357.14$ mg g^{-1}, $b = 0.094$) was recently reported for goethite mineral.[113] Natural minerals (hematite, magnetite and goethite) had also shown appreciable adsorption of As(III) and As(V) from water.[211] The adsorption capacities were: hematite [As(III): $(9.3 \pm 0.2) \times 10^{-6}$, As(V): $(2.9 \pm 0.5) \times 10^{-5}$ mol m^{-2}]; goethite [As(III): $(2.5 \pm 0.1) \times 10^{-6}$, As(V): $(3.0 \pm 0.2) \times 10^{-6}$ mol m^{-2}]; magnetite [As(III): $(3.1 \pm 0.1) \times 10^{-6}$, As(V): $(3.8 \pm 0.2) \times 10^{-6}$ mol m^{-2}]. Adsorption of Cd(II) on boehmite and goethite was shown to have q_m of 3.55 and 5.18 mg g^{-1} respectively.[114] A specific adsorption mechanism was proposed for the process.

Exothermic interactions between *N*-methylimidazole anchored activated palygorskite and Pb(II) yielded Langmuir capacities of 714.29 to 666.67 mg g^{-1} (b: 0.33 to 0.109 L mg^{-1} at 283–313 K).[212]

The presence of $-NH_2$ and –OH groups in hydroxyapatite–chitosan composite favoured adsorption of Pb(II) (q_m: 12.04 mg g^{-1}, b: 0.572 L mg^{-1}), Co(II) (q_m: 10.63 mg g^{-1}, b: 0.349 L mg^{-1}) and Ni(II) (q_m: 8.54 mg g^{-1}, b: 0.211 L mg^{-1}).[213] The hydrated ionic radii of the metal ions (Pb(II) < Co(II) < Ni(II)) ensured that smaller hydrated ions possessing higher ionic mobility and rate of diffusion showed higher adsorption.

Adsorption of Cr(III) and Fe(III) onto chitosan–attapulgite composites was endothermic and the Langmuir capacities increased from 27.03 to 65.36 mg g^{-1} and 36.76 to 62.50 mg g^{-1} respectively (298–318 K).[132] At higher temperature, enlargement of pore volume and surface area along with increased mobility of the ions led to increased adsorption.

Polyaniline–attapulgite composite yielded Langmuir capacities for Hg(II) of 909.1, 813.1 and 781.3 mg g^{-1} at ionic strengths of ($NaNO_3$) 0.01, 0.10 and 1.00 mol L^{-1} respectively.[214] The adsorption capacity of Hg(II) by bare attapulgite and pure polyaniline were <5 mg g^{-1} and <600 mg g^{-1} and it was shown that the fibrous attapulgite acted as a template in the coating of polyaniline, successfully preventing its aggregation and achieved a significantly enlarged surface area. The combined effects led to enhanced Hg(II) removal.

Rectorites had different adsorption capacities for Cr(VI) when modified with dodecyl benzyl dimethyl ammonium chloride (0.97 mg g^{-1}), hexadecyl trimethyl ammonium bromide (2.39 mg g^{-1}) and octadecyl trimethyl ammonium bromide (3.57 mg g^{-1}).[215] The differences were explained on the basis of changes in d-spacing following organic functionalization.

Endothermic adsorption of Pb(II) on beach sand yielded q_m of 22.90 ± 0.27 to 26.80 ± 0.39 μmol g^{-1} (293 to 323 K).[126] The minerals, calcite, quartz and aragonite in the form of carbonates and oxides in the beach sand had negative sites that provided the affinity for Pb(II) cations. The same group of authors reported Langmuir capacity of the beach sand for Zn(II) of 16.9 ± 0.2 μmol g^{-1}.[127]

Iron oxide-coated sand had a larger Langmuir adsorption capacity for As(III) (28.57 μg g^{-1}) in comparison to the uncoated one (5.63 μg g^{-1}) at 300 ± 2 K.[216] The iron oxide-coated sand adsorbed more due to formation of ferrichydroxide in the aqueous solution responsible for coprecipitation of As(III) on the surface of the adsorbent. Li *et al.*[76] used iron oxide nano-particle-immobilized-sand as adsorbent for Cd(II), Cu(II) and Pb(II) with Langmuir capacities of 0.53, 1.26 and 2.09 mg g^{-1} respectively. While ion-exchange was a common process for all the cations, adsorption of Cu(II) was also through inner-sphere surface complexation, and electrostatic attraction was shown to be important in case of Cd(II) and Pb(II). H_2SO_4 treated river sand preferred lower temperature to adsorb Cr(VI) as Langmuir capacities varied from 1.19 mg g^{-1} (298 K) to 1.10 mg g^{-1} (308 K).[129]

During the last few years, nano-scale adsorbents played an active role in metal ion removal scenario. In one such study, Nanoscale zero-valent iron yielded a Langmuir capacity of 135.0 mg g^{-1} at 298 K for As(III).[217] The reactive surface sites were suggested to be stable or metastable iron(II), mixed iron(II)/(III), or iron(III) oxide, hydroxide, or oxyhydroxide. Initially amorphous Fe(II)/(III) and magnetite (or maghemite) were the sites for adsorption, but as the adsorbent corroded over longer periods, more crystalline magnetite and lepidocrocite products were generated for further adsorption of As(III). In addition, As(III) near or in contact with the corroding surface was oxidized to As(V), which was adsorbed by an inner-sphere mechanism. Boparai *et al.*[218] reported q_m of nano zero-valent iron for Cd(II) of 714.30 mg g^{-1} (b: 0.07 L mg^{-1} at 285 K). The standard redox potential of Cd(II) (−0.40 V, 298 K) was very close to that of zero-valent iron (−0.41 V, 298 K) and thus, adsorption was a predominant process.

Adsorption of Cr(VI) on zero-valent iron, Fe–Ni bimetallic nanoparticles and Fe–Ni bimetallic-montmorillonite nanocomposites Kadu and Chikate[62] showed adsorption capacities of 76.92 mg g^{-1} (b = 2.17 L mg^{-1}), 100.00 mg g^{-1} (b = 2.00 L mg^{-1}) and 100.00 mg g^{-1} (b = 3.33 L mg^{-1}) respectively. The lowest adsorption capacity of zero-valent iron was explained on the basis of surface passivation whereas greater uptake of metal–clay composite might be due to synergistic effect of nanoparticles and clay matrix owing to proper dispersion.

It was, however, observed that adsorption of Cr(VI) on magnetite nanoparticles (q_m: 20.13 mg g^{-1}) was more than montmorillonite-supported magnetite nanoparticles (q_m: 13.86 mg g^{-1}) at 298 ± 2 K.[219] The same group of authors[220] used magnetite nanoparticle (Mag), diatomite supported magnetite (MagDt-H) and commercial magnetite (MicroMag) for Cr(VI) adsorption. The magnetite nanoparticles showed the highest monolayer capacity (20.16 mg g^{-1}). Cr(VI) uptake was a

physico-chemical process, including an electrostatic attraction followed by a redox process in which Cr(VI) was reduced to Cr(III) and fixed into iron oxide.

Chen *et al.*[221] reported the use of titanate nanotubes (prepared with microwave intensities of 40, 400 and 700 W) for Pb(II) removal with q_m of 1000, 2000 and 1769 mg g^{-1} respectively at 298 K. Exchange with Na^+ and binding with O-atoms on the adsorbent surface accounted for most Pb(II) removal. In another work, titanate nanotubes were shown to have Langmuir capacities in the order: Pb(II) (2.64 mmol g^{-1}) > Cd(II) (2.13 mmol g^{-1}) > Cu(II) (1.92 mmol g^{-1}) > Cr(III) (1.37 mmol g^{-1}).[99] The differences were explained on the basis of hydration energy of the cations.

Hg(II) adsorption on hybrid mesoporous aluminosilicate sieve (prepared with fly ash and impregnated with zeolite A precursors) yielded Langmuir capacity of 20.66 mg g^{-1} where the electrostatic interactions and ion-exchange mechanism played a role.[80]

Polymetallic sea nodules preferably adsorbed As(V) (q_m: 2.85 to 10.2 mg g^{-1}) than As(III) (q_m: 0.69 to 0.31 mg g^{-1}) (As(III), As(V) 0.2 to 0.1 mg L^{-1}).[222] As(III)–sea nodule surface formed inner sphere complex, while As(V) partially formed inner and partially outer sphere complexes.

Adsorbent prepared from mine tailings had q_m of 20.73 to 46.31 mg g^{-1}, 16.23 to 28.27 mg g^{-1}, 5.36 to 14.96 mg g^{-1}, 3.64 to 5.25 mg g^{-1} and 3.52 to 8.83 mg g^{-1} respectively (303 to 313 K) for Pb(II), Cr(III), Cu(II), Ni(II) and Cd(II).[223] The high tendency of Pb(II) for specific adsorption was due to its high metal electronegativity. Cu(II) and Ni(II) have similar electronegativities and ion radii, but Cu(II) was adsorbed more since it was bound mainly as the hydroxy complex. On the other hand, large ionic radius of Cd(II) worked against its entry into the interlayers and steric hindrance and lower electrostatic attraction limited its complexation

The influence of soil particle size (sand, coarse silt, fine silt and clay) on Cd(II) adsorption was reported by Roth *et al.*[224] The Langmuir capacities were in the range of 0.19 to 0.50 mg g^{-1}. Generally the granulometric part of the soil had better adsorption, with or without organic matter. The authors suggested that organic matter widely influences the isotherms. Coarse and fine silt, and also clay have numerous adsorption sites. Humic substances make the surface more negative and enhance adsorption of metal cations.

Adsorption on a geopolymer at pH 4.0 was in the order of Pb(II) (147.06 mg g^{-1}) > Cd(II) (67.57 mg g^{-1}) > Cu(II) (48.78 mg g^{-1}) > Cr(III) (19.94 mg g^{-1}).[225] The differences were explained on the basis of ion mobility, energy of hydration, *etc.*

Industrial by-products have also been investigated for uptake of metal ions from aqueous system. In one such work, interaction of Cu(II) with limestone yielded q_m of 0.29 mg g^{-1} at pH 7.0 (298 K).[226] Adsorption of Cu(II) was suggested to take place *via* H-bonding and surface precipitation of the metal cations as colloidal insoluble hydroxide, $Cu(OH)_2$, forming successive layers on the adsorbent surface.

By using marble wastes as adsorbent for Zn(II), Gazy and Gad[227] obtained Langmuir capacity of 175.13 mg g^{-1}. Zn(II) ions were chelated to O-atoms on the marble surface together with ion exchange between Zn(II) and Ca(II). Similarly, talc was shown to have Langmuir capacities for Pb(II) of 7.99 to 4.26 mg g^{-1} in the temperature range, 293 to 343 K.[228]

Bagasse fly ash (from sugar industry) yielded exothermic Langmuir capacities of Cr(VI): 2.50 to 2.10 mg g^{-1} and Pb(II): 4.35 to 4.25 mg g^{-1} (303 to 323 K).[229] However, the interactions were endothermic for Cu(II): 2.26 to 2.36 mg g^{-1} and Zn(II) 2.34 to 2.54 mg g^{-1},[230] and for Cd(II): 1.24 to 2.00 mg g^{-1} and Ni(II): 1.12 to 1.70 mg g^{-1} (ref. 231) in the same temperature range. The presence of oxides (SiO_2, Al_2O_3, CaO, Fe_2O_3, MgO) and the minerals, mullite, haematite, kaolinite, α-quartz, γ-alumina, and geolite on fly ash helped adsorption. In another study, fly ash (from thermal power plant) showed exothermic adsorption of Cu(II) (q_m: 5.71 to 5.56 mg g^{-1}, b: 3.97×10^{-3} to 4.35×10^{-3} L mg^{-1}).[232] Pit coal fly ash adsorbed Cu(II) and Zn(II) with Langmuir capacities of 4.59 to 7.61 mg g^{-1} and 4.11 to 7.65 mg g^{-1}, respectively (277 to 333 K).[233]

Adsorption of Cd(II) on two fly ash samples (Afsin-Elbistan and Seyitomer) was pH dependent and q_m varied from 0.08 to 0.29 and 0.01 to 0.23 mg g^{-1} respectively (pH 3.0 to 7.0).[234] The differences were explained on the basis of different chemical composition of the two samples. Adsorption of Cr(VI) and Hg(II) on fly ash (FA) (from thermal power plant) and modified fly ash (impregnated with 0.1 M $Al(NO_3)_3$, IFAAl and 0.1 M $Fe(Cl)_3$, IFAFe) had Langmuir capacities of FA 1.38, IFAAl 1.82, IFAFe 1.67 mg g^{-1} for Cr(VI) and FA 11.00, IFAAl 12.50, IFAFe 13.40 mg g^{-1} for Hg(II).[235] The modified adsorbents were shown to have developed new active sites through electrostatic interactions among $Al(OH)_3$, $Fe(OH)_3$, and SiO_2 leading to improved adsorption.

Fly ash activated with bentonite clay yielded Langmuir capacity of 25.907 mg g^{-1} for Cd(II), which was held to the surface mainly by chemical bonding with ≡SiO− and ≡AlO− groups.[236]

Use of red mud (from aluminium industry) for Cr(VI) and Pb(II) removal yielded q_m of 4.36×10^{-4} to 4.05×10^{-4} mol g^{-1} (b: 0.40×10^{-3} to 0.316×10^{-3} L mol^{-1}) and 3.44×10^{-4} mol g^{-1} to 3.23×10^{-4} mol g^{-1} (b: 15.90×10^{-3} to 2.05×10^{-3} L mol^{-1}) (303 to 323 K) respectively.[237] Adsorption of As(III) and As(V) on activated red mud with a probable ligand-based mechanism yielded q_m of 7.22 and 102.00 mmol g^{-1} respectively.[138]

Langmuir capacities of electric furnace slag for Pb(II) and Cr(VI) increased from 33.78 to 37.04 mg g^{-1} and 32.68 to 39.22 mg g^{-1} respectively.[137] The metal uptake was through calcium-ferrite, $CaO \cdot Fe_2O_3$, $CaO \cdot 2Fe_2O_3$, $4CaO \cdot 7Fe_2O_3$ and calcium-manganese-silicate, $(Ca, Mn)_2SiO_4$ and $CaO \cdot MgO \cdot SiO_2$ phases.

Steel plant wastes had large q_m for Pb(II): furnace sludge (227 and 161 mg g^{-1}) > blast furnace dust (142 and 111 mg g^{-1}) > blast furnace slag (125 and 91 mg g^{-1}) at 298 and 318 K respectively.[238] Blast furnace sludge and dust contained iron oxides while silicates of calcium and aluminum and quartz were the major components of the slag.

Low-cost adsorbents, clarified sludge (steel industry), activated alumina, fuller's earth and fly ash (from thermal power plant) could adsorb Cr(VI)[239] with Langmuir capacities, clarified sludge 26.51 mg g^{-1}; activated alumina 25.57 mg g^{-1}, fuller's

earth 23.58 mg g^{-1} and fly ash 23.86 mg g^{-1} at 303 ± 2 K. Use of clarified sludge for Cd(II) adsorption yielded Langmuir capacity of 36.23 mg g^{-1} at 303 ± 0.5 K.[240] Langmuir capacities of Cu(II) on two sewage sludge ash samples[140] were 3.28 and 4.14 mg g^{-1}.[241] Presence of $CaSiO_2$, $CaOFe_2O_3$, $CaOSiO_2$ phases and traces of $CaO{\cdot}MgO{\cdot}SiO_2$ with Al_2O_3 and FeO might be responsible for the adsorption process. Waste material from boron enrichment process with ulexite, $NaCaB_5O_9{\cdot}8H_2O$, as the main phase adsorbed Cd(II) (q_m: 122.22 mg g^{-1}) and Zn(II) (q_m: 107.65 mg g^{-1}).

Adsorption of Co(II) on two ion exchange resins (IRN77 and SKN 1) yielded Langmuir capacities of 86.17 and 69.44 mg g^{-1} at 298 ± 1 K.[135] In a recent work, dithiocarbamate chelating resin was found to adsorb Hg(II) (q_m = 2.45 mmol g^{-1}) more than Cd(II) (q_m = 2.15 mmol g^{-1}) and Pb(II) (q_m = 1.24 mmol g^{-1}).[136] It was suggested that the hydrophilic character of the resin played an important role in the uptake of metal ions.

2.3. Dubinin–Radushkevich isotherm

Dubinin–Radushkevich (DR) isotherm,[242] which is based on the Polanyi theory,[243] has been found useful in computing energy of molecular adsorption. The DR isotherm predicts heterogeneity of the adsorption energies or adsorption space. This isotherm is applicable from trace to saturation values and the adsorbate properties do not differ from the corresponding bulk phase except for its lower energy.[244]

The isotherm has the following form,

$$q_e = q_{max} \exp(-\beta\varepsilon^2) \quad (5)$$

The linear form will be,

$$\ln q_e = \ln q_{max} - \beta\varepsilon^2 \quad (6)$$

where q_{max} is the theoretical saturation capacity (mol g^{-1}), β (mol^2 kJ^{-2}) is Dubinin–Radushkevich coefficient, related to the mean free energy of adsorption per mol of the adsorbate, and ε is the Polanyi potential given by:

$$\varepsilon = RT \ln(1 + 1/C_e) \quad (7)$$

C_e is the equilibrium solution-phase concentration of the adsorbate, R the universal gas constant (8.314 J mol^{-1} K^{-1}) and T (K) the absolute temperature. The coefficients, q_{max} and β, could be computed from the linear plot of ln q_e *vs.* ε^2.

The Dubinin–Radushkevich coefficient, β, is related to the mean free energy, E (kJ mol^{-1}) of adsorption per mol of the adsorbate and is equivalent to the work done in transferring one mol of adsorbate molecules from the bulk of the solution to the surface of the adsorbent. The relationship between the two is,[245]

$$E = 1/(2\beta)^{1/2} \quad (8)$$

It has been shown that if the magnitude of E is between 8 and 16 kJ mol^{-1}, strong adsorption results from ion-exchange interactions, but if E < 8 kJ mol^{-1}, the adsorption is largely physical in nature.[246–248] Most of the experimental works have been interpreted on this basis.

2.3.1. Clays. Turkish kaolinite had q_{max} of 2.96 × 10^{-4} mol g^{-1} for Pb(II) with free energy of adsorption of 13.78 kJ mol^{-1}, indicating an ion-exchange mechanism.[30] Similarly, the free energy of adsorption of Cu(II) on natural kaolinite was in the range of 10.46 to 10.79 kJ mol^{-1} in the temperature range, 293 to 313 K indicating that Cu(I) ions were held strongly to the surface.[249]

Li *et al.*[37] reported endothermic interaction of Cu(II) on a local bentonite with DR capacities 2.57 × 10^{-4} to 3.24 × 10^{-4} mol g^{-1} (293.15 to 333.15 K). Adsorption was ascribed to ion exchange of H^+/Na^+ with Cu(II) [β: 1.53 × 10^{-2} mol^2 kJ^{-2} (293.15 K), 1.60 × 10^{-2} mol^2 kJ^{-2} (313.15 K), 1.56 × 10^{-2} mol^2 kJ^{-2} (333.15 K)]. The Celtek clay had DR capacities of 5.83 × 10^{-5} and 5.27 × 10^{-5} mol g^{-1} respectively for Cr(III) and Pb(II) at 293 K.[31] However, adsorption was very weak due to very small adsorption energy [(Pb(II)) 0.10 kJ mol^{-1} and (Cr(III)) 0.09 kJ mol^{-1}].

DR capacities of natural bentonite for Zn(II), Cu(II) and Co(II) was influenced by solution pH and increased from 9.28 to 17.29 mg g^{-1}, 7.04 to 12.93 mg g^{-1} and 4.24 to 13.09 mg g^{-1}, respectively (pH: 3.0 to 9.0).[34] Increased adsorption at higher pH was due to bentonite surface becoming negative above the point of zero charge (pzc) of 6.35. The mean adsorption energies were 9.71, 3.72 and 0.74 kJ mol^{-1} respectively for Zn(II), Cu(II) and Co(II) at pH 9.0 (293 K). Thus, the mechanism of adsorption may vary from ion-exchange to weak physical adsorption from Zn(II) to Co(II). Veli and Alyüz[39] observed much lower adsorption energy of natural bentonite for Zn(II) (1.25 kJ mol^{-1}) and Cu(II) (0.53 kJ mol^{-1}) but large adsorption capacity [Zn(II): 7266.07 mg g^{-1}, Cu(II): 2997.73 mg g^{-1}].

Yang *et al.*[38] reported Pb(II) uptake on Na-bentonite with DR capacities of 2.14 × 10^{-3} to 2.67 × 10^{-3} mol g^{-1} (298 to 338 K). Adsorption on Na-bentonite surface was attributed to chemical adsorption (E = 10.01 to 13.06 kJ mol^{-1}) and ion exchange was also contributed in the process.

Turkish vermiculite–Cr(VI) interactions had DR capacity of 1.6 × 10^{-3} mol g^{-1} and mean adsorption energy of 5.9 kJ mol^{-1}.[250] It was shown that adsorption was controlled by Si–OH and Al–OH groups on the vermiculite surface.

Pb(II) cations were taken up by montmorillonite–illite through an ion exchange mechanism with large DR capacities of 39.79 to 50.09 mol g^{-1} (Pb(II) 100–200 mg L^{-1}).[251] Pb(II) cations were shown to be preferentially adsorbed on silanol groups (Si–OH) present on the clay. However, montmorillonite alone had a much lower Cu(II) removal capacity of 13.3844 mg g^{-1}.[252]

2.3.2. Modified clays. The coordinative environment of Cu(II) and the presence of surface hydroxyl groups helped Cu(II) adsorption on hydrated MgO-coated bentonite. The DR capacity was 7.31 ± 0.80 mg g^{-1} (E = 2.81 ± 1.42 kJ mol^{-1}). It is suggested that MgO minimizes the solubility of Cu(II) and resists its redissolution.[59]

Adsorption of Pb(II) on Fe, Mg (hydr)oxide coated bentonite composite had free energy of 8.45 kJ mol^{-1} and DR capacity of 108.82 mg g^{-1}.[60]

2.3.3. Organo-functionalized clays. Sodium montmorillonite modified with dodecylamine adsorbed Cr(VI) with a DR

capacity of 13.897 mg g^{-1} and free energy of 0.540 kJ mol^{-1}.[73] The electrostatic affinity of Cr(VI) to protonated dodecylamine and the surface OH groups in montmorillonite helped the adsorption process.

Sodium dodecylsulfate-montmorillonite yielded DR capacities of 83.0 mmol g^{-1} and 31.9 mmol g^{-1} for Cu(II) and Zn(II) respectively.[171] Introduction of sodium dodecylsulfate to the interlayer space of montmorillonite was shown to increase the negative charge at clay surface favouring adsorption of the metal cations.

Anirudhan and Suchithra[168] reported that DR coefficient, β, of humic acid-immobilized amine-modified polyacrylamide–bentonite composite for Co(II), Cu(II) and Zn(II) adsorption was 8.67, 8.51 and 7.96 kJ mol^{-1} respectively. The comparatively high values indicate adsorption to be taking place through ion exchange.

Chitosan immobilized-bentonite adsorbed Pb(II) (q_{max}: 28.86 mmol g^{-1}), Cu(II) (q_{max}: 18.80 mmol g^{-1}) and Ni(II) (q_{max}: 13.27 mmol g^{-1}).[176] Th cations were bound through $-NH_2$ and –OH groups and the large Pb(II) DR capacity was due to its higher electronegativity.

In another work, Li *et al.*[76] reported DR capacities of tannin-immobilized activated clay for Cr(VI) was in the range of 11.53 to 14.35 mol g^{-1} (300 to 330 K). The porousness of activated clay could make it absorb a small part of Cr(VI), partly Cr in the form of anionic species was adsorbed through esterification reaction with phenolic groups of tannin and the adsorption of reduced Cr(III) ions occurred through the ion exchange reaction in acid solution.

Clay–poly(methoxyethyl)acrylamide composite adsorbed Pb(II) in an endothermic process yielding DR capacities of 8.51×10^{-4} to 9.47×10^{-4} mol g^{-1} (293 to 323 K), the participating groups in adsorption being olefinic double bonds, carbonyl and amine groups present in the composite.[75]

Cu(II) adsorption on bentonite and bentonite–polyacrylamide composite had DR capacities of 2.52 and 3.68 mmol g^{-1} at pH 6.2 and 0.45 and 1.06 mmol g^{-1} at pH 5.0 with DR β of 9.70 and 13.50 kJ mol^{-1}, respectively.[177] The interactions were quite strong and were likely to involve coordination between the lone-pair electrons of N and the empty orbital of Cu(II).

DR capacities of 8-hydroxy quinoline-immobilized bentonite for Pb(II)[71] and Cu(II)[70] were 218.82 to 173.95 mg g^{-1} and 201.89 to 222.37 mg g^{-1} respectively (293 to 323 K). Strong Cu(II) uptake on 2,2′-dipyridyl-immobilized bentonite (93.94 to 76.16 mg g^{-1}, 293 to 323 K)[72] was supported by large DR adsorption energy of 12.12 to 20.71 kJ mol^{-1}.

Hu *et al.*[67] reported an adsorption energy of 13.9 kJ mol^{-1} for Cr(V) adsorption on poly(hydroxo aluminium) and cetyl trimethylammonium bromide modified montmorillonite. Marjanović *et al.*[77] showed that DR capacities of (3-mercaptopropyl)trimethoxysilane functionalized natural and acid-activated sepiolite for Cr(VI) were 2.68 to 1.41 mg g^{-1} and 5.47 to 5.34 mg g^{-1} (pH 2.0 to 4.5) respectively. Better functionalization was achieved in case of the acid-activated sepiolite that increased the number of silanol groups and resulted in higher adsorption capacity. Cr(VI) anions were adsorbed mostly through an electrostatic mechanism involving protonated mercapto groups on the functionalized sepiolite surface. The authors also suggested that Cr(VI) might have been reduced to Cr(III) by mercapto groups, which were then attracted to the sulfonate groups ($-SO_2O^-$), generated by oxidation of the mercapto groups. The adsorption free energy change was only 0.02 and 0.59 kJ mol^{-1} respectively for the two adsorbents and therefore, Cr(VI) anions were held with weak physical forces only. In a recent report, the same authors[78] achieved DR capacities for Cr(VI) of 25.82 and 38.72 mg g^{-1}, respectively with [3-(2-aminoethylamino)propyl]trimethoxy-silane grafted natural and acid-activated sepiolites.

On the other hand, interactions of Pb(II) with mercapto functionalized sepiolite were chemical in nature with adsorption free energy of 14.12 to 15.88 kJ mol^{-1} and DR capacities of 71.34 ± 4.59 to 105.08 ± 3.11 mg g^{-1} in the temperature range of 289.15 to 318.15 K.[79] Pb(II) cations were shown to directly interact with mercapto groups forming stable inner- and outer-sphere complexes.

2.3.4. Zeolites. In a comparative study, zeolite (clinoptilolite as the main component, with quartz and albite) was found to be better adsorbent for Cu(II) than clay (Illite 30%, kaolinite 25%, montmorillonite 5%, albite 7%, quartz 30%) or diatomite (q_{max}: zeolite 0.209, clay 0.151, diatomite 0.062 mmol g^{-1}).[180] Adsorption free energy of 13.30 to 18.50 kJ mol^{-1} indicated ion-exchange type interactions. In another work, natural zeolite yielded DR capacities of 11.52, 0.064 and 0.059 mmol g^{-1} for Pb(II), Cu(II) and Zn(II). A mechanism consisting of ion exchange and adsorption, as well as precipitation of metal hydroxides on active sites of the adsorbent surface was proposed.[253] Natural zeolitic volcanic tuff was shown to adsorb Pb(II) with DR capacities of 6.80, 6.94 and 6.71 mg g^{-1} at 293, 313 and 333 K respectively.[82]

Clinoptilolite adsorbed Co(II) (q_{max}: 0.50 mmol kg^{-1}), Zn(II) (0.29 mmol kg^{-1}), Cu(II) (0.22 mmol kg^{-1}) and Mn(II) (0.15 mmol kg^{-1}).[182] The metal ions were adsorbed in the form of their hexaaqua complexes and the largest Mn(II) showed minimum adsorption and the smallest Co(II) had maximum. In a similar work, Argun[85] observed DR capacities of clinoptilolite for Ni(II) in the range of 1.81 to 1.58 mg g^{-1} (293 to 313 K).

Mordenite with low Si/Al ratio (5 : 1) removed Pb(II) with DR capacities of 60.38 to 104.13 mg g^{-1} (293 to 323 K) and adsorption free energies of 9.57 to 9.95 kJ mol^{-1}.[186]

Endothermic adsorption of Cu(II) on humic acid-immobilized cetylpyridinium bromide-modified zeolite yielded DR capacities of 27.1 to 28.0 mg g^{-1} (298 to 318 K), and adsorption energy of 24.6 to 29.3 kJ mol^{-1}, which indicated strong chemical binding.[88]

Javadian *et al.*[89] reported physisorptive interactions between Cd(II) and zeolite-based geopolymer (from coal fly ash) with mean adsorption energy of 1.581 kJ mol^{-1} and DR capacity of 17.059 mg g^{-1}.

2.3.5. Oxides and modified oxides. Polyacrylamide aerogel had a large DR capacity for Hg(II) (71.69 mg g^{-1}) than silica gel (33.17 mg g^{-1}) and hybrid aerogel (28.49 mg g^{-1}) at 318 K. The adsorption energy was in the range of 12.14 to 14.20 kJ mol^{-1}.[254]

Interaction of hydrous titanium oxide with Cr(III) and Cr(VI) followed ion exchange mechanism with adsorption energy of

9.35 to 11.58 kJ mol^{-1} and 11.84 to 12.66 kJ mol^{-1} (288 to 318 K) respectively.[255] The DR capacities varied from 1.08 to 1.24 mol kg^{-1} (Cr(III)) and 0.60 to 1.70 mol kg^{-1} (Cr(VI)) in the same temperature range.

Adsorption of Se(IV) on iron oxide (q_{max}: 0.109 to 0.089 mmol g^{-1} for 303 to 323 K) was higher compared to that on silicon oxide (q_{max}: 0.092 to 0.054 mmol g^{-1} for 303 to 323 K). Se anions interacted with the oxide surface involving adsorption of SeO_3^{2-} (selenite) and $HSeO_3^-$ (biselenite) on the surface by ligand-exchange. The energy of adsorption was in the range of 7.29 to 6.32 kJ mol^{-1} and 7.87 to 5.72 kJ mol^{-1} for iron oxide and silicon oxide, respectively.[100]

Amino-functionalized Fe_3O_4 magnetic nano-particles[110] could take up Pb(II) with DR capacity of 105.70 mg g^{-1} and adsorption free energy of 10.31 kJ mol^{-1}, with a largely chemical adsorption process.

2.3.6. Other inorganic solids. DR capacities of tannin-immobilized calcined hydrotalcite was highest for Cu(II) (29.8 to 35.4 mg g^{-1}) than Zn(II) (27.7 to 34.8 mg g^{-1}) and Cd(II) (25.2 to 32.8 mg g^{-1}) in the temperature range of 303 to 323 K.[118] The adsorbent was shown to possess high affinity –COOH groups interacting with the metal cations in an ion-exchange mechanism. The adsorption free energies were 9.1 to 15.2 kJ mol^{-1} (Cu(II)), 8.8 to 12.1 kJ mol^{-1} (Zn(II)) and 8.4 to 11.0 kJ mol^{-1} (Cd(II)).

Albadarin *et al.*[205] reported DR capacity of dolomite for Cr(VI) of 7.35 to 3.97 mg g^{-1} (E = 4.87 to 4.37 kJ mol^{-1}). Cr(VI) anions were adsorbed on >(Ca, Mg)OH_2^+ sites with formation of >(Ca, Mg)$Cr_2O_7^-$.

Mn-diatomite had a higher DR capacity (8.06 to 9.66 mg g^{-1}) than diatomite itself (7.30 to 8.41 mg g^{-1}) for Zn(II) at 298 to 313 K.[256] Adsorption free energies were 1.89 to 2.17 kJ mol^{-1} and 2.53 to 3.13 kJ mol^{-1} for diatomite and Mn-diatomite respectively. Both electrostatic interaction and physical adsorption were involved in the mechanism.

Mobasherpour *et al.*[120] observed that nano hydroxyapatite could preferably adsorb Pb(II) (1003.726 mg g^{-1}) compared to Cd(II) (150.028 mg g^{-1}) and Ni(II) (57.812 mg g^{-1}). The authors stated that cations with ionic radii smaller than Ca^{2+} (0.099 nm) showed less chance to be incorporated into the hydroxyapatite structure compared with cations with larger ionic radii. Therefore, precipitation of Ni(II) (0.072 nm) with Ca^{2+} would be less likely compared to that of Pb(II) (0.118 nm) and Cd(II) (0.097 nm).

DR capacities of loamy sand soil for Cr(VI) and Pb(II)[124] was 1525 and 1563 mg kg^{-1} respectively with adsorption energy of 1400 and 335 kJ mol^{-1}. The authors suggested formation of $PbOH^+$ on the adsorbent surface as well as reduction of Cr(VI) to Cr(III) by natural organic matter.

DR capacity of loess soil for Cd(II) increased from 11.17 to 19.32 mg g^{-1} (E = 17.85 to 18.57 kJ mol^{-1}) for temperature variation of 298 to 318 K.[123] The –COOH groups of organic matter in loess soil played a significant role in the uptake of Cd(II) and the adsorption at low pH depended mainly on the protonation or deprotonation of these –COOH groups. Tang *et al.*[202] reported DR capacity of natural Chinese loess soil for Zn(II) in the range of 0.0018 to 0.0021 mol g^{-1}.

The presence of calcite, quartz and aragonite in the form of carbonates and oxides in beach sand created affinity for Pb(II) [q_{max}: (41.3 ± 21.9) to (64.1 ± 22.02) μmol g^{-1} for 293 to 323 K][126] and Zn(II) [q_{max}: 37.5 ± 9.8 μmol g^{-1} at 303 K].[127] The mean adsorption energy was within a narrow range of 11.03 to 12.16 kJ mol^{-1} (Pb(II)) and 11.7 ± 0.6 kJ mol^{-1} (Zn(II)) supporting an ion exchange mechanism. A similar investigation of Pb(II) adsorption on river sand yielded DR capacity of 23.26 ± 0.0502 × 10^{-2} mmol g^{-1}.[126]

Nano zerovalent iron yielded Cd(II) DR capacities of 399.10 to 473.40 mg g^{-1} (285 to 307 K) with E = 54.80 kJ mol^{-1}.[218] The DR capacity and adsorption energy being both large, suggested strong chemical adsorption. Fe–Ni bimetallic nanoparticles had higher Cr(VI) DR capacity (133.35 mg g^{-1}) than those of Fe–Ni bimetallic-montmorillonite nanoparticles (129.07 mg g^{-1}) and zero valent iron (105.70 mg g^{-1}).[62]

2.4. Redlich–Peterson isotherm

When ideal monolayer adsorption is not the case, Redlich–Peterson isotherm[257] is usually applied. This isotherm is considered as a combination of both Freundlich and Langmuir models and has the form,

$$q_e = (K_{RP}\, C_e)/[(1 + a_{RP})\, (C_e)^g] \quad (9)$$

where q_e (mmol g^{-1}) is the solid phase adsorbate concentration at equilibrium, C_e (mmol L^{-1}) is the liquid phase concentration of the adsorbate at equilibrium, K_{RP} (L g^{-1}), a_{RP} (L $[mmol^{1-1/g}]^{-1}$) and g (heterogeneity index, $0 < g < 1$) are adjustable Redlich–Peterson coefficients. The equation has two limiting cases

(i) at $g = 1$, it gives the Langmuir isotherm, *i.e.*

$$q_e = (K_{RP}C_e)/[(1 + a_{RP})C_e] \quad (10)$$

(ii) at $g = 0$, it reduces to Henry's law equation, *i.e.*

$$q_e = (K_{RP}C_e)/[1 + a_{RP}] \quad (11)$$

Rearranging eqn (17) to the form

$$K_{RP}(C_e/q_e) - 1 = a_{RP}(C_e)^g \quad (12)$$

Which can be converted to a linear logarithm form,[258]

$$\ln[K_{RP}(C_e/q_e) - 1] = \ln a_{RP} + g \ln C_e \quad (13)$$

The isotherm coefficients, a_{RP}, K_{RP} and g were obtained from a minimization procedure to solve this equation.

The Redlich–Peterson (RP) isotherm has not found much application because of the difficulties associated with evaluation of the three adsorption parameters. Still, some studies can be found in the literature during the last few years. In such a study, Redlich–Peterson model was applied to Cd(II) adsorption on Fe-montmorillonite and Ca-montmorillonite[65] with the former having large values (Fe-montmorillonite: K_{RP} 508.0 L mg^{-1}, a_{RP} 22.5 L mg^{-1}; Ca-montmorillonite: K_{RP} 2.37 L mg^{-1}; a_{RP} 0.25 L mg^{-1}). The coefficient, g was ~1.0 (0.959 and 0.785) suggesting adsorption mainly at specific homogeneous

sites within the adsorbent. Large number and variety of –OH groups and higher CEC of Fe-montmorillonite resulted in enhanced adsorption by surface complexation and precipitation. Similarly, RP model in adsorption of Hg(II), Cd(II) and Co(II) on phosphate-immobilized-Zr-pillared bentonite yielded (i) K_{RP}: 20.37 L mg^{-1}, a_{RP}: 0.517 mg^{-1}, g: 0.94 for Hg(II), (ii) K_{RP}: 9.98 L mg^{-1}, a_{RP}: 0.20 L mg^{-1}, g: 0.99 for Cd(II) and (iii) K_{RP}: 10.31 L mg^{-1}, a_{RP}: 0.226 L mg^{-1}, g: 0.99 for Co(II). The metal uptake capacity was shown to have been boosed by phosphate immobilization creating well defined porous structure.[159]

Fe pillared, Fe/Cr pillared and Cr pillared bentonite were shown to adsorb Cd(II) with RP parameters, $g \sim 1.0$ for all the three adsorbents (RP model reduces to Langmuir form), and K_{RP} 1.71 L mg^{-1}, a_{RP} 2.28 L mmol^{-1} for Fe pillared bentonite, K_{RP} 1.41 L mg^{-1}, a_{RP} 1.80 L mmol^{-1} for Fe/Cr pillared bentonite and K_{RP} 1.34 L mg^{-1}, a_{RP} 3.43 L mmol^{-1} for Cr pillared bentonite.[63] RP coefficients for adsorption of Pb(II) and Cu(II) on Urea-intercalated-delaminated kaolinite (K_{RP}: 4.0 $\pm$ 0.2 and 3.6 $\pm$ 0.1 L mol^{-1}), urea-intercalated kaolinite (K_{RP}: 3.651 and 3.169 L mol^{-1}) and natural kaolinite (K_{RP}: 2.0 $\pm$ 0.3 and 2.2 $\pm$ 0.2 L mol^{-1}) showed appreciable differences.[154]

Dodecylamine modified sodium montmorillonite was shown to adsorb Cr(VI) with K_{RP}, a_{RP} and g of 2.596 L g^{-1}, 0.184 L mg^{-1} and 0.86 respectively.[73] Cr(VI) anions were held electrostatically to the protonated dodecylamine and surface hydroxyl groups in montmorillonite.

The RP parameters for adsorption of Cr(VI) and Cr(III) on hydrous titanium oxide at 288 K were significantly different, K_{RP}: 2.419 L mg^{-1}, a_{RP}: 0.222 L mg^{-1}, g: 1.082 than for Cr(VI) and K_{RP}: 0.764 L mg^{-1}, a_{RP}: 0.036 L mg^{-1}, g: 1.004 for Cr(III).[255] Ni(II) adsorbed on the same material at 288 $\pm$ 1 to 328 $\pm$ 1 with RP parameters of 34.83 to 47.24 L g^{-1} (K_{RP}), 4.32 to 2.30 L mg^{-1} (a_{RP}) and 0.82 to 0.93 (g).[259]

Pb(II) adsorption on natural apatite and synthetic hydroxyapatite had K_{RP}: 0.532 L mg^{-1}, a_{RP}: 3.05 L mg^{-1}, g: 0.410 and K_{RP}: 38.7 L mg^{-1}, a_{RP}: 82.6 L mg^{-1}, g: 0.797 respectively.[121]

Guerra *et al.*[179] reported Pb(II), Mn(II) and Zn(II) adsorption on 3-aminopropyltriethoxysilane modified nontronite with K_{RP} (L g^{-1}) of Pb 25.034, Mn 23.916, Zn 22.218; a_{RP} ({mmol L^{-3}}$^{-g}$) of Pb 0.984, Mn 0.988, Zn 0.993 while the parent nontronite had K_{RP} (L g^{-1}): Pb 13.451, Mn 13.925, Zn 12.217; a_{RP} ({mmol L^{-3}}$^{-g}$): Pb 0.812, Mn 0.889, Zn 0.951. The g values were ~1.0. Organic functionalization was seen to have positive influence on K_{RP}.

Amino functionalized silica gel with three different loadings of aminopropyl group yielded K_{RP} from 0.062 to 0.002 L g^{-1} (g = 0.95) for Cu(II).[115] Another material, aminated mesoporous alumina adsorbed Cu(II) with K_{RP} 2.22 L mg^{-1}, a_{RP} 0.55 L mg^{-1}, g 0.80 while Cu(II) on simple protonated mesoporous alumina had K_{RP} 2.63 L mg^{-1}, a_{RP} 0.37 L mg^{-1}, g 0.90.[112] Mg-mesoporous alumina held Ni(II) with K_{RP}: 9.93 L g^{-1}, a_{RP}: 2.18 L g^{-1}.[260] The large values were explained on the basis of interconnected pore system of mesoporous alumina that reduced transport limitations and enhanced the accessibility of the active sites.

Cr(VI) adsorption on zerovalent iron, Fe–Ni bimetallic nanoparticles and Fe–Ni bimetallic-montmorillonite nanoparticles K_{RP} of 3.16 $\times$ 10^3 to 4.60 $\times$ 10^3 L g^{-1}; a_{RP}: 56.88 to 64.71 L mg^{-1} with $g \sim 1.0$.[62]

2.5. Temkin isotherm

Temkin isotherm[261] is based on the assumption that the adsorption heat decreases linearly with coverage instead of a logarithmic decrease as implied in the Freundlich isotherm[262,263] and that there is a uniform distribution of binding energies. The isotherm has the form,[264]

$$q_e = (RT/b_T)\ln(K_T C_e) \quad (14)$$

or

$$q_e = B \ln K_T + B \ln C_e \quad (15)$$

where $B = RT/b_T$ and the Temkin coefficients, K_T (L mmol^{-1}) and B (kJ mol^{-1}) are related respectively to equilibrium binding energy and the heat of adsorption. Plot of q_e *versus* ln C_e can be used to determine the values of K_T and B. Temkin isotherm requires that the adsorption process is accompanied by a uniform distribution of binding energies, which is hardly possible while considering adsorption from solutions on to a solid. Thus, while Temkin equation is excellent for predicting the gas phase equilibrium (when organization in a tightly packed structure with identical orientation is not necessary), it is found that complex systems, particularly liquid-phase adsorption equilibria are usually not appropriate to be represented by Temkin isotherm.[265]

It is thus found in the literature that in those few cases (of adsorption from solutions) where application of Temkin isotherm was attempted, the interpretations of the results were inconsistent and incomplete, particularly with respect to values of the Temkin coefficieny, K_T.[62,73,89,99,121,158,169,218,254,260]

2.6. Toth isotherm

To obtain a general relationship for the interactions of adsorptive molecules and the energetically heterogeneous solid surfaces, Toth[266] observed that a heterogeneous surface would have a higher uptake of adsorptive at the same relative equilibrium pressure than a homogeneous surface. The Toth isotherm is strictly applicable to adsorption of gases on solids, but the equation has been extended to adsorption from solutions with the following common form:[255]

$$q_e = (Q_{max} b_T, C_e)/([1 + (b_T C_e)^{1/n}]^n) \quad (16)$$

where Q_{max} (mg g^{-1}), b_T (mg L^{-1})^n and n (dimensionless parameter) are Toth coefficients. The linear from of the eqn (26) is,

$$C_e^{1/n}/q_e = [1/(Q_{max} b_T)] + (1/Q_{max}) C_e \quad (17)$$

The three-parameter Toth equation is not easy to solve and this has resulted in only a few applications of the same. Debnath and Ghosh[255] reported Toth capacities of hydrous TiO_2 for Cr(III) and Cr(VI) in the range of 21.71 mg g^{-1} to 64.13 mg g^{-1} and 10.43 mg g^{-1} to 29.99 mg g^{-1} respectively (288 K to 318 K). The Toth coefficient, n, had values of Cr(III): 1.185 to 1.474 and Cr(VI): 0.987 to 1.029.

Montmorillonite–Cu(II) interaction yielded Toth capacity of 25.124 mg g^{-1} with $n = 1.230$.[252] Cu(II) cations were adsorbed by an ion exchange mechanism at permanent charge sites and also by the formation of complexes with surface hydroxyl groups of the adsorbent. The Toth capacity of zeolite for Pb(II) (0.433 mmol g^{-1}) was found to be higher than that for Cu(II) (0.410 mmol g^{-1}) and Zn(II) (0.201 mmol g^{-1}) with '*n*' varying between 0.90 to 0.99.[253]

3. Molecular simulation of adsorption

There are some studies in which molecular simulation has been used to predict the adsorption isotherms. However, the output of a simulation is the absolute number of molecules present in the framework, whereas experimental results are often reported as the excess amount adsorbed.[267]

Kremleva *et al.*[268] carried out DF calculations on supercell slab models of kaolinite edge surfaces, using the plane-wave based *ab initio* simulation to interactions of uranyl groups with kaolinite edge surfaces. The (010) surface of kaolinite edge facets was expected to be highly reactive that could preferentially adsorb metal cations. In considering bidentate uranyl adsorption complexes at (010) edge surfaces, three types of deprotonated adsorption sites, namely, (i) pure aluminol (Al–OH) sites, (ii) mixed silanol–aluminol sites within the same substrate layer of kaolinite and (iii) bridging silanol–aluminol sites between neighboring layers, were taken into consideration. Adsorption at the bridging sites was found to be essentially as stable as complexes at aluminol sites, while complexes at mixed aluminol–silanol sites within a single kaolinite layer were energetically less favorable. Uranyl adsorption was accompanied by hydrolysis resulting in uranyl mono- or dihydroxide as the adsorbate. Comparison of energetically preferred adsorption complexes on the (001) and (010) surfaces of kaolinite showed no characteristic structural feature that would differentiate between uranyl adsorption on these two types of surfaces.

The *ab initio* molecular dynamics simulation for Li^+-, Na^+- and K^+-montmorillonites was studied by considering three types of isomorphic substitutions in the montmorillonite layer: tetrahedral (T_{sub}), octahedral (O_{sub}) and both (OT_{sub}).[269] The authors observed that for all types of montmorillonites, K^+ remained bound to the surface, confirming its role as a swelling inhibitor. On the other hand, Li^+ showed a tendency to hydrate and coordinate to four H_2O molecules in all the cases, except for the OT_{sub} substituted montmorillonite where one of the two Li^+ cations remained bound to the oxygen atoms close to the substituted tetrahedral site. Na^+ possessed an intermediate behaviour and could bind to the surface for T_{sub} montmorillonite but got hydrated for O_{sub}. The inner/outer complex formation of the cations depended on the relative water-cation and surface-cation affinity. The binding energy between alkali cations and water was highest for Li^+, followed by Na^+ and K^+, the ions being bound to 4, 5, and 6 solvating water molecules, respectively. Moreover, increase in the cation size and polarizability, enhances the interactions with the surface, following the sequence $Li^+ < Na^+ < K^+$. From the molecular electrostatic potential maps, it was shown that the effects of tetrahedral and/or octahedral substitutions in montmorillonite were to adjust the negative charge carried by the surface oxygen atoms, thereby tuning the cation-surface affinity and the inner/outer complex formation.

The adsorption behaviour of V(V) on goethite surface and the acid–base behaviour of the adsorbent surface were theoretically studied by Peacock and Sherman.[270] It was shown that at pH ~ 6.0 to 9.0, adsorption was concentration dependent that reflected the formation of polynuclear complexes in solution. V(V) adsorbed on α-FeOOH surface as the mononuclear VO_2^+ (pH 1.0 to 4.0) and $VO_3(OH)^{2-}$ ions (pH > 4.0). Adsorption was accompanied by the formation of inner-sphere surface complexes resulting from bidentate corner-sharing between doubly and singly protonated VO_4^{3-} tertrahedra and FeO_6 polyhedra. The authors fitted the experimental V(V) adsorption data to the reactions,

$$2FeOH_2^+ + VO_2 = Fe_2O_2V(OH)_2^+ + 2H^+$$

and

$$2FeOH + HVO_4^{2-} = Fe_2O_2VO(OH)^0 + 2OH^-$$

The same group of authors investigated adsorption of Cu(II) onto goethite (α-FeOOH), hematite (α-Fe_2O3) and lepidocrocite (γ-FeOOH) at pH 2.0–7.0 and showed that Cu(II) adsorbed as $(CuO_4H_n)^{n-6}$ and binuclear $(Cu_2O_6H_n)^{n-8}$ complexes.[271] These could form inner-sphere complexes with iron (hydr)oxide surfaces by corner-sharing with two or three edge-sharing $Fe(O,OH)_6$ polyhedra. No evidences was found for surface complexes resulting from either monodentate corner sharing or bidentate edge-sharing between $(CuO_4H_n)^{n-6}$ and $Fe(O,OH)_6$ polyhedra. With the bidentate $(\equiv FeOH)_2Cu(OH)_2^0$ and tridentate $(\equiv Fe_3O(OH)_2)Cu_2(OH)_3^0$ surface complexes, the experimental Cu(II) adsorption data could be expressed as,

$$3(\equiv FeOH) + 2Cu^{2+} + 3H_2O \rightarrow (\equiv Fe_3O(OH)_2)Cu_2(OH)_3^0 + 4H^+$$

and

$$2(\equiv FeOH) + 2Cu^{2+} + 2H_2O \rightarrow (\equiv Fe_3OH_2)Cu(OH)_2^0 + 2H^+$$

The non-coulombic interactions of Cd(II), Cu(II) and Zn(II) with (001) surface of muscovite mica were studied by atomistic simulation techniques and a set of specific interatomic potentials.[272] The surface experienced only minimal relaxation. The study indicated absence of strong bonding of Cd(II), Cu(II) and Zn(II) to the perfect (001) surface of muscovite. The bond lengths (2.6 and 2.8 Å) were much longer than those observed by experiment suggesting that only weak interactions exist between metal cation and adsorbent surface, pointing to physisorption rather than chemisorption. The lack of reactivity was explained by considering the stability of the SiO_2 units that make up the surface in which all oxygen bonds were satisfied. The replacements of 25% Si by Al imparted some residual charge to the surface, which was not enough to lead to chemisorption. Adsorption onto 2 : 1 layered silicate surface was enhanced by isomorphic charge distribution and higher pH as

collaborated by experimental results. The increased adsorption at pH > 6.0 indicated complexation of metal cations to AlOH and SiOH groups at edge sites of mica. Stable defects on a surface could offer new sites for the binding of metal cations and Cu(II) and Zn(II) might be attached to these sites forming four M–O bonds. On the basis of the solvated structures, the authors concluded that the binding of Cu(II) and Zn(II) from solution and the associated loss of K^+ ions into solution were favoured. Zn(II) could combine more strongly than Cu(II). The theoretical study also indicated that Cd(II) did not chemisorb into the defect sites, which might be due to the separation between the oxygens of the tetrahedral layer and those of the octahedral layer, which selectively accommodate smaller ions. Cd(II) could form a much less stable structure on the mica surface by binding to two oxygen atoms of the defect sites and the stability of this configuration was increased by the presence of water molecules. Cd(II) preferably formed outer sphere complexes rather to bind directly with either the smooth muscovite surface or edge sites, which was supported by experimental data.

Kaludjerovic-Radoicic and Raicevic[121] studied the adsorption of Pb(II) on natural apatite and hydroxyapatite and the experiments were simulated in which 0.2 g of adsorbent reacted with 0.483 mmol Pb(II) L^{-1} (as nitrate). According to the Visual MINTEQ calculations, 99.97% of Pb(II) could be adsorbed on hydroxyapatite, while the experimental value was 99.60%. The calculations showed the presence of two solids at equilibrium, namely, pyromorphite (HPM) and hydroxyapatite (HAP), and that HAP dissolved to form HPM until there were Pb(II) present in the solution. Only 0.03% of initial Pb(II) concentration remained in solution, indicating that the main mechanism of Pb(II) removal from the solution was dissolution of HAP followed by HPM precipitation, though the experimental data did not show any new solid phase formation. The reason for this could be the low concentration of HPM or the poor crystallinity of the newly formed solid phase. Visual MINTEQ calculations showed that synthetic HAP was an appropriate adsorbent for Pb(II). However, a significant difference between calculated and experimental values of Pb(II) removal was observed for natural apatite (calculated: 99.95%, experimental: 41.6%). Visual MINTEQ predicted two solids at Pb(II)–apatite equilibrium, namely, fluorapatite and pyromorphite. According to the calculations, natural apatite dissolved to provide PO_4^{3-} ions for HPM formation. The large difference between experimental and calculated values of Pb(II) removal indicated that dissolution–precipitation mechanism suggested by this model could not describe Pb(II)–natural apatite interactions. Adsorption of Pb(II) by HAP was shown to lead to encapsulation of HAP particles by insoluble pyromorphite, preventing the process of Pb(II) immobilization. On the other hand, apatite could form apatite/Pb(II) solid solution instead of the pyromorphite, which allow diffusion of Pb(II) from the surface into the HAP particles resulting in slow but continuous uptake of Pb(II).

Dou *et al.*[273] reported that As(V) primarily reacted with Fe–OH sites of Fe–Ce bimetal oxide with the formation of monodentate mononuclear and bidentate binuclear surface complexes of As(V), which coexisted. The existence of monodentate complex might be due to the existence of Ce atoms in the bimetal oxide. Moreover, molecular simulation studies showed that protonated monodentate complex and deprotonated bidentate complex preferred to co-exist at Fe–Ce surface under a significantly high surface loading. Protonated monodentate complex was found to be dominant at pH < 8.0, while deprotonated bidentate complex was dominant at pH > 8.0. By increasing the protonated monodentate complex, As(V) surface loading could be increased.

4. Conclusion and future perspective

From the large number of works reviewed here, it is observed that the adsorption capacities of metal cations and anions on inorganic adsorbents are mainly evaluated on the basis of Freundlich and Langmuir isotherm models. The maximum uptake capacities of different adsorbents provide some idea of their effectiveness for each type of metal cation/anion. Most of these adsorbents have good removal capacities, sometimes even better than activated carbons. Different modification processes often enhance the uptake capacities; however, the reverse observations are also there.

Although the suitability of the equilibrium isotherm model is important for a specific adsorbate–adsorbent process, some adsorption studies have been reported without the use of any isotherm model. These have not been covered in this review.

Despite the fact that the influences of experimental parameters on adsorption capacities for various adsorbate–adsorbent systems are not very straight forward, yet some general conclusions can be drawn. A few of them are;

(i) The nature of the surface functional groups considerably influences adsorption of cations and anions.

(ii) Pre-treatment (*e.g.* acid-treatment, pillaring, organic functionalization, *etc.*) of the solid in various ways serve to change the number and distribution of surface active sites and thereby, influences adsorption capacities.

(iii) The solution pH affects the adsorbent surface by placing a layer of hydroxyl or hydrogen ions on the surface which influences adsorption of cations and anions as well as the mechanism of uptake.

(iv) Increase in solution temperature enhances the mobility of the ions and transport limitation, if any, is minimized. Results indicate both increase and decrease in the adsorption capacities of solids with change in temperature.

(v) Adsorption capacity is likely to be affected by the way in which the adsorbate–adsorbent mixture was agitated (*e.g.* stirring speed). However, this angle was not studied much except in one or two studies.

This literature review shows remarkable variations in the mechanisms of adsorption from one system to another. The mechanisms suggested belong to ion exchange, ligand exchange, electrostatic interaction, formation of inner and outer sphere complexes, chelation, hydrogen bonding, acid–base interaction, *etc.*, and in many cases, more than one mechanism has been predicted as operating simultaneously. There are large differences in how the adsorption capacities are represented and in a considerable number of publications, no attention seems to have been given to use a uniform pattern of units, many have just ignored the use of units.

Nomenclature

C_e	Equilibrium liquid phase concentration
q_e	Solid phase concentration
K_F	Freundlich adsorption capacity
n	Freundlich adsorption intensity, Toth coefficient
q_m	Langmuir capacity
b	Langmuir adsorption equilibrium constant
q_{max}	Dubinin–Radushkevich capacity
β	Dubinin–Radushkevich coefficient related to the mean free energy of adsorption per mol of the adsorbate
ε	Polanyi potential
R	Universal gas constant
K	Absolute temperature
E	Mean free energy
K_{RP}	Redlich–Peterson coefficient
a_{RP}	Redlich–Peterson coefficient
g	Redlich–Peterson heterogeneity index
K_T	Temkin equilibrium binding energy
B	Temkin coefficient related to enthalpy of adsorption
Q_{max}	Toth capacity
b_T	Toth coefficient
CEC	Cation exchange capacity

References

1 S. Hong, C. Wen, H. Jing, F. Gan and Y.-S. Ho, *J. Hazard. Mater.*, 2009, **167**, 630–633.
2 M. I. El-Khaiary, *J. Hazard. Mater.*, 2008, **158**, 73–87.
3 K. Y. Foo and B. H. Hameed, *Chem. Eng. J.*, 2010, **156**, 2–10.
4 W. J. Weber, Jr, Adsorption theory, concepts, and models, in *Adsorption Technology: A Step-by-Step Approach to Process Evaluation and Application*, ed. F. L. Slejko, Marcel Dekker, New York, 1985, p. 1.
5 F. E. Bernardin, Jr, Experimental design and testing of adsorption and adsorbates, in *Adsorption Technology: A Step-by-Step Approach to Process Evaluation and Application*, ed. F. L. Slejko, Marcel Dekker, New York, 1985, p. 37.
6 W. J. Thomas and B. Crittenden, Fundamental of adsorption equilibria, in *Adsorption Technology and Design*, Butterworth-Heinemann, Oxford, 1998, ch. 3, p. 31.
7 D. Mohan and C. U. Pittman Jr, *J. Hazard. Mater.*, 2007, **142**, 1–53.
8 Q. U. Jiuhui, *J. Environ. Sci.*, 2008, **20**, 1–13.
9 V. K. Gupta, P. J. M. Carrott, M. M. L. R. Carrott and Suhas, *Crit. Rev. Environ. Sci. Technol.*, 2009, **39**, 783–842.
10 A. Bhatnagar and M. Sillanpää, *Chem. Eng. J.*, 2010, **157**, 277–296.
11 S. Wang and Y. Peng, *Chem. Eng. J.*, 2010, **156**, 11–24.
12 K. G. Bhattacharyya and S. Sen Gupta, *Adv. Colloid Interface Sci.*, 2008, **140**, 114–131.
13 S. Sen Gupta and K. G. Bhattacharyya, *Phys. Chem. Chem. Phys.*, 2012, **14**, 6698–6723.
14 S. Sen Gupta and K. G. Bhattacharyya, Natural and treated montmorillonites as scavengers of toxic metals from water, in *Application of Adsorbents for Water Pollution Control*, ed. A. Bhatnagar, Bentham Science Publishers, USA, 2012, p. 291.
15 M. Borowko, Adsorption on heterogeneous surfaces, in *Adsorption Theory, Modelling, and Analysis*, Surfactant Science Series, ed. J. Toth, Marcel Dekker, New York, 2002, vol. 107, p. 105.
16 I. Langmuir, *J. Am. Chem. Soc.*, 1916, **38**, 2221–2295.
17 A. L. Myers and J. M. Prausnitz, *AIChE J.*, 1965, **11**, 121–129.
18 J. H. De Boer, *The Dynamical Character of Adsorption*, Oxford University Press, London, 2nd edn, 1968.
19 M. M. Dubinin, *Chem. Rev.*, 1960, **60**, 235–266.
20 D. M. Ruthven, *Principles of Adsorption and Adsorption Processes*, Wiley, New York, 1984.
21 H. M. F. Freundlich, *J. Phys. Chem.*, 1906, **57**, 385–470.
22 W. J. Weber, Jr, P. M. McGinley and L. E. Katz, *Water Res.*, 1991, **25**, 499–528.
23 A. W. Adamson and A. P. Gast, *Physical Chemistry of Surfaces*, Wiley-Interscience, New York, 1997.
24 J. Zeldowitsch, *Acta Physicochim. URSS*, 1934, **1**, 961–973.
25 Md. Ahmaruzzaman, *Adv. Colloid Interface Sci.*, 2008, **143**, 48–67.
26 H. Jobstmann and B. Singh, *Water, Air, Soil Pollut.*, 2001, **131**, 203–215.
27 V. Chantawong, N. W. Harvey and V. N. Bashkin, *Water, Air, Soil Pollut.*, 2003, **148**, 111–125.
28 P. Turan, M. Doğan and M. Alkan, *J. Hazard. Mater.*, 2007, **148**, 56–63.
29 F. Arias and T. K. Sen, *Colloids Surf., A*, 2009, **348**, 100–108.
30 A. Sari, M. Tuzen, D. Citak and M. Soylak, *J. Hazard. Mater.*, 2007, **149**, 283–291.
31 A. Sarı, M. Tuzen and M. Soylak, *J. Hazard. Mater.*, 2007, **144**, 41–46.
32 S. Wang, Y. Dong, M. He, L. Chen and X. Yu, *Appl. Clay Sci.*, 2009, **43**, 164–171.
33 S. M. Dal Bosco, R. S. Jimenez, C. Vignado, J. Fontana, B. Geraldo, F. C. A. Figueiredo, D. Mandelli and W. A. Carvalho, *Adsorption*, 2006, **12**, 133–146.
34 Ş. Kubilay, R. Gürkan, A. Savran and T. Şahan, *Adsorption*, 2007, **13**, 41–51.
35 T. K. Sen and D. Gomez, *Desalination*, 2011, **267**, 286–294.
36 N. Karapinar and R. Donat, *Desalination*, 2009, **249**, 123–129.
37 J. Li, J. Hu, G. Sheng, G. Zhao and Q. Huang, *Colloids Surf., A*, 2009, **349**, 195–201.
38 S. Yang, D. Zhao, H. Zhang, S. Lu, L. Chen and X. Yu, *J. Hazard. Mater.*, 2010, **183**, 632–640.
39 S. Veli and B. Alyüz, *J. Hazard. Mater.*, 2007, **149**, 226–233.
40 S. Q. Zhang and W. G. Hou, *Colloids Surf., A*, 2008, **320**, 92–97.
41 S. I. Abu-Eishah, *Appl. Clay Sci.*, 2008, **42**, 201–205.
42 Q. Fan, D. Shao, Y. Lu, W. Wu and X. Wang, *Chem. Eng. J.*, 2009, **150**, 188–195.
43 J.-S. Yang, J. Y. Lee, Y.-T. Park, K. Baek and J. Choi, *Sep. Sci. Technol.*, 2010, **45**, 814–823.
44 M.-q. Jiang, Q.-p. Wang, X.-y. Jin and Z.-l. Chen, *J. Hazard. Mater.*, 2009, **170**, 332–339.

45 R. A. Shawabkeh, O. A. Al-Khashman, H. S. Al-Omari and A. F. Shawabkeh, *Environmentalist*, 2007, **27**, 357–363.
46 K. G. Bhattacharyya and S. Sen Gupta, *Ind. Eng. Chem. Res.*, 2007, **46**, 3734–3742.
47 S. Sen Gupta and K. G. Bhattacharyya, *J. Hazard. Mater.*, 2006, **128**, 247–257.
48 K. G. Bhattacharyya and S. Sen Gupta, *Appl. Clay Sci.*, 2008, **41**, 1–9.
49 K. G. Bhattacharyya and S. Sen Gupta, *Colloids Surf., A*, 2008, **317**, 71–79.
50 K. G. Bhattacharyya and S. Sen Gupta, *Sep. Sci. Technol.*, 2007, **42**, 3391–3418.
51 K. G. Bhattacharyya and S. Sen Gupta, *Sep. Sci. Technol.*, 2008, **43**, 3221–3250.
52 K. G. Bhattacharyya and S. Sen Gupta, *Adsorption*, 2006, **12**, 185–204.
53 S. Sen Gupta and K. G. Bhattacharyya, *Appl. Clay Sci.*, 2005, **30**, 199–208.
54 K. G. Bhattacharyya and S. Sen Gupta, *Colloids Surf., A*, 2006, **277**, 191–200.
55 K. G. Bhattacharyya and S. Sen Gupta, *Ind. Eng. Chem. Res.*, 2006, **45**, 7232–7240.
56 K. G. Bhattacharyya and S. Sen Gupta, *Sep. Purif. Technol.*, 2006, **50**, 388–397.
57 K. G. Bhattacharyya and S. Sen Gupta, *Desalination*, 2011, **272**, 66–75.
58 B. I. Olu-Owolabi, D. B. Popoola and E. I. Unuabonah, *Water, Air, Soil Pollut.*, 2010, **211**, 459–474.
59 E. Eren, A. Tabak and B. Eren, *Desalination*, 2010, **257**, 163–169.
60 M. Ranđelović, M. Purenović, A. Zarubica, J. Purenović, B. Matović and M. Momćilović, *J. Hazard. Mater.*, 2012, **199–200**, 367–374.
61 A. Mockovčiaková, Z. Orolínová and J. Škvarla, *J. Hazard. Mater.*, 2010, **180**, 274–281.
62 B. S. Kadu and R. C. Chikate, *J. Environ. Chem. Eng.*, 2013, **1**, 320–327.
63 F. Tomul, *Ind. Eng. Chem. Res.*, 2011, **50**, 7228–7240.
64 L.-g. Yan, X.-q. Shan, B. Wen and G. Owens, *J. Hazard. Mater.*, 2008, **156**, 499–508.
65 P. Wu, W. Wu, S. Li, N. Xing, N. Zhu, P. Li, J. Wu, C. Yang and Z. Dang, *J. Hazard. Mater.*, 2009, **169**, 824–830.
66 P. Wu, Q. Zhang, Y. Dai, N. Zhu, Z. Dang, P. Li, J. Wu and X. Wang, *Geoderma*, 2011, **164**, 215–219.
67 B. Hu, H. Luo, H. Chen and T. Dong, *Appl. Clay Sci.*, 2011, **51**, 198–201.
68 J. Su, H.-G. Huang, X.-Y. Jin, X.-Q. Lu and Z.-L. Chen, *J. Hazard. Mater.*, 2011, **185**, 63–70.
69 S. Sen Gupta and K. G. Bhattacharyya, *J. Colloid Interface Sci.*, 2006, **295**, 21–32.
70 Ö. Gök, A. Özcan, B. Erdem and A. S. Özcan, *Colloids Surf., A*, 2008, **317**, 174–185.
71 A. S. Özcan, Ö. Gök and A. Özcan, *J. Hazard. Mater.*, 2009, **161**, 499–509.
72 B. Erdem, A. Özcan, Ö. Gök and A. S. Özcan, *J. Hazard. Mater.*, 2009, **163**, 418–426.
73 A. S. K. Kumar, R. Ramachandran, S. Kalidhasan, V. Rajesh and N. Rajesh, *Chem. Eng. J.*, 2012, **211–212**, 396–405.
74 W. A. Carvalho, C. Vignado and J. Fontana, *J. Hazard. Mater.*, 2008, **153**, 1240–1247.
75 M. Şölener, S. Tunali, A. S. Özcan, A. Özcan and T. Gedikbey, *Desalination*, 2008, **223**, 308–322.
76 W. Li, Y. Tang, Y. Zeng, Z. Tong, D. Liang and W. Cui, *Chem. Eng. J.*, 2012, **193–194**, 88–95.
77 V. Marjanović, S. Lazarević, I. Janković-Častvan, B. Potkonjak, Đ. Janaćković and R. Petrović, *Chem. Eng. J.*, 2011, **166**, 198–206.
78 V. Marjanović, S. Lazarević, I. Janković-Častvan, B. Jokić, D. Janaćković and R. Petrović, *Appl. Clay Sci.*, 2013, **80–81**, 202–210.
79 X. Liang, Y. Xu, L. Wang, Y. Sun, D. Lin, Y. Sun, X. Qin and Q. Wan, *Chemosphere*, 2013, **90**, 548–555.
80 M. Liu, L. Hou, B. Xi, Y. Zhao and X. Xia, *Appl. Surf. Sci.*, 2013, **273**, 706–716.
81 M. A. Shavandi, Z. Haddadian, M. H. S. Ismail, N. Abdullah and Z. Z. J. Abidin, *J. Taiwan Inst. Chem. Eng.*, 2012, **43**, 750–759.
82 M. Karatas, *J. Hazard. Mater.*, 2012, **199–200**, 383–389.
83 S. Wang, T. Terdkiatburana and M. O. Tadè, *Sep. Purif. Technol.*, 2008, **62**, 64–70.
84 D. Nibou, H. Mekatel, S. Amokrane, M. Barkat and M. Trari, *J. Hazard. Mater.*, 2010, **173**, 637–646.
85 M. E. Argun, *J. Hazard. Mater.*, 2008, **150**, 587–595.
86 Y.-h. Xu, T. Nakajima and A. Ohki, *J. Hazard. Mater.*, 2002, **92**, 275–287.
87 A. Nezamzadeh-Ejhieh and M. Kabiri-Samani, *J. Hazard. Mater.*, 2013, **260**, 339–349.
88 J. Lin, Y. Zhan and Z. Zhu, *Colloids Surf., A*, 2011, **384**, 9–16.
89 H. Javadian, F. Ghorbani, H.-a. Tayebi and S. M. H. Asl, *Arabian J. Chem.*, 2013, DOI: 10.1016/j.arabjc.2013.02.018, article in press.
90 M. R. Panuccio, A. Sorgonà, M. Rizzo and G. Cacco, *J. Environ. Manage.*, 2009, **90**, 364–374.
91 L. A. Rodrigues, L. J. Maschio, R. E. da Silva and M. L. C. P. da Silva, *J. Hazard. Mater.*, 2010, **173**, 630–636.
92 T. Sheela, Y. A. Nayaka, R. Viswanatha, S. Basavanna and T. G. Venkatesha, *Powder Technol.*, 2012, **217**, 163–170.
93 V. Venkatesham, G. M. Madhu, S. V. Satyanarayana and H. S. Preetham, *Procedia Eng.*, 2013, **51**, 308–313.
94 T. Sheela and Y. A. Nayaka, *Chem. Eng. J.*, 2012, **191**, 123–131.
95 T. K. Sen and M. V. Sarzali, *Chem. Eng. J.*, 2008, **142**, 256–262.
96 Q. Su, B. Pan, S. Wan, W. Zhang and L. Lv, *J. Colloid Interface Sci.*, 2010, **349**, 607–612.
97 Q. Chen, D. Yinb, S. Zhu and X. Hu, *J. Colloid Interface Sci.*, 2012, **367**, 241–248.
98 A. Nilchi, S. R. Garmarodi and S. J. Darzi, *Sep. Sci. Technol.*, 2010, **45**, 801–808.
99 W. Liu, T. Wang, A. G. L. Borthwick, Y. Wang, X. Yin, X. Li and J. Ni, *Sci. Total Environ.*, 2013, **456–457**, 171–180.
100 R. R. Sheha and E. A. El-Shazly, *Chem. Eng. J.*, 2010, **160**, 63–71.

101 N. N. Nassar, *J. Hazard. Mater.*, 2010, **184**, 538–546.
102 I. Akin, G. Arslan, A. Tor, M. Ersoz and Y. Cengeloglu, *J. Hazard. Mater.*, 2012, **235–236**, 62–68.
103 Y.-H. Huang, C.-L. Hsueh, C.-P. Huang, L.-C. Su and C.-Y. Chen, *Sep. Purif. Technol.*, 2007, **55**, 23–29.
104 S. Zhang, H. Niu, Y. Cai, X. Zhao and Y. Shi, *Chem. Eng. J.*, 2010, **158**, 599–607.
105 Y. Zhang, M. Yang and X. Huang, *Chemosphere*, 2003, **51**, 945–952.
106 Q. Zhang, B. Pan, W. Zhang, B. Pan, Q. Zhang and H. Ren, *Ind. Eng. Chem. Res.*, 2008, **47**, 3957–3962.
107 M. Ozmen, K. Can, G. Arslan, A. Tor, Y. Cengeloglu and M. Ersoz, *Desalination*, 2010, **254**, 162–169.
108 Y. Jin, F. Liu, M. Tong and Y. Hou, *J. Hazard. Mater.*, 2012, **227–228**, 461–468.
109 A. Z. M. Badruddoza, Z. B. Z. Shawon, T. W. J. Daniela, K. Hidajat and M. Shahab Uddin, *Carbohydr. Polym.*, 2013, **91**, 322–332.
110 Y. Tan, M. Chen and Y. Hao, *Chem. Eng. J.*, 2012, **191**, 104–111.
111 T. K. Naiya, A. K. Bhattacharya and S. K. Das, *J. Colloid Interface Sci.*, 2009, **333**, 14–26.
112 S. Rengaraj, Y. Kim, C. K. Joo and J. Yi, *J. Colloid Interface Sci.*, 2004, **273**, 14–21.
113 A. Jaiswal, S. Banerjee, R. Mani and M. C. Chattopadhyaya, *J. Environ. Chem. Eng.*, 2013, **1**, 281–289.
114 F. Granados-Correa, N. G. Corral-Capulin, M. T. Olguín and C. E. Acosta-León, *Chem. Eng. J.*, 2011, **171**, 1027–1034.
115 V. Manu, H. M. Mody, H. C. Bajaj and R. V. Jasra, *Ind. Eng. Chem. Res.*, 2009, **48**, 8954–8960.
116 A. Heidari, H. Younesi and Z. Mehraban, *Chem. Eng. J.*, 2009, **153**, 70–79.
117 X. Liang, Y. Xu, G. Sun, L. Wang, Y. Sun and X. Qin, *Colloids Surf., A*, 2009, **349**, 61–68.
118 T. S. Anirudhan and P. S. Suchithra, *Indian J. Chem. Technol.*, 2010, **17**, 247–259.
119 D. Zhao, G. Sheng, J. Hu, C. Chen and X. Wang, *Chem. Eng. J.*, 2011, **171**, 167–174.
120 I. Mobasherpour, E. Salahi and M. Pazouki, *Arabian J. Chem.*, 2012, **5**, 439–446.
121 T. Kaludjerovic-Radoicic and S. Raicevic, *Chem. Eng. J.*, 2010, **160**, 503–510.
122 C. P. Wang, J. Z. Wu, H. W. Sun, T. Wang, H. B. Liu and Y. Chang, *Ind. Eng. Chem. Res.*, 2011, **50**, 8515–8523.
123 Y. Wang, X. Tang, Y. Chen, L. Zhan, Z. Li and Q. Tang, *J. Hazard. Mater.*, 2009, **172**, 30–37.
124 B. Fonseca, H. Maio, C. Quintelas, A. Teixeira and T. Tavares, *Chem. Eng. J.*, 2009, **152**, 212–219.
125 R. Ahmed, T. Yamin, M. S. Ansari and S. M. Hasany, *Adsorpt. Sci. Technol.*, 2006, **24**, 475–486.
126 S. I. H. Taqvi, M. I. Bhanger, S. W. Shah and S. M. Hasany, *Sep. Sci. Technol.*, 2006, **41**, 531–547.
127 S. I. H. Taqvi, S. M. Hasany and M. I. Bhanger, *Sep. Purif. Technol.*, 2008, **61**, 153–160.
128 S.-M. Lee, C. Laldawngliana and D. Tiwari, *Chem. Eng. J.*, 2012, **195–196**, 103–111.
129 S. Yadav, V. Srivastava, S. Banerjee, C.-H. Weng and Y. C. Sharma, *Catena*, 2012, **100**, 120–127.
130 N. Gupta, A. K. Kushwaha and M. C. Chattopadhyaya, *J. Taiwan Inst. Chem. Eng.*, 2012, **43**, 125–131.
131 H.-P. Chao and S.-H. Chen, *Chem. Eng. J.*, 2012, **193–194**, 283–289.
132 X. Zou, J. Pan, H. Ou, X. Wang, W. Guan, C. Li, Y. Yan and Y. Duan, *Chem. Eng. J.*, 2011, **167**, 112–121.
133 M. M. Abou-Mesalam, *Colloids Surf., A*, 2003, **225**, 85–94.
134 M. M. Abou-Mesalam, *Adsorption*, 2004, **10**, 87–92.
135 S. Rengaraj and S.-H. Moon, *Water Res.*, 2002, **36**, 1783–1793.
136 A. F. Shaaban, D. A. Fadel, A. A. Mahmoud, M. A. Elkomy and S. M. Elbahy, *J. Environ. Chem. Eng.*, 2013, **1**, 208–217.
137 L. Ćurković, Š. Cerjan-Stefanović and A. Rastovèan-mioè, *Water Res.*, 2001, **35**, 3436–3440.
138 H. Genç-Fuhrman, J. S. Tjell and D. Mcconchie, *Environ. Sci. Technol.*, 2004, **38**, 2428–2434.
139 V. K. Gupta, A. Rastogi and A. Nayak, *J. Colloid Interface Sci.*, 2010, **342**, 135–141.
140 N. Atar, A. Olgun and S. Wang, *Chem. Eng. J.*, 2012, **192**, 1–7.
141 I. Langmuir, *J. Am. Chem. Soc.*, 1918, **40**, 1361–1403.
142 S. Kundu and A. K. Gupta, *Chem. Eng. J.*, 2006, **122**, 93–106.
143 A. B. Pérez-Marín, V. Meseguer Zapata, J. F. Ortuno, M. Aguilar, J. Sáez and M. Llorens, *J. Hazard. Mater.*, 2007, **139**, 122–131.
144 R. A. K. Rao and M. Kashifuddin, *Arabian J. Chem.*, 2012, DOI: 10.1016/j.arabjc.2012.01.010, article in press.
145 M. H. Al-Qunaibit, W. K. Mekhemer and A. A. Zaghloul, *J. Colloid Interface Sci.*, 2005, **283**, 316–321.
146 J. A. Hefne, W. K. Mekhemer, N. M. Alandis, O. A. Aldayel and T. Alajyan, *Int. J. Phys. Sci.*, 2008, **3**, 281–288.
147 L. Zhi-rong and Z. Shao-qi, *Process Saf. Environ. Prot.*, 2010, **88**, 62–66.
148 C.-H. Weng, C.-Z. Tsai, S.-H. Chu and Y. C. Sharma, *Sep. Purif. Technol.*, 2007, **54**, 187–197.
149 C.-H. Weng, Y. C. Sharma and S.-H. Chu, *J. Hazard. Mater.*, 2008, **155**, 65–75.
150 M. G. A. Vieira, A. F. A. Neto, M. L. Gimenes and M. G. C. da Silva, *J. Hazard. Mater.*, 2010, **177**, 362–371.
151 S. Kocaoba, *Desalination*, 2009, **244**, 24–30.
152 Y. Liu, D. Xiao and H. Li, *Sep. Sci. Technol.*, 2007, **42**, 185–202.
153 A. A. El-Bayaa, N. A. Badawy and E. A. AlKhalik, *J. Hazard. Mater.*, 2009, **170**, 1204–1209.
154 D. L. Guerra and C. Airoldi, *J. Braz. Chem. Soc.*, 2009, **20**, 19–30.
155 M. Eloussaief and M. Benzina, *J. Hazard. Mater.*, 2010, **178**, 753–757.
156 A. P. Singh, K. K. Srivastava and H. Shekear, *Indian J. Chem. Technol.*, 2009, **16**, 136–141.
157 R. Yu, S. Wang, D. Wang, J. Ke, X. Xing, N. Kumada and N. Kinomura, *Catal. Today*, 2008, **139**, 135–139.
158 D. L. Guerra, C. Airoldi, V. P. Lemos and R. S. Angélica, *J. Hazard. Mater.*, 2008, **155**, 230–242.
159 T. S. Anirudhan, C. D. Bringle and P. G. Radhakrishnan, *Chem. Eng. J.*, 2012, **200–202**, 149–157.

160 B. I. Olu-Owolabi and E. I. Unuabonah, *Appl. Clay Sci.*, 2011, **51**, 170–173.
161 M. G. Mostafa, Y.-H. Chen, J.-S. Jean, C.-C. Liu and Y.-C. Lee, *J. Hazard. Mater.*, 2011, **187**, 89–95.
162 M. Al-Harahsheh, R. Shawabkeh, A. Al-Harahsheh, K. Tarawneh and M. M. Batiha, *Appl. Surf. Sci.*, 2009, **255**, 8098–8103.
163 L. Yun, W. U. Pingxiao, D. Zhi and Y. E. Daiqi, *Acta Geol. Sin.*, 2006, **80**, 219–225.
164 K. G. Bhattacharyya and S. Sen Gupta, *Appl. Clay Sci.*, 2009, **46**, 216–221.
165 B. Sarkar, Y. Xi, M. Megharaj, G. S. R. Krishnamurti, D. Rajarathnam and R. Naidu, *J. Hazard. Mater.*, 2010, **183**, 87–97.
166 D. L. Guerra, H. C. P. Oliveira, P. C. C. da Costa, R. R. Vian and C. Airoldi, *Catena*, 2010, **82**, 35–44.
167 D. L. Guerra and C. Airoldi, *J. Solid State Chem.*, 2008, **181**, 2507–2515.
168 T. S. Anirudhan and P. S. Suchithra, *Chem. Eng. J.*, 2010, **156**, 146–156.
169 R. Huang, B. Wang, B. Yang, D. Zheng and Z. Zhang, *Desalination*, 2011, **280**, 297–304.
170 S. Dultz, J.-H. An and B. Riebe, *Appl. Clay Sci.*, 2012, **67–68**, 125–133.
171 S.-H. Lin and R.-S. Juang, *J. Hazard. Mater.*, 2002, **92**, 315–326.
172 S.-Z. Li and P.-X. Wu, *J. Hazard. Mater.*, 2010, **173**, 62–70.
173 D. L. Guerra, R. R. Viana and C. Airoldi, *Mater. Res. Bull.*, 2009, **44**, 485–491.
174 G. Balomenou, P. Stathi, A. Enotiadis, D. Gournis and Y. Deligiannakis, *J. Colloid Interface Sci.*, 2008, **325**, 74–83.
175 D. L. Guerra, V. P. Lemos, R. S. Angélica and C. Airoldi, *Colloids Surf., A*, 2008, **322**, 79–86.
176 C. M. Futalan, C. C. Kan, M. L. Dalida, K.-J. Hsien, C. Pascua and M.-W. Wan, *Carbohydr. Polym.*, 2011, **83**, 528–536.
177 G. Zhao, H. Zhang, Q. Fan, X. Ren, J. Li, Y. Chen and X. Wang, *J. Hazard. Mater.*, 2010, **173**, 661–668.
178 D.-W. Cho, B.-H. Jeon, C.-M. Chon, Y. Kim, F. W. Schwartz, E.-S. Lee and H. Song, *Chem. Eng. J.*, 2012, **200–202**, 654–662.
179 D. J. L. Guerra, J. Goco, J. Nascimento and I. Melo, *J. Saudi Chem. Soc.*, 2013, DOI: 10.1016/j.jscs.2013.03.008, article in press.
180 M. Šljivić, I. Smičiklas, S. Pejanović and I. Plećaš, *Appl. Clay Sci.*, 2009, **43**, 33–40.
181 N. Bektaş, S. Aydın and M. S. Öncel, *Sep. Sci. Technol.*, 2011, **46**, 1005–1016.
182 E. Erdem, N. Karapinar and R. Donat, *J. Colloid Interface Sci.*, 2004, **280**, 309–314.
183 N. Bektaş and S. Kara, *Sep. Purif. Technol.*, 2004, **39**, 189–200.
184 S. Çoruh, *Desalination*, 2008, **225**, 41–57.
185 W. Qiu and Y. Zheng, *Chem. Eng. J.*, 2009, **145**, 483–488.
186 X. S. Wang, L. He, H. Q. Hu and J. Wang, *Sep. Sci. Technol.*, 2008, **43**, 908.
187 E. A. Shukla, E. Johan, T. Henmi and N. Matsue, *Procedia Environ. Sci.*, 2013, **17**, 279–284.
188 R. Leyva-Ramos, A. Jacobo-Azuara, P. E. Diaz-Flores, R. M. Guerrero-Coronado, J. Mendoza-Barron and M. S. Berber-Mendoza, *Colloids Surf., A*, 2008, **330**, 35–41.
189 M.-J. Yu, X. Li and W.-S. Ahn, *Microporous Mesoporous Mater.*, 2008, **113**, 197–203.
190 Y. J. O. Asencios and M. R. Sun-Kou, *Appl. Surf. Sci.*, 2012, **258**, 10002–10011.
191 V. Kailasam, E. Rosenberg and D. Nielsen, *Ind. Eng. Chem. Res.*, 2009, **48**, 3991–4001.
192 M. Ghoul, M. Bacquet and M. Morcellet, *Water Res.*, 2003, **37**, 729–734.
193 N. Chiron, R. Guilet and E. Deydier, *Water Res.*, 2003, **37**, 3079–3086.
194 R. Qu, Y. Zhang, W. Qu, C. Sun, J. Chen, Y. Ping, H. Chen and Y. Niu, *Chem. Eng. J.*, 2013, **219**, 51–61.
195 A. Naeem, M. T. Saddique, S. Mustafa, S. Tasleem, K. H. Shah and M. Waseem, *J. Hazard. Mater.*, 2009, **172**, 124–128.
196 X. Guo, J. Lu and L. Zhang, *J. Taiwan Inst. Chem. Eng.*, 2013, **44**, 630–636.
197 Y.-J. Tu, C.-F. You, C.-K. Chang, S.-L. Wang and T.-S. Chan, *Chem. Eng. J.*, 2012, **198–199**, 440–448.
198 S. Mustafa, M. Waseem, A. Naeem, K. H. Shah and T. Ahmad, *Desalination*, 2010, **255**, 148–153.
199 S. Mustafa, M. Waseem, A. Naeem, K. H. Shah, T. Ahmad and S. Y. Hussain, *Chem. Eng. J.*, 2010, **157**, 18–24.
200 T. Mahmood, S. U. Din, A. Naeem, S. Mustafa, M. Waseem and M. Hamayun, *Chem. Eng. J.*, 2012, **192**, 90–98.
201 Y. Zhang, M. Yang, X.-M. Dou, H. He and D.-S. Wang, *Environ. Sci. Technol.*, 2005, **39**, 7246–7253.
202 X. Tang, Z. Li, Y. Chen and Z. Wang, *Desalination*, 2009, **249**, 49–57.
203 Y. T. Liu, M. K. Wang, T. Y. Chen, P. N. Chiang, P. M. Huang and J. F. Lee, *Environ. Sci. Technol.*, 2006, **40**, 7784–7789.
204 S. Milicevic, T. Boljanac, S. Martinovic, M. Vlahovic, V. Milosevic and B. Babic, *Fuel Process. Technol.*, 2012, **95**, 1–7.
205 A. B. Albadarin, C. Mangwandi, A. H. Al-Muhtaseb, G. M. Walker, S. J. Allen and M. N. M. Ahmad, *Chem. Eng. J.*, 2012, **179**, 193–202.
206 M. Prasad, S. Saxena and S. S. Amritphale, *Ind. Eng. Chem. Res.*, 2002, **41**, 105–111.
207 Q. Fan, Z. Li, H. Zhao, Z. Jia, J. Xu and W. Wu, *Appl. Clay Sci.*, 2009, **45**, 111–116.
208 A. Maiti, S. DasGupta, J. K. Basu and S. De, *Ind. Eng. Chem. Res.*, 2008, **47**, 1620–1629.
209 M. I. Kandah, *Sep. Purif. Technol.*, 2004, **35**, 61–70.
210 Z. Zhu, L. Li, H. Zhang, Y. Qiu and J. Zhao, *Sep. Sci. Technol.*, 2010, **45**, 262–268.
211 J. Giménez, M. Martínez, J. de Pablo, M. Rovira and L. Duro, *J. Hazard. Mater.*, 2007, **141**, 575–580.
212 Y. Chang, H. Liu, F. Zha, H. Chen, X. Ren and Z. Lei, *Chem. Eng. J.*, 2011, **167**, 183–189.
213 N. Gupta, A. K. Kushwaha and M. C. Chattopadhyaya, *J. Taiwan Inst. Chem. Eng.*, 2012, **43**, 125–131.
214 H. Cui, Y. Qian, Q. Li, Q. Zhang and J. Zhai, *Chem. Eng. J.*, 2012, **211–212**, 216–223.

215 Y. Huang, X. Ma, G. Liang, Y. Yan and S. Wang, *Chem. Eng. J.*, 2008, **138**, 187–193.
216 V. K. Gupta, V. K. Saini and N. Jain, *J. Colloid Interface Sci.*, 2005, **288**, 55–60.
217 S. R. Kanel, B. Manning, L. Charlet and H. Choi, *Environ. Sci. Technol.*, 2005, **39**, 1291–1298.
218 H. K. Boparai, M. Joseph and D. M. O'Carroll, *J. Hazard. Mater.*, 2011, **186**, 458–465.
219 P. Yuan, M. Fan, D. Yang, H. He, D. Liu, A. Yuan, J. X. Zhu and T. H. Chen, *J. Hazard. Mater.*, 2009, **166**, 821–829.
220 P. Yuan, D. Liu, M. Fan, D. Yang, R. Zhu, F. Ge, J. X. Zhu and H. He, *J. Hazard. Mater.*, 2010, **173**, 614–621.
221 Y.-C. Chen, S.-L. Lo and J. Kuo, *Colloids Surf., A*, 2010, **361**, 126–131.
222 S. Maity, S. Chakravarty, S. Bhattacharjee and B. C. Roy, *Water Res.*, 2005, **39**, 2579–2590.
223 T. Shi, S. Jia, Y. Chen, Y. Wen, C. Du, H. Guo and Z. Wang, *J. Hazard. Mater.*, 2009, **169**, 838–846.
224 E. Roth, V. Mancier and B. Fabre, *Geoderma*, 2012, **189–190**, 133–143.
225 T. W. Cheng, M. L. Lee, M. S. Ko, T. H. Ueng and S. F. Yang, *Appl. Clay Sci.*, 2012, **56**, 90–96.
226 S. E. Ghazy and A. H. Ragab, *Indian J. Chem. Technol.*, 2007, **14**, 507–514.
227 S. E. Ghazy and A. H. M. Gad, *Indian J. Chem. Technol.*, 2008, **15**, 433–442.
228 N. Chandra, N. Agnihotri, P. Sharma, S. Bhasin and S. S. Amritphale, *J. Sci. Ind. Res.*, 2005, **64**, 674–678.
229 V. K. Gupta and I. Ali, *J. Colloid Interface Sci.*, 2004, **271**, 321–328.
230 V. K. Gupta and I. Ali, *Sep. Purif. Technol.*, 2000, **18**, 131–140.
231 V. K. Gupta, C. K. Jain, I. Ali, M. Sharma and V. K. Saini, *Water Res.*, 2003, **37**, 4038–4044.
232 K. Nath, J. P. Gor, P. N. Shah and K. Modi, *J. Sci. Ind. Res.*, 2007, **66**, 170–177.
233 L. Tofan, C. Paduraru, D. Bilba and M. Rotariu, *J. Hazard. Mater.*, 2008, **156**, 1–8.
234 B. Bayat, *J. Hazard. Mater.*, 2002, **95**, 275–290.
235 S. S. Banerjee, M. V. Joshi and R. V. Jayaram, *Sep. Sci. Technol.*, 2004, **39**, 1611–1629.
236 M. Visa, *Appl. Surf. Sci.*, 2012, **263**, 753–762.
237 V. K. Gupta, M. Gupta and S. Sharma, *Water Res.*, 2001, **35**, 1125–1134.
238 A. Bhatnagar, A. K. Jain, A. K. Minocha and S. Singh, *Sep. Sci. Technol.*, 2006, **41**, 1881–1892.
239 A. K. Bhattacharya, T. K. Naiya, S. N. Mandal and S. K. Das, *Chem. Eng. J.*, 2008, **137**, 529–541.
240 T. K. Naiya, A. K. Bhattacharya and S. K. Das, *J. Colloid Interface Sci.*, 2008, **325**, 48–56.
241 S.-C. Pan, C.-C. Lin and D.-H. Tseng, *Resour., Conserv. Recycl.*, 2003, **39**, 79–90.
242 M. M. Dubinin and L. V. Radushkevich, The equation of the characteristic curve of activated charcoal, *Proc. Acad. Sci. USSR, Phys. Chem. Sect.*, 1947, **55**, 331–333.
243 M. Polanyi, *Trans. Faraday Soc.*, 1932, **28**, 316–333.
244 S. M. Hasany and R. Ahmad, *Sep. Sci. Technol.*, 2004, **39**, 3509–3525.
245 J. P. Hobson, *J. Phys. Chem.*, 1969, **73**, 2720–2727.
246 F. Helfferich, *Ion exchange*, McGraw-Hill, New York, 1962.
247 M. S. Onyango, Y. Kojima, O. Aoyi, E. C. Bernardo and H. Matsuda, *J. Colloid Interface Sci.*, 2004, **279**, 341–350.
248 A. Ozcan, E. M. Oncu and A. S. Ozcan, *Colloids Surf., A*, 2006, **277**, 90–97.
249 X.-S. Wang, J. Wang and C. Sun, *Adsorpt. Sci. Technol.*, 2006, **24**, 517–530.
250 A. Sari and M. Tuzen, *Sep. Sci. Technol.*, 2008, **43**, 3563–3581.
251 J. U. K. Oubagaranadin and Z. V. P. Murthy, *Ind. Eng. Chem. Res.*, 2009, **48**, 10627–10636.
252 J. U. K. Oubagaranadin and Z. V. P. Murthy, *Appl. Clay Sci.*, 2010, **50**, 409–413.
253 J. Perić, M. Trgo and N. V. Medvidović, *Water Res.*, 2004, **38**, 1893–1899.
254 H. Ramadan, A. Ghanem and H. El-Rassy, *Chem. Eng. J.*, 2010, **159**, 107–115.
255 S. Debnath and U. C. Ghosh, *J. Chem. Thermodyn.*, 2008, **40**, 67–77.
256 N. Caliskan, A. R. Kul, S. Alkan, E. G. Sogut and İ. Alacabey, *J. Hazard. Mater.*, 2011, **193**, 27–36.
257 O. Redlich and D. L. Peterson, *J. Phys. Chem.*, 1959, **63**, 1024.
258 Y. C. Wong, Y. S. Szeto, W. H. Cheung and G. McKay, *Adsorption*, 2008, **14**, 11–20.
259 S. Debnath and U. C. Ghosh, *Chem. Eng. J.*, 2009, **152**, 480–491.
260 S. Rengaraj, J.-W. Yeon, Y. Kim and W.-H. Kim, *Ind. Eng. Chem. Res.*, 2007, **46**, 2834–2842.
261 M. I. Tempkin and V. Pyzhev, *Acta Phys. Chim. USSR*, 1940, **12**, 327–356.
262 C. Aharoni and M. Ungarish, *J. Chem. Soc., Faraday Trans. 1*, 1977, **73**, 456–464.
263 Y. S. Ho, J. F. Porter and G. McKay, *Water, Air, Soil Pollut.*, 2002, **141**, 1–33.
264 A. Ahmad, M. Rafatullah, O. Sulaiman, M. H. Ibrahim and R. Hashim, *J. Hazard. Mater.*, 2009, **170**, 357–365.
265 Y. Kim, C. Kim, I. Choi, S. Rengraj and J. Yi, *Environ. Sci. Technol.*, 2004, **38**, 924–931.
266 J. Toth, *Acta Chim. Acad. Sci. Hung.*, 1962, **15**, 415–430.
267 T. Düren, Y.-S. Bae and R. Q. Snurr, *Chem. Soc. Rev.*, 2009, **38**, 1237–1247.
268 A. Kremleva, S. Krüger and N. Rösch, *Geochim. Cosmochim. Acta*, 2011, **75**, 706–718.
269 P. Mignon, P. Ugliengo, M. Sodupe and E. R. Hernandez, *Phys. Chem. Chem. Phys.*, 2010, **12**, 688–697.
270 C. L. Peacock and D. M. Sherman, *Geochim. Cosmochim. Acta*, 2004, **68**, 1723–1733.
271 C. L. Peacock and D. M. Sherman, *Geochim. Cosmochim. Acta*, 2004, **68**, 2623–2637.
272 H. M. Steele, K. Wright, M. A. Nygren and I. H. Hillier, *Geochim. Cosmochim. Acta*, 2000, **64**, 257–262.
273 X. Dou, Y. Zhang, B. Zhao, X. Wu, Z. Wu and M. Yang, *Colloids Surf., A*, 2011, **379**, 109–115.

